The usage of magnetic particles in research on cells migration in the zebrafish embryo (*Danio rerio*) system.

A thesis submitted to the University of Sheffield

For the degree of Doctor of Philosophy

By

Pawel Karol Lysyganicz

September 2018

Declaration

I hereby declare that this thesis has not been and will not be, submitted in whole or in part to another University for the award of any other degree.

Pawel Karol Lysyganicz

Acknowledgements

Many people had their contribution to the creation, improvement, and polishing of this work. Here I would like to thank them all for their help.

First of all, I wanted to thank my parents for their help and allowing me to climb so high in pursuit of my career path.

Secondly, I wanted to give my sincere thanks to my supervisors Jarema Malicki and Sarah Staniland for guidance and mentoring.

I wanted to give my gratitude to my advisors Elisabeth Seward and Tanya Whitfield for their guidance help in focusing my attention on the most immediate aspects of my work.

I wanted to thank members of mechanosensation network Paul Evans, Gwendoline Reilly, Matthew Bryan for making this PhD genuinely interdisciplinary experience.

I wanted to thank members of both labs in which this PhD work was created. With special thanks to Andrea Rawling, Niedharsan Pooranahandran and Khodor Hazime for teaching me techniques and always having time for scientific consultation. Special ones for Zainab Taher with who made my work with magnetosomes much funnier and a lot easier as we learned a lot together by mistakes and constant improvement.

I owe big thanks to Karishma Chhabria amazing young scientist who helped me with data analysis and revived my curiosity of science behind walls of biology.

Many people contributed to this work in the non-scientific matter. Listing them all would probably occupy too many pages of this work, therefore, I have to mention by name only a few Magdalena Widziołek, Kunal Chopra, Jane Zhang, Gustavo A Escobar-Palafox, Ania Mastela, and Joanna Majewska thank you for always being there for me and helping to cope with the pressure created by this work.

Thank you all,

Pawel Karol Lysyganicz

Table of content

List of Abbreviations

ATP – Adenosine triphosphate

BacMPs - Bacterial magnetic nanoparticles

dpf – Days post fertilisation

ECM - Extracellular matrix

e.m.f – Electromotive force

ER - Endoplasmic reticulum

Fgreen - Fluorescence of green signal

Fred - Fluorescence of red signal

GFP – Green fluorescent protein

hpf – Hours post fertilisation

HATs - Histone acetyltransferases

HDAC - Histone deacetylase

MIP- Maximum intensity projection

MNPs – Magnetic nanoparticles

MRI – Magnectic Resonance Imiging

MTOC - Microtubule-organizing centre

MTs - Microtubules

PCM – Pericentriolar matrix

PTM – Posttranscriptional modification

PTU – Propylthiouracil

RFP – Red fluorescent protein

TAT- Tubulin acetyltransferase

TEM- Transmission electron microscopy

TSA – Trichostatin A

Sirt- Sirtuin

SPION – Supermagnetic Iron oxide nanoparticles

List of figures:

Abstract

Migration of cells is a crucial process in establishing a healthy and functional organism. The goal of this work is to develop a system, which allows changing the migration pattern of cells during early zebrafish (*Danio rerio*) development using magnetic nanoparticles (MNPs). To achieve this goal, I used two approaches; first, I exerted forces on the plasma membrane by moving the particles within a cell. Secondly, I tried to attach particles to GFP labelled centrin2 in centrosomes. I obtained magnetic nanoparticles from two sources - bacterial magnetic particles (BacMPs) also known as magnetosomes, extracted from *Magnetospirillum magneticum* AMB-1, and artificially synthesised magnetic nanoparticles from ADEMTECH. I described behaviours of particles under magnetic force outside and within the cells. I proved that functionalised magnetic nanoparticles could be delivered to cells both, *in vitro* (HeLa cells) and *in vivo* (developing embryos), where they are stored into vesicles and do not interact with actin directly. I tested the change in migration patterns in zebrafish embryos expressing centrin2 fused with green fluorescence protein (GFP), and H2B fused with red fluorescence protein (RFP). Several studies have suggested a role for HDACs proteins in cell migration and centrosome behaviour. Thus, I generated and described the phenotypes *of hdac6*$^{-/-}$*, hdac10*$^{-/-}$ and *sirt2*$^{-/-}$ homozygote mutant zebrafish lines including a combination of these mutants (Boggs et al., 2015; Ran et al., 2015; Szyk et al., 2014). I planned to test the involvement of these proteins in centrosome positioning against nucleus in migrating cells. In summary, my work shows that magnetic nanoparticles are promising tools for non-invasive, acute, and controllable exertion of force on cells *in vivo* and *in vitro*.

Chapter 1. Introduction

1.1 Mechanical forces

Embryonic development is a complex and sophisticated process, during which masses of dividing cells create advanced structures such as kidneys, eyes, the heart, and the brain. It is a time when the anterior-posterior and dorsal-ventral axes and left-right asymmetry of the body are established. During early stages of development, embryos of various organisms share common features, and overall development is very similar (Kimmel et al., 1995; Solnica-Krezel et al., 2012; Tam et al., 1997). Conservation of early stages of development across distant species highlights the importance of studying this phenomenon. Disorders in this process may lead to various major foetal malformations (Beckman et al., 1984). It shows the importance of conducting studies on early embryonic stages both from a scientific and medical point of view.

Events during early embryonic development are strictly controlled by genetic information and morphogens (Keller et al., 2003). However, research suggests the role of an additional player - mechanically induced stimuli- as being equally important for development (Mammoto et al., 2010; Patwari et al., 2008). It has been shown that endogenous and exogenous mechanical forces regulate a large number of cellular behaviours, including cell turnover (proliferation or apoptosis) (Ranft et al., 2010; Campinho et al., 2013). The most investigated aspect of it is the interaction between ECM and cells attachment to it through integrins (Parsons et al., 2010). We still lack the full understanding of how physical interactions between cells may affect their development, division, and differentiation (Klein et al. 2010; Chen et al. 1997; Mammoto et al. 2004). Different types of forces can affect these processes in various ways. Thus now, five types of mechanical forces can be distinguished, including spring forces, osmotic pressure, surface tension, tension forces (traction and pre-stress), and shear stress (Mammoto and Ingber 2010). For example, stem cell differentiation *in vitro* correlates with contraction of non-muscle myosin (Lecuit et al., 2007). Mechanical forces regulate the behaviour of cells at the cellular, tissue and organisation level. Several examples illustrate this. The orientation of the left/right asymmetry is controlled by the mechanical force of fluid flow generated by the cilia movement. Remodelling during vasculogenesis also depends on fluid flow from the cardiac cycle. Drosophila

gastrulation is dependent on the activity of non-muscle myosin (Keller, et al., 2003; Lecuit et al., 2007; Mammoto et al., 2010).

All cells are exposed to constant mechanical stresses, and they respond to these mechanical forces by triggering various signalling pathways. Signals activated via mechanotransduction next to the changed in cell polarisation have been shown to be important in orchestrating cell dynamics and contractility (Heisenberg & Bellaïche, 2013). An excellent example of this is the activation of RhoA small GTPases, which through control over myosin II were shown to play a vital role in remodelling the actin cytoskeleton and controlling intercellular tension (Mammoto et al., 2004; Asparuhova et al., 2009; Mammoto et al., 2010; Lessey et al., 2012; Etoc et al., 2013). Futhermore myosin-actin network in apical junctions was show shown to play a key role in transmitting forces across the tissue (Campinho et al., 2013; Martin et al., 2010). Another well-described pathway connected with sensing mechanical properties of growing tissue is the Hippo pathway. Evidence suggests that internal cell tension is a master regulator for this pathway (Yu et al., 2013). Studies indicate the role of this pathway in controlling cell proliferation, apoptosis, tissue size and even responding to gravitational force in Drosophila, fish and mammals (Harvey et al., 2012; Porazinski et al., 2015; Udan et al.,2003). Another good example evidence demonstrating the importance of mechanical cues comes from investigating the role of the friction force generated by anterior axial mesoderm progenitors migrating towards the animal pole and neurectoderm progenitors moving in the opposite direction, towards the vegetal pole in the neural anlage of the developing zebrafish embryo (Smutny et al., 2017). A way for cells to respond to mechanical stimuli is calcium efflux from the endoplasmic reticulum (ER) supported by Ca2+ influx through plasma membrane calcium transporters such as TRPM7 (Kim et al., 2015). Importance of mechanical forces has risen in terms of wound and bone healing. During the wound healing process, the mechanical tension and rigidity of ECM are increases by contraction of the myofibroblasts. That creates positive feedback further stimulating the differentiation of myoblasts. The impact on wound healing, of these changes in tension and rigidity, was experimentally proven on mice. Mechanical tensions were inflicted on the wounds by stretching and splinting, it resulted in increased activity of myofibroblasts and led to the intensification of scarring which resembled human hypertrophic scars (Agha et al., 2011; Rosińczuk et al.,2016). Further research has shown that the decrease of the

rigidity or declining mechanical stress of ECM can and decrease the expression of α-SM actin and myofibroblasts' ability of contraction and induce apoptosis (Wipff et al., 2007). α-SM actin genes are directly activated by mechanical signaling, received from integrins (Wang et al.,2003). Mechanical signals and following stimulation of TGF-β1 in myofibroblasts, stimulate synthesis of collagen and other ECM, what results in change of mechanical properties of the wounded tissue (Leask et al.,2004).

Mechanical forces affect pathways trough healing of fractured bones occurs. Studies have shown that time taken to heal can be modulated by changes in the mechanical environment. What effects in change the proportions of gene expression patterns of cells and different tissue types in the healing bone (Carter, 1987.; Palomares et al., 2009). In biomechanical research, we can distinguish two approaches external and internal fixation (Betts & Müller, 2014). The external fixation is used in research conducted on larger animals when the internal is used I study on the smaller animal (Gardner et al., 2013). However it is well documented that stiffness affect cells fate being able to alter its differentiation into adipocytes or osteoblasts (Park et al., 2012; Sun et al., 2018), lack in knowledge about the true bone geometry and exact tissue composition makes difficult to determine strains tissues are experiencing (Betts & Müller, 2014). That results in difficulties in creating accurate models.

Cells shape, position and organisation, were successfully predicted with mathematical models using in calculations concept of energy minimalisation based on the combined activities of cortical tension and adhesion. This model is called the Cellular Potts Model (El Yacoubi et al., 2006). This model allowed to predict the behaviour of cells Drosophila ommatidium and in germ-layer progenitor cell segregation during vertebrate gastrulation (Kafer et al., 2007; Krieg et al., 2008). These are only a few examples of how cells respond to mechanical forces and how it influences a cell, tissue and the whole organism's fate.

In my research, I used mechanical forces to trigger the change in the behaviour of migrating cells.

1.1.1 Role of cilia in mechanosensation

Cilia are microscopic microtubule-based structures necessary for the function of many signal transduction cascades, including those involved in vision, hearing, olfaction, and embryonic patterning. Fluid flow caused by cilia beating is responsible for establishing left-right asymmetry in a developing embryo (Delling et al., 2016; Patwari et al., 2008). Dysfunction of cilia leads to a number of diseases known as ciliopathies. Typically, a cilium contains nine doublets of outer microtubules (so-called 9+0 configuration). In addition, most motile cilia contain an additional two doublets in the centre (9+2). Acetylation of microtubules is a dynamic and reversible process regulated by two groups of competing enzymes, histone acetyltransferases (HATs) and histone deacetylases. Acetylation of tubulin lysine40 (K40) is believed to enhance ciliary stability (Pugacheva et al., 2007; Szyk et al., 2014). This is important, for example, because cells disassemble their cilia before they divide. Imbalances in this process may affect cancer progression.

Cilia's antenna-like shape led to researchers to hypothesise their role in mechanosensing and modulating response to environmental cues (Patwari et al., 2008). Cilia receive physical and molecular cues that orchestrate a cell growth and differentiation. Ciliary membranes feature receptors detecting signals for Hedgehog, PDGF-a and Wnt pathways, and extracellular forces (Nikonova et al., 2015). It is speculated that cilia are responsible for detection and response to compression in chondrocytes (Ruhlen et al., 2014). This idea emerged from the observation of chondrocyte cilia bending when the extracellular matrix (ECM) was present and straightening in the absence of ECM. It is under discussion whether or is not the mechanical response of primary cilia is Ca2+ dependent (Delling et al., 2016; Ruhlen et al., 2014). Both cilia and centrosomes share and interact with structures called the centrioles, a small organelle (200 nm wide and 400 nm long) containing a cylindrical array of nine triplet microtubules (Dutcher, 2003).

1.2 Model organism – Zebrafish (*Danio rerio*)

Over the years, the zebrafish (*Danio rerio*) has become a very important model organism for developmental biology, oncology, neurobiology, genetics, regenerative medicine and teratology (Jing & Malicki, 2009; Kimmel et al., 1995; Marlow et al., 1998;

Novorol et al., 2013; Ruprecht et al., 2015; Topczewski et al., 2001; Wei & Malicki, 2002). This particular model has a number of advantages, the most important being its small size, fully sequenced genome, transparent body and rapid development. Zebrafish share many similarities with mammalian organisms. Owing to conserved roles of signalling pathways playing critical roles in development, between zebrafish and other animals, this model has become important in many fields of research (Asaoka et al., 2014; Glickman et al., 2003; Kim et al., 2010; Menegola et al., 2006). One of the characteristics of zebrafish that is particularly important in my research is oviparity, which allows for precise observation of embryonic development from the single cell stage to the shaping of the notochord (Glickman et al., 2003). These attributes make zebrafish embryos the suitable organism, for my experiments, to monitor changes in the early stages of development using microscopy techniques.

1.3 Cell migration in early zebrafish development

Cell migration plays a key role during morphogenesis in establishing and maintaining the proper organisation of multicellular organisms. Morphogenesis can be seen as a result of masses of cells migrating to shape the body axis. The process starts at gastrulation when the notochord domain is formed, and mesoderm cells form an array through convergence and extension movements, into narrow, elongated structures that define the primary axis of the embryo (Glickman et al.,2003). This complicated process is mediated by a change in cell polarity coordinated by non-canonical Wnt signalling, reorganization of the actin cytoskeleton, orientation of adhesion complexes on migrating plasma membranes, localized release of intercellular Ca2+, and activation of Rho GTPases (Blaser et al., 2006; Glickman et al., 2003; Heisenberg et al., 2000). The migration of the cells is mostly driven by actin activity (Krause et al., 2014), which leads to the establishment of leading and rear edges in migrating cells. The leading edge usually creates membrane protrusions called lamellipodia - activated by GTPase Rac, or filopodia - associated with activation of Cdc42 (Nobes et al., 1995; Ridley et al., 1992). These structures are created by reorganisation of the actin cytoskeleton, which is mediated by the actin-related protein 2/3 (ARP2/3) (Krause et al., 2014). Alternatively, cells can form blebs to lead migration by contractions of the actomyosin cortex (Charras et al., 2008). This kind of migration is suggested to play a vital role in the migration of primordial zebrafish germ cells. The

process is driven by the chemokine SDF-1, which initiates formation of protrusions at sites of higher levels of free calcium where activation of myosin contraction occurs. Higher concentration of calcium is achieved by polarised activation of the receptor CXCR4 (Blaser et al., 2006).

Cell migration can be divided into two types: single cell migration and collective migration (Mayor et al., 2016; Wong et al., 2014). The latter allows large groups of cells to migrate with the same speed in the same direction. This type of migration has been shown to be more efficient than single cell migration. Although single cells migrate with higher velocity, their migration is shorter and quickly and frequently changes direction. (Mayor et al., 2016). Single cell migration is triggered either by biochemical cues or physical interactions. In clustered migration leader and follower, cells can be distinguished. Collectively migrating cells coordinate their responses, ensuring that cells otherwise immobilised or migrating in other directions will follow the leading cells (Mayor et al., 2016; Wong et al., 2014).

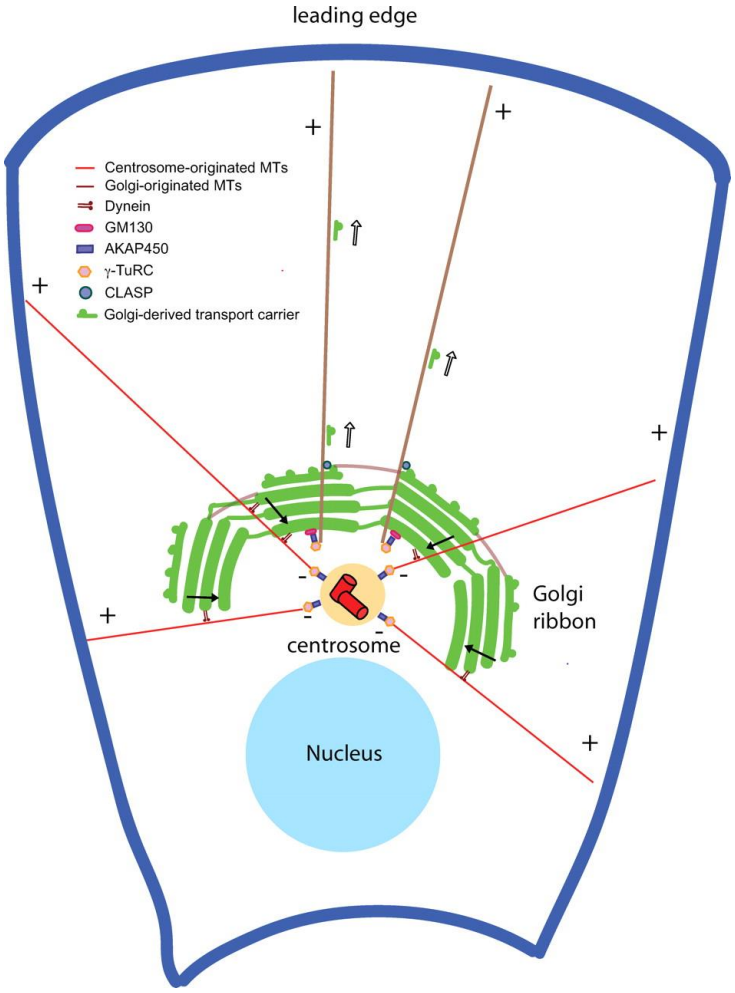

Fig. 1 Golgi- and centrosome-nucleated microtubules in cell migration. The centrosome nucleates a radial array of microtubules (red) whose minus ends (−) are anchored at the centrosome and whose plus ends (+) extend into the cell periphery. This population of microtubules depends on γ-TuRC complexes and the large scaffold protein AKAP450 for their nucleation and functions in maintaining the pericentriolar localization of the Golgi ribbon by a dynein-mediated mechanism (closed arrows). In contrast, the Golgi apparatus nucleates microtubules (brown) that extend asymmetrically toward the leading edge of a migrating cell. Microtubule nucleation at the Golgi requires the peripheral Golgi protein GM130, which recruits AKAP450 and γ-TuRC complexes to the Golgi apparatus. Golgi-nucleated microtubules are coated with CLASP proteins and are necessary for the formation of the Golgi ribbon from dispersed stacks. In addition, they are required for cell migration by facilitating polarized protein transport to the leading edge of a cell (open arrows) (Sütterlin & Colanzi, 2010).

As mentioned earlier, to migrate cells have to polarise and create leading and rear edges (Mayor et al. 2016). Imaging of migrating cells has revealed that the nucleus moves away from the leading edge to position the stationary microtubule-organising centre (MTOC) between the nucleus and the leading edge, which is needed for directed migration (Fig.1) (Sütterlin & Colanzi, 2010; van Bergeijk et al., 2015). Both actin and microtubule cytoskeleton are central players in terms of obtaining polarity by migrating cells. Proteins for both of these structures can self-assemble into functional and complex structures such as actin comets or mitotic spindle-like structures, in the presentence of ATP (Woodham et al., 2014). These cellular level rearrangements lead to the shaping of zebrafish body axes, by elongating along the mediolateral axis cells take on a bipolar shape. The primary role in this process is played by actin-based cytoskeletal machinery, which mediates motility, and perhaps also orients associated adhesion complexes on corresponding plasma membranes which are explained by mediolateral interaction behaviour theory (Heisenberg et al., 2000).

According to the mediolateral interaction behaviour theory, shaping the notochord requires a single force-generating cellular machine, where the force is distributed across a group of cells, producing both convergence and extension movements and leading to both narrowing and elongation of the field (Heisenberg et al., 2000). This hypothesis assumes that motile and adhesive cells within the mesoderm become polarised along one particular axis, the mediolateral axis.

1.3.1. Centrosome

The centrosome was formally described by Edouard Van Bened and Theodor Boveriin the late 1800's. This cell structure plays a crucial role in various cell process such as cell division, vesicle trafficking, cell migration, signalling and on top of that, acts as a microtubule-organising centre (MTOC) (Tang et al., 2012). Centrosomes in animal cells are formed of γ-tubulin ring complexes (γ-TuRCs), pericentriolar material, centrioles, tubulins and a number of other centrosome-associated proteins (Wilkinson et al. 2004). Centrioles are cylindrical structures with nine-fold radial symmetry and triplets of short microtubules creating the core of the centrosome (Bobinnec et al., 1998). A Key protein of the centrosome is γ–tubulin, this protein is well conserved across different animal species (Kollman et al.,2011). γ–tubulin works as a starting point for tubulin polymerisation in mitotic spindle poles of early cleavage stages during

cell division (Dekens et al., 2003). In many non-dividing cells, the centrioles migrate to the cell surface where the mother centriole forms a basal body that organises the formation of a cilium or flagellum (Kobayashi, 2011).

An excellent example of the transition of centrosomes into basal bodies was provided by research conducted on algae Chlamydomonas. It was shown that the same microtubule structures function as centrioles within centrosomes at the spindle poles during cell division and as basal bodies for the formation of flagella during interphase (Dutcher et al., 2003).

When considered from a mechanistic perspective, human diseases resulting from centriolar aberrations are expected to reflect defects in (1) centriole biogenesis, (2) centrosome structure, function, and positioning, or (3) the formation or maintenance of cilia and flagella. Dysfunctions of this organelle may lead to severe clinical conditions such as Huntington disease and lissencephaly (Sathasivam et al., 2001; Tanaka et al., 2004).

It has been shown that centrosomes occupy non-random locations that differ between cell types. In interphase of post-mitotic cells, centrosomes dictate the organisation of microtubules, which is essential for determining cell, polarity, shape and motility (Desai and Mitchison, 1997; Keating and Borisy, 1999). The interaction between the nucleus and centrosome is so strong that among some cell types it can even affect organelle shape. In other cell types, centrioles also have determined orientations of their long axis. For example, in pig kidney embryo cells, the mother centrioles tend to be oriented perpendicular to the substrate (Vorobjev and Chentsov, 1982).

Centriole orientation is also regulated in migrating cells. Directional cell migration depends on centrosome-derived microtubules (MTs) for Golgi polarisation and subsequent vesicle trafficking to the leading edge (Petrie et al., 2009; Kaverina and Straube, 2011; Luxton and Gundersen, 2011). Laser ablation studies reveal a centrosome requirement for the initial Golgi organisation, but once the MTOC is established, centrosome loss has negligible effects (Miller et al., 2009; Vinogradova et al., 2012). In contrast to centrosome loss, it is unclear whether excess centrosomes impairs cell migration. It has been shown that the presence of even one extra

centrosome in endothelial cells leads to a cascade of defects during interphase, resulting in disrupted cell migration and perturbed vessel sprouting (Kushner et al., 2014). In macrophages and lymphocytes, centrioles oriented themselves vertically with respect to the cell surface over which the cells are migrating (Gudima et al., 1988). Furthermore, primary cilia in migrating cells tend to point in the direction of cell movement (Albrecht-Buehler, 1977; Katsumoto et al., 1994; Schneider et al., 2010).

Interestingly recent research has shown centrosomes as nucleating centres not only for microtubules but actin skeleton as well (Farina et al., 2016). This interaction between actin and centrosomes is mediated by the nucleation-promoting factor WASH in combination with the Arp2/3 complex and is modulated by pericentriolar matrix material 1 (PCM1) (Farina et al., 2016).

Amid zebrafish gastrulation, the centrosome position is highly polarised along the anteroposterior and mediolateral embryonic axes (Sepich et al., 2011). Centrosomes first polarise along a superficial-deep axis through the ectoderm and mesoderm and later become polarised within the planes of the mesoderm and ectoderm between mid and late gastrulation. This planar polarisation of centrosomes might reflect changes in the movements of polarised cells; especially, medial or lateral positioned centrosomes can reflect medial or lateral cell rearrangement, respectively.

1.4 Role of HDACs in centrosome behaviour, migration and ciliogenesis.

Posttranslational modifications (PTMs) of tubulin affects its properties in significant ways. For instance, lack of tubulin tyrosine ligase, which restores carboxy-terminal Y on the unpolymerized tubulin, leads to early death in mice as a result of the disturbance in neuronal development (Erck et al., 2005). Glutamylation and glycylation compete for glutamate sites within the carboxy-terminal tail domains (Rogowski et al., 2009). In ciliated cells of primates, glycylation is limited only to single glycine on the side chain of tubulin (Rogowski et al., 2009). In zebrafish, it was shown that morpholino knockdown of Tubulin tyrosine ligase-like (TTLL), TTLL3 glutamylase leads to a reversal in the pattern of cilia beating in the pronephros. Knockdown of

TTLL6 slows down cilia beating frequency. Glutamylation was shown crucial for cilia motility in Chlamydomonas (Kubo et al., 2014) and impairment in glutamylation leads to phenotypes associated with ciliopathies in zebrafish (Pathak et al., 2014). Glutamylation was shown to play a role in cilia length and stability (Wloga et al., 2017). The PMT on which I focus in this work is acetylation of tubulin.

Acetylation of lysine 40 (K40) of α-tubulin is one of the best described PTM of tubulin. This modification is performed by acetyltransferases (HATs) (αTAT1, MEC17) and takes place on the lumenal surface of the microtubule (Leroux, 2010; Quinones et al., 2011) (Fig.2). However, recent studies revealed that K40 is not the only residue of tubulin that may undergo acetylation, other acetylation sites are for example K60. K96 or K112 (Sadoul et al., 2016). Acetylation of α-Tubulin has been shown not to be essential for cell survival, yet can affect cell polarisation and function (Song et al., 2015). There is a study that describes how acetylation of α-tubulin of microtubules prolongs its lifespan from 5-10 min to hours, as well as help it to withstand mechanical stress (Rymut et al., 2015; Szyk et al., 2014). Due to significant levels of acetylated tubulin within axons, it was suggested that disturbances in this process might lead to neurodegenerative diseases such as Parkinson disease, Alzheimer disease, Rett syndrome, and Charcot– Marie–Tooth (CMT) disease (Dubey et al., 2015; Zhang et al., 2015). Recently, changes in acetylation and deacetylation of tubulin have been linked with many diseases including non-Hodgkin lymphoma, metastasis, cystic fibrosis (CF), and obesity (Boggs et al., 2015; Forcioli-Conti et al., 2016; Hayashi et al., 2014; Rymut SM et al., 2013). Homeostasis in the ratio between acetylated and non-acetylated tubulin is achieved by acetyltransferases (HATs) and Histone deacetylases (HDACs) (Fig.2).

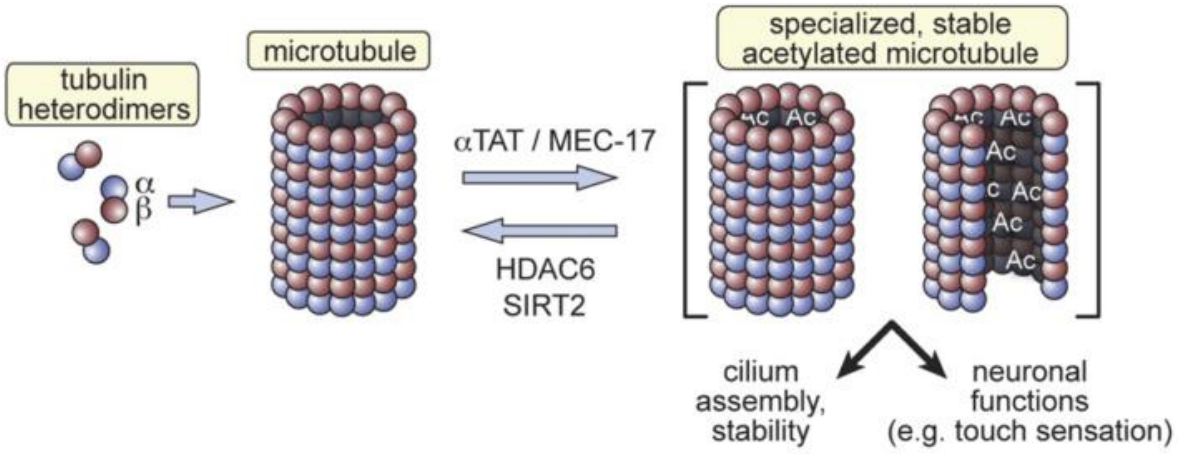

Fig. 2 Acetylation of α-tubulin by the tubulin acetyltransferase αTAT/MEC-17 emerged in the ancestral eukaryote, likely to promote cilium formation and stability. Additional functions evolved in metazoans, including neuronal roles in touch sensation. Tubulin acetylation is countered by the deacetylases HDAC6 and SIRT2 (Leroux, 2010).

Histone deacetylases are divided into four classes. Members of class1 (HDAC1, 2, 3 and 8), class2 (which in turn is subdivided into 2 subclasses) IIa (HDAC4,5,7,9) and IIb (HDAC6 and 10), and class 4 (HDAC11) have a zinc-dependent catalytic domain with a high degree of homology and less conserved accessory domains, with regulatory functions. Class 3 members are called sirtuins. They are NAD-dependent deacetylase enzymes and are related to the yeast protein Sir2. (Sirt1-7) (Guo et al. 2007; Menegola et al. 2006; Zhao et al., 2010). Class 1 enzymes are widely expressed, class 2 and 4 proteins are tissue specific. Moreover, class 1 and 4 HDACs are constitutively localised in the nucleus, while class 2 and 3 HDACs shuttle between the nucleus and the cytoplasm (Menegola et al., 2006).

HDAC6 and Sirt2 are proven to deacetylate acetylated K40 tubulin. Moreover, HDAC6 has been shown to localise in cilia and deacetylase axoneme tubulin what is suggested to be required for resorption of the cilium (Pugacheva et al., 2007). Recently HDACs were shown to negatively control centrosome duplication (Ling et al. 2012). Among them are HDAC1 and HDAC6, which suggested the possibility of these two proteins cooperating in other cilia-related processes such as retinal neurogenesis, retina development or deacetylation of ciliary tubulin (Leyk, Daly et al., 2017; Pugacheva et al., 2007; Yamaguchi, 2005). The function of HDAC10 is poorly understood, but since it shares a highly conserved Catalytic Domain1 with HDAC6, it was suggested that HDAC10 might be involved in tubulin deacetylation (Haberland et

al., 2009). However, the latest research has proven that HDAC10 is not engaged in tubulin deacetylation and its primary substrate is acetylated spermidine (Hai et al., 2017).

1.5 Magnetism

Magnetic rocks were known to humanity since around 4000 years ago. The first mention of strange rocks attracting iron ore, found in Magnesia (Asia Minor), comes from the ancient Greek culture. These rocks are magnetite, the same material from which the magnetic core of most magnetosomes, synthesised by magnetotactic bacteria, is made of. Now we know that these rocks confine their properties to one of the fundamental physical forces – magnetism. Till the 18th century magnetisation was the only way to create magnets. That means magnetite was rubbed against iron or steel to induce their magnetic fields. This method was changed when the effects of electricity on the magnetic field was discovered. Magnetization is one of the three principal effects caused by the electric current; two others were found years earlier – temperature and chemical effects. This crucial discovery was made in 1819 by the professor of physics at Copenhagen – Hans Christian Oersted. Oersted noticed that a compass needle was deflected by a wire when electric current was passed through. This discovery led to the creation of electromagnets.

Magnetism and gravity are both forces depending on distance but unlike gravity, which always attracts the objects – magnetism can both attract and repel. Objects creating the magnetic field have two poles – north (N) and south (S). When dipole objects are facing each other with the same pole (N, N or S, S poles), they will repel each other, but when they are facing opposite poles, they will attract each other (N, S poles). Evidence for the existence of magnetic monopoles is inconclusive.

The magnetic field is the space in which the forces act on the moving electric charges, and the body having a magnetic moment, regardless of their movement. The magnetic field next to the electric field is a manifestation of the electromagnetic field. Depending on the reference system, in which an observer is, the same phenomenon can be described as a sign of the electric field, magnetic field or both. Solids with magnetic properties can be classified by their magnetisation, which explains how they

react to an external magnetic field. Magnetization can be calculated with the following equation:

M=ϰH Where M=magnetization, ϰ=magnetic susceptibility, H=magnetic field strength. Magnetic susceptibility determines the strength of magnetisation as a function of magnetic field strength. Substances can be divided into three groups according to their magnetic properties: diamagnetic, paramagnetic and ferromagnetic. The criterion of this division is their response to the magnetic field.

ϰ<0 – Diamagnet

ϰ>0 – Paramagnet

ϰ>>0 – Ferromagnet

ϰ=-1 - superconductor, a perfect diamagnet

These properties depend on an internal arrangement of atoms bound into large groups within a metal. These groups containing around 1012 atoms are called domains. The direction in which all the atomic magnets point is called the axis of the domain. In unmagnetised iron, domains are aproximately of the same size and their axes point in random directions. As a result, they cancel each other, and the magnetic field cannot be detected (*without specialised instruments). In a magnetised iron, the domains align in a way that they do not cancel themselves anymore, and the magnetic field can be detected outside the iron. Magnetization can be obtained in three ways, (i) by extending domain boundaries (Fig.3 a-b), (ii) by rotating axes opposing magnetic field about 180 degrees (Fig.3 b-c), and (iii) domain whose axis is at an angle to the magnetic field can be drawn round so that the axis is in line with the field (Fig.3 c-d). Once the iron is saturated, atomic magnets arrange themselves in a “tail-head” manner, which results in the creation of two magnets when the magnet is cut. Saturation can be partially or completely removed by heating or rough treatment, which leads to the restoration of random alignment of domain axes within the magnet. Addition of cobalt or aluminium

to the alloy makes this “reset” more difficult while in the pure iron removal of a source of magnetic field is enough to remove magnetisation.

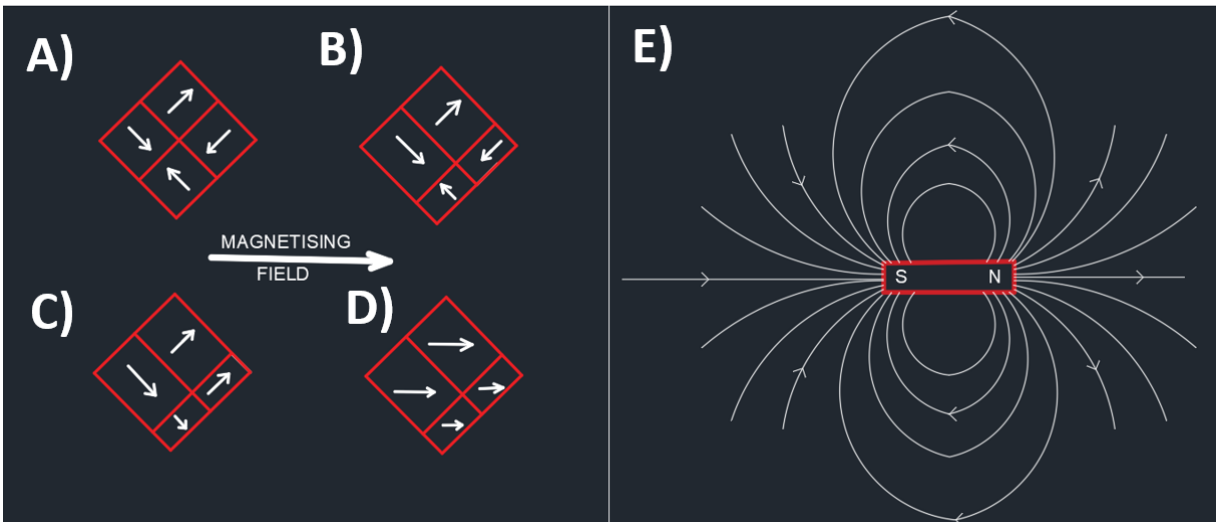

Fig. 1 Magnetisation. A) non magnetisated alloy with equal domains canceling each other. B) change in domain sizes under the magnetic field resulting in magnetisation of the alloy. C) rotation around 180 degrees of magnetisation axes of around half of domains. D) Alignment of magnetic axes of domains resulting in a magnetic saturation of the alloy. E) The magnetic field created by magnetically saturated alloy.

The key concepts describing electromagnetism are Magnetic B- H- fields, Ampere’s Law, Faraday’s Law, The Lorentz Force and the Biot-Savart Law. Magnetic fields H-B- are vector fields. Magnetic field B is mostly known as a magnetic flux density and describes the total number of magnetic lines of force passing through a specified area in a magnetic field. The formula describes the relationship between these two

$$B=\mu_0\mu_r H.$$

Where μ_0 is the permeability of free space and μ_r is the relative permeability.

Oersted's observation let to the description of electromagnetism – a theory that unified electric current and magnetism. This theory led to the formulation of Ampere’s Law, which describes the relation of the integrated magnetic field around a closed circuit to the electric current passing through the loop. This law lets us calculate the magnetic field associated with a given current and vice versa. The equation to describe this law is:

$$I_{enc}=H \times 2\pi r$$

Where Ienc is total enclosed current. If Amperian loop surrounds a coil of N turns carrying the current I, then the total confined current is NI.

Faraday's Law of Magnetic Induction describes the force that sets electricity in motion – electromotive force (e.m.f). This law says that "when the magnetic field through a circuit changes, an e.m.f. is induced in the circuit, which is proportional to the rate of change of field". The direction of an induced e.m.f. is always opposite change producing it. If the magnetic field is (approximately) uniform over the wire loop then, remembering that B is the magnetic flux density, the formula is

$$emf=-d((BxA))/dt$$

As a total linear e.m.f. Induced in multiple coils is additive, and therefore:

$$emf=-n(d(BxA))/dt$$

Where emf – electromotive force (Volts), B - pseudo-magnetic induction (teslas), A - vector direction of the surface, t – time (seconds), n = number of coils

The Lorentz Force describes the force that affects electrically charged particles – electrons or protons in the magnetic field. The equation describing the force affecting particles depends on electric and magnetic fields.

$$F=q(E+vxB)$$

Where F – force (Newtons), q – electric charge (coulombs), E - vector of electric field strength (volts / meter), B - pseudo magnetic induction (teslas), v - particle velocity vector (meters / second).

Biot-Savart Law allows computing magnetic induction for a known current inducing magnetic field. All contributors to the induction vector derived from the conductor elements have at the same point in the same direction that is perpendicular to the plane in which the guide and the point are located. Therefore, magnetic field lines have the shape of circles lying in a plane perpendicular to the conductor.

$$\mathrm{B} = \int \frac{\mu_0 I}{4\pi r^2} \mathrm{dl\ x\ r\hat{}}$$

where B is the magnetic field density (a vector), l is the differential element of the wire in the direction of conventional current (a vector), r is the distance from the wire to the

point at which the magnetic field is being calculated, r̂ is the unit vector from the wire element to the point at which the magnetic field is being calculated.

This theoretical knowledge enabled me to design a system containing either the bar magnet or electromagnetic tweezers, allowing me to manipulate magnetic nanoparticles with controllable and measurable force within cells *in vitro* and migrating zebrafish cells.

1.6 Magnetic nanoparticles

Several methods are used in changing localisation in organelles within cells (van Bergeijk et al., 2015). Among the most frequently used ones are disruption of the cytoskeleton, disruption of motor proteins, fixing morphology on micropatterns, physical linking of motors or anchors to organelles relocate specific organelles or internalisation of magnetic particles within cells or organelles (van Bergeijk et al., 2015). All of these techniques have their advantages and disadvantages. For instance, disruption of the cytoskeleton leads to changes in cell morphology and impairment in motor protein function and affects multiple organelles (van Bergeijk et al., 2015). These reasons led me to focus on magnetic nanoparticles as an acute method for strict control of applied force through the application of the magnetic field.

Before nanoparticles can be considered for use in living systems, they are required to meet the following criteria: they need to be biocompatible (non-toxic to the cells), biodegradable, maintain physical properties after surface modification, and they must not affect stem cell characteristics (Alphandéry, 2014). Fullfiling hese requirements minimalise nonspecific and side effects of introducing foreign object to cells. Further, they should be active at therapeutic doses, chemically stable in physiological conditions, ideally, have regulatory approval, and cause minimal or no transfer of by-products to surrounding cells or tissue (Markides et al., 2012).

Magnetic nanoparticles are used in various ways in environmental, biomedical and clinical fields. Iron oxide particles were shown to be demonstrably efficient in removal of heavy metals such as Pb(II), Hg(II), Cu(II) and Co(II). However, efficiency seemed to be dependent on amine groups with which particles were functionalised (Wanna et al., 2016). Other studies have shown that wastewater containing Cd^{2+}, Cr^{6+}, Cu^{2+} and Ni^{2+} can be purified with iron oxides. These studies have found that this process mostly

depends on particles size and electrostatic attraction (Li et al., 2008; Shen et al., 2009). Removal of Cr(VI) and As(V) pollutants from water by Fe_2O_3 nanoparticles has been studied. The removal mechanism was attributed to electrostatic interactions with the polarized oxygen atoms on the iron oxide surface at low pH values (Chowdhury & Yanful, 2010; Hu et al.,2007). Numerous studies have shown the impact of the size of the particles on their efficiency in removing pollutants from the water. For example, reducing the size of particles from 500 to 100 nm increased its reactivity 50-90 times (Lin et al., 2008). Other research has shown that decreasing size from 50 nm to 8 nm increased removal capacity of the particles 7 folds (Shen et al., 2009).

Nanoparticles are used more and more in the field of biomedical research. It is well documented that cells can take up NPs ranging from 10–200 nm in size mostly by endocytosis (Apopa et al., 2009; Markides et al., 2012; Moise et al., 2017; Tay et al., 2014). The amount of up taken nanoparticles has been demonstrated to reach picograms per cell, but it depended greatly on the type of coating (Markides et al. 2012).

Recent studies have shown a different cell response to nanoparticles treatment (Albanese et al., 2012; Kolosnjaj-Tabi et al., 2013; Mao et al., 2015; Markides et al., 2012; Vagida et al., 2016). For example, titanium dioxide (TiO2), silicon dioxide (SiO2) or hydroxyapatite (Ha) nanoparticles were demonstrated to affect cell motility *in vitro* strongly. To explain this, researchers suggest a possible physical interaction between nanoparticles and the microtubule cytoskeleton (Tay et al., 2014). This interaction is suggested to disrupt microtubules and prevent them from balancing tension created by actin, leading to a significant increase in adhesive properties of the cells and subsequently impairing their ability to migrate (Tay et al., 2014). This interaction was suggested to occur due to physical and not chemical processes resulting from nano size of particles. This interaction has not been reported for magnetic nanoparticles.

Magnetic nanoparticles were used successfully for *in vitro* activation of Rac-GTPase, leading to actin cytoskeleton remodelling and morphological changes. 500 nm particles labelled with ATTO-647N and functionalised with HaloTag ligand were introduced into NIH3T3 fibroblasts expressing Rac-GDPase fused with HaloTag. Then, application of around 30 pN force to attached to Rac-GTPase particles activation of Rac1 pathway what lead to changes in an actin cytoskeleton (Etoc et al., 2013). This

data shows that nanoparticles can be used to bind to specific proteins inside living cells.

Another successful use of magnetic particles *in vitro* was reported in the spatial and temporal accumulation of proteins in HeLa cells. This study showed the impact of the size of nanoparticles on their intercellular distribution and motility. In this study, functionalised magnetic nanoparticles were bound to HT-eGFP in a click reaction and accumulated on one side of the cell by application of femto-Newton force (Etoc et al., 2015).

In a different study, supermagnetic iron oxide nanoparticles (SPION) were successfully used to change the shape of cells (Shen et al., 2014). Additionally, this study also showed that nanoparticles are stored in lysosomes and that applying magnetic force can alter the position of lysosomes within the cell. Moreover, another group has demonstrated that under magnetic force, migrating cells that contained particles were attracted towards a magnetic force. Researchers did not notice significant cytotoxicity of nanoparticles. (Shen et al., 2014). However, just like the studies as mentioned above, this research was performed in cell culture.

Injection of ferrofluid into the developing Drosophila melanogaster embryo and application of magnetic force was successfully used to express the mechanosensitive gene twist in stomodeal cells. Application of uncontrolled external forces and magnetic force were compared with respect to rescuing twist expression. To achieve that, some stomodeal cells were photo ablated to decrease tension created by surrounding cells, which resulted in lower twist expression. To rescue the phenotype, either an external force (50 mm tip) or magnetic force (magnetic tweezers) that affected injected ferrofluid inside the cell in a controllable manner was used. In both cases, the tension that was created was sufficient to rescue twist expression (Desprat, 2008). This work showed that magnetic manipulation could be used to alter development at the whole tissue level.

Finally, magnetic nanoparticles are becoming widely used in medical research. The possibility of various modifications of the particles surface makes them a promising tool for drug delivery, drug formulation, hyperthermia treatments, radio immunotherapy, gene therapy and magnetofection, peptide and antibodies therapeutics and drug encapsulation and release (Mohammed et al., 2017). Being able to externally

manipulate allows for a targeted accumulation of particles delivering drugs, chemotherapeutics etc. MNPs can be triggered to release drugs with temperature increase caused by heating of particles in a high-frequency magnetic field - a process called hyperthermia (Bañobre-López et al., 2013; Hedayatnasab et al., 2017). Studies show that hyperthermia can be successfully used in killing cancer cells *in vivo* (Behrouzkia et al., 2016; Prosnitz et al., 1999). Several explanations for the mechanism how hyperthermia affects and kills cancer cells for example by stimulation of antitumour immune responsivity, impairing DNA damage response making cancers cell more prone to treatments targeting DNA (Skitzki et al., 2009; Tempel et al., 2019). MNP is used in MR Imaging (Sosnovik et al., 2008)

All these data suggest magnetic particles to be a potent tool in research on mechanosensation. In my study, I wanted to utilise the natural advantages of naturally biosynthesised magnetic particles – magnetosomes.

1.5.1 Magnetosomes

` In my research, I used naturally biosynthesised nanomagnets coated with a phospholipid layer – magnetosomes. Discovered by Blakemore in 1975 (Blakemore et al. 1975), these nanostructures are biomineralized by a diverse group of Gram-negative bacteria. The uniform shape and size of magnetosomes, of each species, suggests that the process of biomineralisation remains under the strict control of the cell. The majority of genes essential for participating in magnetosome formation by magnetotactic bacteria are grouped in four conserved gene clusters within a large unstable genomic region called the magnetosome island (MAI) (Murat et al. 2010a). In most magnetotactic bacterial strains, magnetosomes consist of magnetite, Fe_3O_4, with a typical particle size between 35 and 120 nm. However, in some cases, crystals larger than 200 nm have also been found. In several magnetotactic bacteria species isolated from sulphuric environments, magnetosomes consist of an iron-sulphide mineral called greigite (Fe_3S_4), which is ferrimagnetically ordered, as well as magnetite (Murat et al., 2010). Synthesis of magnetosomes involves three major steps. The first step is the invagination of the cytoplasmic membrane to create a magnetosome membrane. This step is driven by GTPases such as Mms16, MpsA and Mms24. This process is followed by the attachment of these vesicles to filamentous protein to create chains - by the interaction between MamK and MamJ proteins

(Arakaki et al., 2008). In the second stage, iron transporters such as MamB/MamM transport supersaturating ferrous ions from the cytoplasm to the vesicles. This process demands strict control due to the harmful effects of a high concentration of iron inside the cell. In the last step, magnetite is nucleated by an increase of the pH inside the vesicle (Arakaki et al., 2008). The presence of membrane proteins establishes many of the magnetosomal membrane features.

An advantage of magnetosomes compared to artificially created magnetic nanoparticles is that their phospholipid bilayer contains glycolipids, sulpholipids, phospholipids (in the weight ratio of 1:4:6), free fatty acids such as palmitoleic acid and oleic acid and unique surface proteins. (Gorby et al., 1988). These properties have allowed researchers to modify the magnetosomal membrane in various ways, allowing it to bind antibodies, drugs, nucleic acids or isotope-labelled particles (Sun et al., 2011).

Furthermore, genetic engineering techniques have been successfully applied to express functional proteins on bacterial magnetosomal surfaces in the AMB-1 strain of *Magnetospirillum magneticum*. Bacterial magnetosome-specific proteins were used as anchor proteins, localising various functional proteins on bacterial magnetic particles and facilitating their proper orientation. To date, various kinds of heterologous proteins, such as luciferase, protein A, the estrogen receptor, and the dopamine receptor have been interpolated onto BacMPs (Yoshino et al., 2008; Yoshino et al., 2005; Yoshino et al., 2006). These modifications allow using magnetosomes in various ways. For instance, BacMPs containing protein A (protein A-BacMPs) on their surface have been used for cell separation (Yoshino et al., 2006; Yoshino et al., 2005, 2008), and flow-cytometric analysis showed that target cells were successfully separated with a purity of more than 95%. Because of their strong magnetic susceptibility, magnetosomes are being tested to be used in antitumor hyperthermia therapy. Magnetic hyperthermia is a procedure in which magnetic nanoparticles are taken up by the tumour cells and heated under an alternating magnetic field (AMF) (Alphandéry et al. 2012). As an effect, the heat produced locally by the nanoparticles induces anti-tumour activity. Moreover, magnetosomes do not seem to to be cytotoxic when taken up by cells via endocytosis, as they are stored in lysosomes and oxidised to iron di- or trivalent (Alphandéry et al. 2012).

1.7 Aims

Cell migration and way how cells polarise themselves during this event are crucial in shaping multicellular organisms. It is documented in the literature that how the cells migrate can be modulated with mechanical cues, which play an important role in this process (Collinet et al., 2015; Heisenberg & Bellaïche, 2013; Nobes & Hall, 1995; Solnica-Krezel & Sepich, 2012; Wong et al., 2014). Mathematical simulations conducted by the Oster group predicted that mechanical forces could orchestrate complex process such as gastrulation without any other factors needed (Weliky & Oster, 1990). Over the years many techniques testing the role of these mechanical forces were discovered, optimised and applied in research . Among them techniques involving usage of magnetic nanoparticles and the magnetic force (Bryan et al., 2010; Desprat et al., 2008; Etoc et al., 2013; Henstock et al., 2014; Rotherham et al., 2017). These magnetic techniques were proven to be successfully used in altering the migration and behaviour of cells *in vitro* (Shen et al., 2014; Steketee et al., 2011). Growing number of cases when magnetic particles were used intracellularly to reach intercellular targets or modify cells behaviour creates promising corner stone for progressing these research to *in vivo* models (Desprat et al., 2008; Etoc et al., 2013; Etoc et al., 2015; Master et al., 2015; Shen et al., 2014).

Cell polarisation is one of key event determining organised migration in case of many cells (Woodham & Machesky, 2014). During this process cytoskeleton, organells and membrane proteins are reorganised in the way that rear, and lead edges are established (Kaverina & Straube, 2011; Solnica-Krezel & Sepich, 2012; Thiam et al., 2016; Woodham & Machesky, 2014). Centrosomes being microtubules organising centres are one of the organelles which polarisation is suggested to play an important role in direction of which the cell migrates (Kushner et al., 2014). MTOC orchestrates extending microtubules which modifications, specially acetylation, are known to affect cell migration (Bance et al., 2018; Boggs et al., 2015; Rymut & Kelley, 2015; Zuo et al., 2012). Acetylation of tubulin is carried by aTAT and MEC17 and deacetylation by HDAC6 and Sirt2 proteins (Hubbert et al., 2002; Leroux, 2010; Wloga et al., 2017; Zhang et al., 2015). Interestingly HDAC6, Sirt2 and other proteins from HDAC family have been found as components of the centrosome (Ling et al., 2012).

The aim of this PhD is to evaluate if magnetic nanoparticles, both synthesised by magnetotactic bacteria *Magnetospirillum magneticum* AMB-1 and man-made, can be used as a tool for non-invasive induction of responses to mechanical stimuli, either to exert pressure on the cell membrane or manipulate the position of centrosomes inside cells (Fig.4). Our hypothesis based on literature data assumes that it is plausible to affect cell migration using force generated by magnetic particles in a magnetic field. What will later allow investigating the role of the position of the individual organelle and role of specific proteins in responses to the mechanical stimuli?

This research covers five major areas; (i) functionalisation and description of particles for their physical and biological features (ii) internalization of particles in HeLa cells and their interaction with actin, (iii) delivery of nanoparticles and their impact on migration pattern in developing zebrafish embryo, (iv) developing a magnetic setup to induce particles movement and visualise its impact on the embryo, and (v) description of zebrafish HDACs (*hdac*1$^{-/-}$, *hdac*6$^{-/-}$, *hdac*10$^{-/-}$ *sirt*2$^{-/-}$ and double and triple) mutants, a model for testing this system in the future.

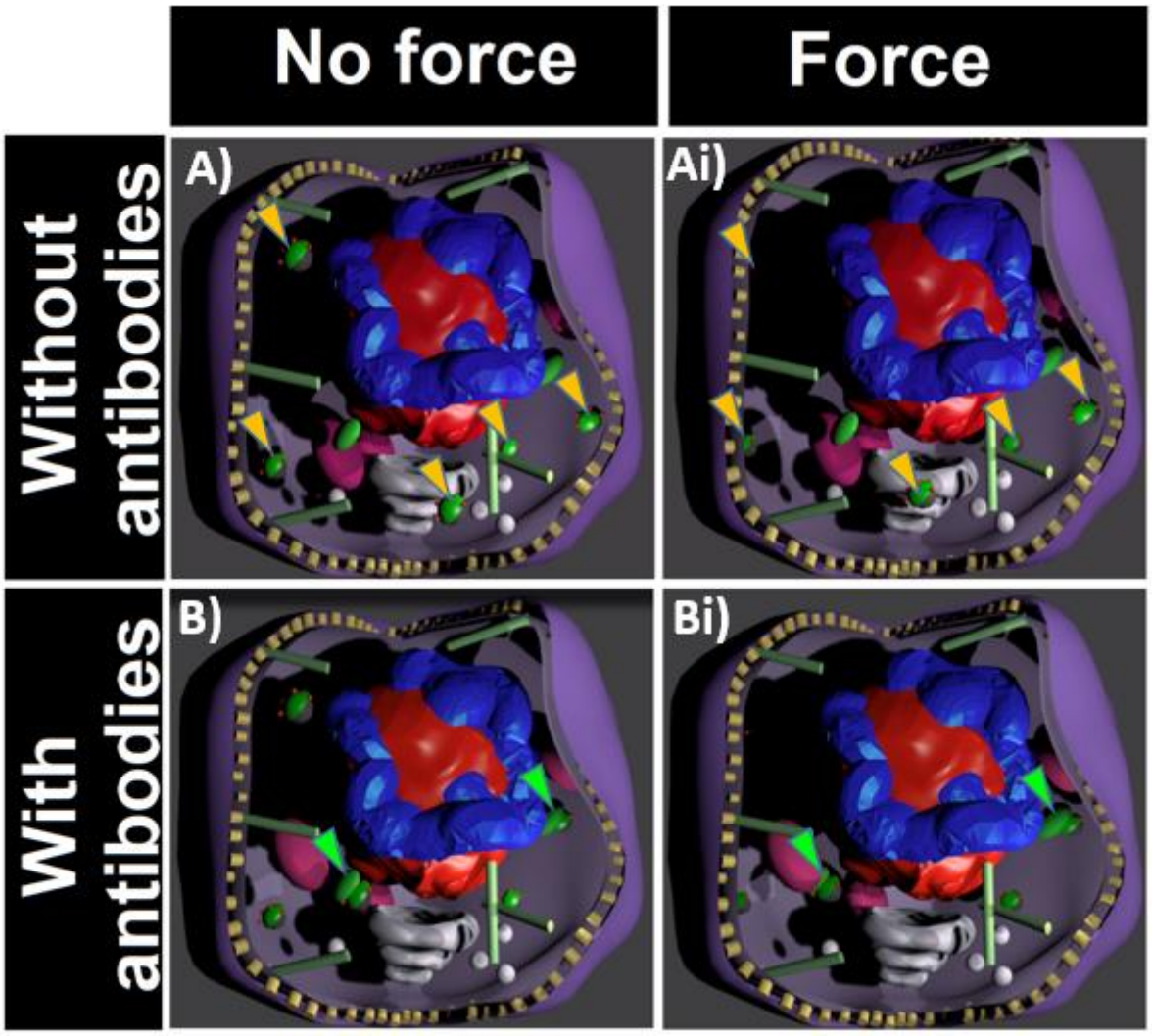

Fig. 2 An outline of the project aims. Images show a schematic cell containing functionalised magnetic nanoparticles (yellow arrowhead). Panels A) and Ai) show a movement of particles within a cytoplasm. Panels B) and Bi) show the displacement of particles and attached centrosomes (green arrowheads) under the magnetic force.

Chapter 2. Materials and methods

2.1 Zebrafish strains, maintenance and fin-clipping

2.1.1 Maintenance

Zebrafish were maintained in accordance with UK Home Office regulations, UK Animals (Scientific Procedures) Act 1986, under the project licence issued to Dr Jarema Malicki: 40/3624 and my personal licence: 37807. Both adult and embryonic zebrafish were maintained at 28 C degree, on a 14:10 hours light/dark cycle. Adults were fed with live artemia or dry food twice daily.

To obtain homozygote embryos and wild-type embryos, the parent fish were incrossed using pair mating. This was done using breeding tanks that include an internal tank with a perforated bottom permeable for embryos to pass through and escape being ingested by the adults. The collected embryos were sorted into Petri dishes, containing the E3 medium, with approximately 40 embryos per dish. The embryos were kept at 28 C degrees and regularly monitored for any developmental abnormalities. Dead embryos are removed to prevent contamination.

To obtain double, triple and quadruple mutants or transgenic lines, fish were outcrossed with partners giving the highest chance of the desired combination of alleles.

2.1.2 Strains

The H2B-RFP line was obtained from Dr Malicki's lab. The Centrin2: GFP line was kindly donated by Bill Harris (Novorol et al., 2013). The double transgenic line H2B-RFP; Centrin2-GFP was obtained by crossing the Centrin2-GFP line with the H2B-RFP line. Embryos positive for both red and green fluorescence were selected. The Claudin: GFP line was received from Dr Tanya Whitfield. The 4xGTIIC:eGFP transgenic line was donated by Prof. Brian Link (Miesfeld et al., 2014). *Hdac6*$^{-/-}$, *hdac10*$^{-/-}$, *hdac6*$^{-/-}$, *hdac10*$^{-/-}$ double mutant and *sirt2* mosaic were made by Dr Niedharsan Pooranachandran in Dr Jarema Malicki's lab. *Hdac6*$^{-/-}$ was mutated using TALEN, while *hdac10*$^{-/-}$ and *sirt2*$^{-/-}$ were generated using CRISPR. *Hdac1*$^{+/-}$ was made by Dr Vincent Cunliffe (Harrison et al., 2011). Triple mutants were created by injecting sirt2 CRISPR/Cas9 into the *hdac6*$^{-/-}$ and *hdac10*$^{-/-}$ double mutant background. The G0

was outcrossed with either *hdac6*$^{-/-}$ / *hdac10*$^{-/-}$ double mutants or Wild Type fish. 3-month-old F1 animals were, and from fins, genetic material was obtained. This was followed by PCR for *sirt2*. PCR products were digested with the restriction enzyme HindII. Undigested PCR products were sent for sequencing, following which *hdac6*$^{-/-}$ and *hdac10*$^{-/-}$ mutants were identified. The *hdac1*$^{+/-}$ / *hdac6*$^{-/-}$ / *hdac10*$^{-/-}$ triple mutant strain was created by outcrossing *hdac1*$^{+/-}$ fish with the double mutant *hdac6*$^{-/-}$ / *hdac10*$^{-/-}$. Pairs positive for *hdac*1 mutation were identified by screening offspring. Triple heterozygotes obtained from the first cross were outcrossed with double mutant homozygotes for *hdac6* and *hdac10* to increase the chance of obtaining *hdac1*$^{+/-}$ / *hdac6*$^{-/-}$ / *hdac10*$^{-/-}$ genotype. Wild types, heterozygotes, and homozygotes were identified by using 3% low melting agarose gel (MetaPHOR).

2.1.3 Fin clipping

Adult fish were anaesthetised in 4.2 ml tricaine per 100 ml of water. Tranquillized fish were positioned on a spatula in such a way the way that tail fin was exposed. A small portion of the fin was cut off (less than a third of the entire tail) using scissors and transferred to a 96-well plate. At the start and between every fin clip scissors and tweezers were sterilised in 70% ethanol solution. Fish were kept in separate tanks labelled individually.

2.1.3 Handling embryos

Embryos used in experiments were obtained either by pairing fish or by marbling if the identity of the parents was not necessary. Embryos were collected and transferred to Petri dishes containing E3 media, with ~40 per plate. Dead embryos and other contaminants were removed with a Pasteur pipette and discarded into a container containing bleach. Embryos were subdivided into groups of 40 per dish and cleaned at evening on the same day.

2.1.4 Behavioural test – drop test

Adult fish were dropped from a height of 15 cm, into a tank. Their reaction was recorded for 10 minutes. Fish were tracked for pattern and velocity of movement. Water was changed between every experiment.

2.1.5 PTU and TSA treatment

Hdac1$^{-/-}$ embryos used in experiments were treated with 0.1 mM of PTU in E3 from day 0. The medium was changed daily.

For TSA experiments, fish were treated with 50/100/200 nM of TSA from day 0 and 50 nM of TSA at day 1. The medium was changed daily. Fish were inspected at day 3 and 5.

2.2 Solutions

2.2.1 PCR, SDS-PAGE and Western blot

2.2.1.1 PCR ready mix

For one reaction 10 µl ready mix, 7µl MiliQ water, 1 µl 10 µM primer forward, 1 µl 10 µM primer reverse, 1 µl of template DNA were used

hdac6 Primers: Forward-5'-TTGTTTTTCTAGGATGTTCAAGGA-3',

Reverse-5'-GGTTTTTCAGTTTTATGCACATT-3'

hdac10 Primers: Forward-5'-CTGTCGCCATTTTACTGTGG-3',

Reverse-5'-TTTGCTTGTGCTCACCTGAC-3'

sirt2 Primers: Forward-5'-GCAGTCTTTTCTCGCGAACA-3',

Reverse-5'-GCAGCAAAGTGTTCATGAAGC-3'

2.2.1.2 SDS-Page

Running buffer 4xcc: 1,5 M TRIS, 8 mM Na2EDTA, 0.4 % SDS pH adjusted to 8.8 with HCl.

Stacking buffer 4xcc: 0.5 M TRIS, 8 mM Na2EDTA, 0.4 % SDS pH adjusted to 6.8 with HCl

Migration buffer 1xcc: 2 mM Na2EDTA, 50 mM TRIS, 380 mM glycine, 0.2% SDS

2.2.1.3 Western blot

10x RUNNING BUFFER: 30.3g Tris, 144.0g glycine, 10.0g SDS

10x TRANSFER BUFFER: 30.3g Tris, 144.0g glycine, 10.0g SDS

1x TRANSFER BUFFER with 20% methanol

20x PBS: 160,0.0g NaCl, 4.0 g KCl, 4.8g KH2PO4, 71.6 Na2HPO4 x 12H2O

1x PBST: 1xPBS, 0.05% Tween 20

1x TBST: 50mM Tris, 150 mM NaCl, 0.1% Tween 20,0. pH 7.6

PONCEAU S: 2% Ponceau, 30% TCA

2.2.2 Basic buffers and solutions

1M KOH (Sigma Aldrich) – 56.11g of KOH tablets per 1 litre of MiliQ water

1M NaOH (Sigma Aldrich) – 40.00g of NaOH per 1 litre of MiliQ water

1M Tris-HCl (Sigma Aldrich) - 157.60g of tris base per litre of MiliQ water, pH adjusted with HCl (36% Sigma Aldrich) to reach pH=7.5 or 8.

1M HEPES buffer (Sigma Aldrich) - 238.30g of HEPES per litre of miliQ water, pH was adjusted by adding HCl or KOH to reach 7.5.

PBS (10x concentrated) NaCl – 80g, KCl – 2g, Na2HPO4 – 14.2g, KH2PO4 - 2.4g per litre of miliQ.

2.2.3 Immunostaining and fixation solutions

4% PFA: 2 g of paraformaldehyde + 50 ml of warm PBS. KOH was added drop by drop until PFA dissolved. After dissolving, PFA was aliquoted in 1ml Eppendorf tubes and stored in -20 C degree .

0.1% PBST: 50 ml of PBS + 50 µl of Triton.

1% PBST: 50 ml 0.1% PBST + 500 µl of Triton.

Blocking buffer: 9 ml of 0.1 %PBST, 1ml of goat serum.

30% Sucrose: 15g of sucrose were dissolved in 50 ml of PBS.

Mounting Medium 4 ml*: 2 ml glycerol, 80 mg n-Propyl Gallate, 800 □L 1 M Tris-HCl pH 8.0,0. 1.2 ml MiliQ

*This solution goes yellow within a few days at room temperature but can still be used. Store at 4 C degrees. It is photo/thermostable.

G-buffer: 2mMTris-HCL [pH 8.0], 0.2mMCaCl2, 0.5mM DTT, 0.2mM ATP

F-buffer: G-buffer + 50 mM KCl, 1 mM MgCl2 + 1mM EGTA

2.2.4 Mounting solutions

2% Methylcellulose – 2g of methylcellulose was dissolved in 100ml of warm E3 media. The solution was then frozen at -20 C degree , overnight. The following day, the solution was thawed at room temperature and frozen once again for 1h. This process was repeated until the solution became transparent. At this point, the methylcellulose was transferred into 20ml syringes and frozen for long-term storage.

3% agarose – 1.5g of agarose was dissolved in 50 ml E3 media and boiled in a microwave then stored at room temperature.

1% low temperature melting agarose – 0.5g of low temperature melting agarose was dissolved in 50 ml E3 media and boiled in a microwave then stored in room temperature.

2.2.5 Media

DMEM – DMEM was purchased from Gibco Thermofisher, Penicillin/Streptomycin (P/S) Solution was added to 1% final concentration and foetal bovine serum (FBS) to 10% final concentration. The medium was stored at 4 C degree .

DSMZ 380 media for *Magnetospirillum magneticum* AMB-1 strain growth - KH2PO4 -1.36g, NaNO3-0.24g, L(+)-Tartaric acid- 0.74g, Succinic acid- 0.74g, Na-acetate- 0.10g, Resazurin - 1mg were dissolved in 2000ml of N2 saturated MiliQ water; pH was adjusted to 6.5 with 1M KOH. Media was subdivided into 400 ml bottles and autoclaved. After cooling bottles were transferred to the cabinet (at 30 C° and 99% nitrogen gas Whitley VA 500 workstation cabinet) and 1ml Na-thioglycolate solution was added to each bottle. The media was left for two days. If they were free of contaminations Welfer´s mineral solution(1ml), Welfer´s vitamin solution (4 ml) and

Ferric quinate (0.01M) solution (0,0.16ml) were added. Resazurin solution changes colour from blue to purple due to changes in pH (acidic) and oxygen depletion with time solution turns to dark blue colour. After 2 days if contamination does not appear medium is ready to be used.

Welfer´s vitamin solution - Folic acid -2.00mg, Biotin -2.00mg, Pyridoxine-HCl-10.00mg, Thiamine-HCl -5.00mg, Riboflavin -5.00mg, Nicotinic acid- 5.00mg, D-Ca-pantothenate- 5.00mg, Vitamin B12- 0.10mg, P-Aminobenzoic acid- 5.00mg, Lipoic acid- 5.00mg were dissolved in 1000 ml of N2 saturated MiliQ water and sterilized by microfiltration with 0.22mm filter, then kept in room temperature in darkness.

Welfer´s mineral solution - The nitrilotriacetic was dissolved in 250ml of degassed MiliQ, and pH was adjusted to 6.5 with NaOH then, the minerals were added: Nitrilotriacetic acid- 1.50g, MgSO4.7H2O- 3.00g, MnSO4.7H2O- 0.50g, NaCl- 1.00g, FeSO4. 7H2O- 0.10g, CoSO4. 7 H2O- 0.18g, CaCl2. 2H2O- 0.10g, ZnSO4. 7H2O- 0.18g, CuSO4. 5H2O- 0.01g, KAl(SO4)2.12H2O- 0.02g, H3BO3- 0.01g, Na2MoO4.2H2O- 0.01g, NiCl2.6H2O- 0.03g, Na2SeO3-0.30mg. Final pH was adjusted to 7.0. The mineral solution was sterilised by filtration with 0.22mm filter and kept at room temperature in darkness.

0.01M Ferric quinate - FeCl3.6H2O– 0.45g, Quinic acid- 0.19g were dissolved in 20 ml of N2 saturated miliQ water. *This solution has to be prepared fresh every time due to a high level of salt precipitation.

Na-thioglycolate solution– 0.10g of Na-thioglycolate was dissolved in 5 ml of degassed MiliQ water and filtrated with 0,.22mm filter.

2.2.6 Antibiotics and drugs

50 mM carbenicillin stock solution - 1.05g of carbenicillin disodium salt (Sigma Aldrich) was dissolved in 50 ml of miliQ, sterilised by filtration and aliquoted 0.5 ml in Eppendorf tubes and stored in -20 C degree .

50 mM kanamycin stock solution - 1.45g of kanamycin sulfate (Sigma Aldrich) was dissolved in 50 ml of miliQ, sterilised by filtration and aliquoted 0.5 ml in Eppendorf tubes and stored in -20 C degree .

TSA 50 µM stock solution – 0.75 mg of TSA were dissolved in 50 ml of 10% DMSO. Aliquoted into 1 ml Eppendorf tubes and stored at -20 C degree .

2.2.7 Solution to work with magnetosomes

Magnetosomes lysis buffer – 0.5g N-Lauroylsarcosine sodium salt dissolved 50 ml of 50 mM NaOH.

10 000k Dextran – 3g of 10 000k Dextran was dissolved in 10 ml PBS, aliquoted into Eppendorf tubes and stored at -20 C degree

Lysozyme – 0.5g of lysozyme were dissolved in PBS, aliquoted into Eppendorf tubes and stored at -20 C degree

EZ-Link NHS-Biotin solution– (Thermo Fisher Scientific) – 1mg was dissolved in 0,0.1 ml of HEPES buffer. The solution is stable for around 4h on ice 4 C degree .

BODIPY FL solution – BODIPY FL dye (Thermo Fisher) was diluted x100 in HEPES buffer, divided into 10 µl aliquots and stored at -20 C degree .

Bovine Serum Albumin solution – 10mg of BSA (Thermo Fisher) was dissolved in 1ml of HEPES buffer.

2.3 Molecular techniques

2.3.1 DNA extraction from zebrafish fin

Water from wells containing fin clips was removed with a pipette. 50 µl of 50mM NaOH was added to every well. Next samples were incubated at 98^{o} C for 20 min. 5 µl of 1M Tris-HCl (pH 8) was added to each well to neutralise pH. Following this procedure DNA can be stored at -20 C degree for further usage.

2.3.2 PCR, enzyme digestion and sequencing

PCR was performed in 20 µl of volume. With following settings 94^{o} C:2min, (94^{o} C:30sec 52^{o} C*:30 sec 72 ^{o} C:30 sec)x32 72 ^{o} C:2min. *52 ^{o} C for hdac6 and hdac10 primers and 54 ^{o} C for sirt2. PCR products were kept at -20 ^{o}C.

The product of PCR reaction was checked o 1% agarose gel with using U:Genius3 gel imaging machine.

For genotyping, 5 µl of the *sirt2* product was digested for 2h in 37 ^{o}C with 0.05 µl HincII enzyme and 0.5 µl of NEBuffer 3.1. Wild-type was identified by the appearance of 2 bands on 1% agarose gel heterozygotes by 3 and homozygotes by appearance of 1 band these samples were sent for sequencing.

3 µl of PCR product was sent for sequencing to "Core Genomic Facility" of Sheffield University. Along with 20µl of 10 times diluted primers in MiliQ for the appropriate gene (*sirt2, hdac6 or hdac10*). Results were analysed with Snapgene software.

2.3.3 SDS-PAGE, Western blot

Running gel 10% (for 2 gels) – 4.5 ml Acrylamide/ Bis-acrylamide 40 % (1:29), 4.5ml Running buffer 4x concentrated, 8.9 ml MiliQ, 0.1 ml Ammonium persulfate 10%, 0.01 ml TEMED (µl).

Stacking gel (for 4 gels) -0.9 ml Acrylamide/ Bis-acrylamide 40 % (1:29), 2 ml Stacking buffer 4x concetrated, 5 ml MiliQ, 0.1 ml Ammonium persulfate 10%, 0,0.01 ml TEMED

Gels were prepared following standard BioRad protocol.

2.4 Nanoparticles

2.4.1 Magnetosomes

2.4.1.1 *Magnetospirillum mageticum* AMB-1 bacteria growth

1 ml aliquot of frozen (-80 C degree) *Magnetospirillum mageticum* AMB-1 was thawed on ice. Bacteria were inoculated into 50 ml bottle with DSMZ 380 media and incubated in Whitley VA 500 workstation cabinet (1% oxygen and 99% nitrogen) at 30.1 C° for 3-4 days. Groth of bacteria was checked on a magnetic stirrer. Speed was increased slowly, and a torch was kept against the bottle wall. When bacteria grew free of contamination grey swirl was visible. Then bacteria were transferred in an aseptic way into 400 ml bottle. Bacteria were left to grow for 7-28 days in Whitley VA 500

workstation cabinet (1% oxygen gas and 99% nitrogen) at 30.1 C°. Bacteria growth were checked on the magnetic stirrer in the same way as above. Once density reached the desired level, a bar magnet was attached to the wall in the middle of the bottle (Fig.6) (in this way only viable bacteria are gathered) and left in Whitley VA 500 workstation cabinet overnight. After removing the magnet black/ grey patch of bacteria should be visible. These bacteria were used to inoculate another bottle of 400 ml DSMZ 380 media, and the remaining media were used to harvest magnetosomes.

2.4.1.2 Preparing stock of *Magnetospirillum mageticum* AMB-1

The magnet was attached to the wall of a 400ml bottle with growing bacteria and left overnight, so bacteria gathered next to the magnet. Collected bacteria with 770 µl of DSMZ 380 media were transferred into Eppendorf tubes, containing 330µl sterile glycerol, in an aseptic way. The resulting solution was mixed by shaking and transferred to -80 C° freezer. Following day one tube was inoculated into 50 ml bottle to test the quality of the prep.

2.4.1.3 Collecting magnetosomes and magnetic nanoparticles with a neodymium magnet and washing procedure

Eppendorf tube with magnetic nanoparticles was positioned on ice it the way that one of the poles of the neodymium magnet was touching its wall. After 10 min, the layer of magnetic particles was visible and the wall of the tube. The magnet was slowly removed. The supernatant was removed with a pipette tip on the opposite wall to the particles. Samples were washed with 1 ml of HEPES buffer three times to remove any contaminations.

2.4.1.4 Harvesting magnetosomes

400 ml of bacterial culture were subdivided into 50 ml falcon tubes. Falcon tubes were balanced and centrifuged at 4700 rpm for 45 minutes at 4C° (Heraeus megafuge 40R centrifuge Thermo scientific). The supernatant was discarded and black/grey pellet containing bacteria collected and subdivided into 4 Eppendorf tubes. Tubes were left for 4h on a neodymium magnet rack (0.1-1 T), and media was removed and replaced with 0.5 ml of HEPES buffer. To obtain magnetosomes without membranes bacteria were suspended in Magnetosomes lysis buffer. To obtain magnetosomes containing membranes bacteria were suspended in 10 mM Tris-HCl buffer (pH 7.4).

Samples were sonicated on ice for 1 hour (10 min pulse every 25 min, 50% amplification) using microprobe tip sonicator (Sonics Vibra cell USA). After sonication magnetosomes were collected on the side of Eppendorf tube by using the neodymium magnet and the remaining of the solution was removed, and magnetosomes were washed four times with 25 mM HEPES buffer (pH 7.5). Magnetosomes prepared this way can be stored for two weeks at 4°C. Freezing is damaging to the membranes so only magnetosomes without membrane can be stored at -20°C.

2.4.1.5 Labeling magnetosomes membranes with BODIPY FL.

Harvested magnetosomes were incubated with 0.01% BODIPY FL (final concentration) for 1 hour on ice in darkness and washed four times for 30 min with HEPES buffer to remove unbound BODIPY FL. Fluorescence of labelled magnetosomes was inspected with an Olympus FV1000 confocal microscope, and neodymium magnet was used to check their response to a magnetic field.

2.4.1.6 Labeling magnetosomes with EZ-Link NHS-Biotin and fluorescent streptavidin.

100 µl of magnetosomes solution was mixed by pipetting for 2 min. Magnetosomes were then collected with a magnet and washed with cold (4°C) HEPES buffer and kept on ice 4°C. 2 µl of EZ-Link NHS-Biotin were added, and the solution was incubated for 1 hour on ice in darkness. Every 15 min solution was mixed by pipetting. Subsequently, magnetosomes were collected with the magnet as above. The supernatant was removed, and 0.5 ml of BSA solution was added, to remove unbound EZ-Link NHS-Biotin followed by incubation for 30 min on ice. Magnetosomes were collected with a magnet as above and washed three times for 15 min each wash with cold HEPES buffer. 5µl of fluorophore-conjugated streptavidin (Alexa Fluor 488 or 594) (Thermo Fisher) was added, and the resulting solution was incubated for 1hour on the ice and mixed every 15 min. Magnetosomes were collected with the magnet and washed five times as above. At this step, magnetosomes were inspected with Zeiss Z1 Observer microscope (20x, 40x lens) and their response to magnetic field was evaluated with a neodymium magnet.

2.4.2 ADEMTECH particles

500nm MasterBeads, coated with streptavidin were ordered from ADEMTECH company and stored at 4°C. For experiments, 100x dilution in HEPES buffer was used.

2.4.3 50 nm synthesised nanoparticles

2.4.3.1 Reverse room temperature co-precipitation of magnetite at silicon coating.

A heart Shaped flask was set up with nitrogen entering through the centre port and rubber seals on the two outside ports with a hypodermic needle in one to allow nitrogen to escape. A stirrer bar was placed in the flask, and 8 ml of Milli Q water was added.

0.1489g of $Fe_2(SO_4)_3$ and of 0.139g $FeSO_4$ were weighted and dissolved in miliQ water in the heart-shaped flask. Using a luer lock syringe with fluidics tubing and a syringe pump driver (Harvard apparatus 11PLUS) NaOH was added at rate 50 µl/min. The reaction was left to run for 160 minutes after which the nitrogen supply and the needles were removed, and the solution was poured into a beaker and magnetite was washed with miliQ. The water was removed, and particles were left in a vacuum desiccator overnight to dry.

Magnetite particles were dispersed in 40 ml of ethanol and sonicated at 80% amplitude for 10 min under a nitrogen atmosphere. 6ml of miliQ was added then 3 ml of ammonium hydroxide (30%) followed by 0.4 ml of Tetraethylorthosilicate (TEOS) resulting solution was stirred for 5 hours. The particles were washed and left in the vacuum desiccator overnight to dry.

To further modify their surface 10 mg of particles were suspended in 50 ml of toluene and sonicated at 80% for 10 min to fully disperse them. 2 ml of ammonia and 0.2 ml of APTES were added and stirred for 1h. then washed with toluene and miliQ water.

2mg of modified magnetic nanoparticles were washed three times with PBS. 1 ml of 2.5% glutaraldehyde in PBS was added. Subsequently, particles were sonicated for 1h in a sonic bath. Collected particles were washed three times in PBS 10-100µg/ml of Anti-GFP mouse antibodies or AlexaFluor 594 labelled streptavidin was added to particles in the final volume of 1ml. Particles were incubated overnight on a roller at 4°C.

2.4.5 Functionalisation of magnetic nanoparticles (magnetosomes and ADEMTECH particles)

100µl of streptavidin labelled magnetosomes or 100µl of 100 times diluted ADEMTECH magnetic nanoparticles were incubated with 1 µl biotinylated anti-GFP antibodies (Thermo Fisher), and 5 µl biotinylated ATTO 594 dye or both, for 1 hour on the ice. Samples were divided into two tubes 20 µl and 80 µl. 20 µl was incubated with 100 µg GFP for 1 hour on ice. The efficiency of functionalisation was inspected with fluorescent signals co-localization with Z1 observer microscope (5x, 20x, 40x lenses) and with the neodymium magnet. Functionalised particles were stored at 4°C for no more than two weeks.

2.4.5 Transmission electron microscopy (TEM) of *M. magneticum* AMB-1 and magnetic nanoparticles.

1.5 ml of DSMZ 380 media with magnetotactic bacteria were centrifuged at 4700 rpm for 45 minutes at 4°C (Heraeus megafuge 40R centrifuge Thermo scientific). The supernatant was removed, and bacteria were suspended in 0.5 ml of HEPES buffer. Following this, magnetosomes, magnetic nanoparticles and *M. magneticum* were prepared for the experiment. 10 µl of the solution containing magnetic particles was mounted onto the carbon-coated copper grid and left for 1 min to sediment on the grid. Excess of liquid was removed with filter paper and vacuum pump. Grids were stored in the special container.

2.4.6 Actin pulldown

ADEMTECH particles, magnetosomes without membrane and magnetosomes were incubated for 1h on ice with 3µM actin or Alexa 488 labelled actin for imaging in F-Buffer. Magnetosomes were washed, and the supernatant was used for SDS-PAGE to estimate actin bounding to the magnetosomes' membrane proteins.

Magnetosomes incubated with fluorescently labelled actin were transferred on a coverslip and imaged with Zeiss Z1 Observer microscope (lens 20x, 40x, 100x).

2.4.7 Calculating force exerted on magnetic particles

Functionalised ADEMTECH particles were suspended in HEPES, 25%, 50%, 75% and ~97% glycerol solutions. The magnetic force was applied at 2cm away from the

droplet for 2 minutes from the right direction. Time-lapse was made with Zeiss Z1 Observer 5x lens. Stokes law was used to calculate the force:

$$F=6\pi\eta Rv$$

Where F-frictional force, η-viscosity of the solution, R-radius of the particle, v= velocity (Etoc et al., 2013). η for glycerol solutions were Based on the parameterisation in Cheng (2008) Ind, Eng, Chem, Res, 47 3285-3288,

2.5 Injections

2.5.1 Preparing needles

The capillary glass was set (World Precision Instruments, Inc.#TW100-4) to a needle puller. Glass capillary was heated and pulled to make a glass needle. Needles were stored on a petri dish with a small roll of blue tag on it, preventing them from moving and being damaged. Tip of the needle was broken by forceps under a microscope so that there was a small opening at the narrow end of the needle tip.

2.5.2 Preparation of agarose plates for injection

3g of agarose (Invitrogen, 15510-207) was mixed in 300 ml of E3 media. Solution heated up in a microwave oven for 2 min. Hot agarose was poured into 10 cm Petri dishes to fill them up halfway, and a plastic imprinting tool was placed on top of it. Once the agarose cooled down to room temperature, the plastic mould was removed, and grooves, where embryos can be placed for injection, were imprinted. This plate can be used up to a month if kept at 4 C degree

2.5.3 Preparing nanoparticles solutions for injecting

Particles were held on ice (4 C degree), before loading the needle solution was roughly mixed by pipetting for 2 min to disperse clustered particles. Then particles were loaded to an already broken needle and quickly injected into embryos. All particles due to their magnetic properties start to clump in Eppendorf tube and in the needle causing clogging.

2.5.3.1 Non coated particles

To non-coated particles 30% 10 000 dextran was added to reach concentration of 10% 10 000 (Da) dextran. It increased the viscosity of the solution and slowed down clumping.

2.5.3.2 Cell membrane labelling

To mark membranes – BODIPY FL solution was dissolved in magnetic nanoparticles solutions in ratio 1:100 just before loading the solution into the needle.

2.5.4 Injection set up

The microinjector was switched on, and the needle was loaded with the magnetosomes, ADEMTECH magnetic particles. The needle was placed in the needle holder. Injections were performed on embryos within 30 min after fertilisation (1 cell stage). Each embryo was injected with 0.2 µl of the solution. What in ADEMTECH (10 mg/ml) particles case corresponds after 100x dilution to approximately 0.02 µg of particles and 0.014 µg of iron oxide.

2.6 Cell cultures

2.6.1 Cell growth and incubation with magnetic particles

MDCK1 and Hela cells were grown in 10ml of DMEM media with 1% P/S and 10% foetal bovine serum (FBS) till they reach 90% confluency. Then cells were detached from the flask using 1-3 ml of trypsin/EDTA and cultivated in 1 ml of DMEM medium on glass bottom µ-Dish (Ibidi) covered with poly-L-Lysine. Once culture reached 50% confluency, the cells were washed with PBS, and the new 1 ml of DMEM containing 10 µl of functionalised nanoparticles was added - cells were grown overnight. Cells were cultivated in 37^{o}C.

2.6.2 Covering glass bottom µ-Dish (Ibidi) with poly-L-Lysine

The glass bottom µ-Dish was treated with 0.1% to 0.001% Poly-L-Lysine and placed at 4^{o}C, followed by incubation at 37^{o}C for 1 hour, rinsed with ddH2O then allowed the glass coverslips to dry completely.

2.7 Samples preparation and imaging

2.7.1 Immunochemistry

Zebrafish embryos (1,2,3 or 5 dpf) were treated with 4.2 ml tricaine per 100 ml of E3 media for 20 min. Then they were transferred to 1ml of 4% PFA and fixed overnight in a cold room (4 C degree), overnight. Samples were washed three times PBST for 2 min and twice for 30 min.

2.7.1.1 Whole mount staining

Samples were incubated for 3h in blocking buffer at the room temperature. Followed by three washes for 2 min and twice for 30 min in PBST. Next, samples were incubated overnight with blocking buffer containing anti-acetylated tubulin antibodies (rabbit)at 1:500 dilutions (correct for the rest), anti-gamma tubulin antibodies (mouse) 1:200 or anti glutaminated tubulin (GT335) (mouse) 1:200 on the orbital shaker and washed 3 times for 2 min and twice for 30 min with PBST. Samples were incubated with secondary anti-rabbit Alexa Fluor 488 and anti-mouse Alexa Fluor 564 (Thermo) antibodies (1:500) for 4h in darkness, at the room temperature and washed three times for 2 min and twice for 30 min with PBST. Samples were then incubated with 0.1µg/ml DAPI for 20 min and washed once with PBST. The embryos were mounted in agarose.

2.7.1.2 Cryosections preparation and staining

Cryosections were performed on embryos aged 1 to 3 dpf. After fixation and permeabilisation embryos were washed with PBST. Samples were placed in 1 ml of 30% sucrose solution and incubated overnight (till embryos sunk) on an orbital shaker. Subsequently, half of the liquid was removed and replaced with cryosectioning-embedding medium (OCT) media and left for 4hour incubation. Pasteur pipette was cut to obtain ¼ inch cylindrical rings which were put on slide glass an filled up with OCT medium. Approximately ten embryos were transferred into one ring with tweezers and positioned in the way that head was touching slide glass. The slide glass with the embryos was transferred to the box with dry ice to freeze the OCT medium. Once frozen razor was used to remove the plastic ring and cylinder was mounted on cryostat chuck by using more OCT medium. The chuck was installed in cryostat chamber. Sections were taken at 15-20 µm thickness depending on the tissue examined, and collected on superfrost slides. The slides were dried at RT for at least 2 hours before

storage at 4 C degree . The samples were rehydrated for 30 min with 0.25 ml per slide of PBST. PBST was removed and replaced with the same volume of blocking buffer and incubated for 1 hour. The sections were rinsed with PBST and incubated overnight in 4 C degree with primary antibodies (anti-acetylated tubulin rabbit 1:500 and anti-gamma tubulin mouse 1:200) diluted in blocking solution. Samples were rinsed twice and washed for 30 min with PBST then secondary antibodies were added and incubated in darkness in room temperature for 4 hours. Samples were rinsed twice and washed for 30 min with PBST and counterstained with DAPI and washed. 20 µl of mounting medium was placed on the sample and covering glass was sealed with nail polish.

2.7.1.3 Cell cultures staining

DMEM medium was removed, and cells were washed with PBS twice then 1-2 ml of 4% PFA was added, and cells were fixed for 30 min. Cells were washed thrice with PBS (10 min each). PBS was removed then, 1-2 ml of 0.5% Triton-X in PBS was added, and cells were incubated for 5-10 min. Subsequently, cells were washed twice with PBS (10 min each). PBS was replaced with 1% bovine serum albumin (BSA) and incubated for 30 min followed by once with PBS.

2.7.1.3.1 Microtubule cytoskeleton staining

Cells were incubated with anti-acetylated tubulin mouse primary antibodies; dilution 1:500 in BSA/PBS overnight in 4^{o}C then washed three times with PBS (10 min each). Secondary antibodies anti-mouse Alexa Fluor488 were diluted in 1% BSA/PBS (1:1000) and incubated for 2 hours in the dark then washed twice with PBS (10 min each time). Subsequently, 1-2 ml of PBS with 2µl of DAPI were added, and cells were incubated for 5 min and were washed twice with PBS. 1 ml of mounting media was added, and cells were imaged with Z1 observer microscope (40x, 100x lenses).

2.7.1.3.2 Phalloidin staining

Phalloidin staining was performed following to Thermo Fisher protocol.

2.7.2 Preparing embryos injected with magnetic particles for imaging.

7 to 8 hours old embryos were dechorionated with tweezers and left for 30 min to identify damaged embryos. In this time sharp edges of glass bottom µ-Dish (Ibidi) were

covered with 3% agarose. Next embryos were transferred with Pasteur pipette on the centre of glass bottom μ-Dish and covered with 1% low melting agarose. Subsequently, embryos were rotated to face the glass bottom of a dish with their forming body axis. Dishes were left for 15 min to let agarose to , and 1.5 ml of E3 were added to prevent the sample from drying.

2.7.3 TEM samples of nanoparticles uptake by HeLa cells

HeLa cells were grown in 10ml of DMEM media with 1% P/S and 10% foetal bovine serum (FBS) till they reach 60% confluency. Subsequently, 100 μl of magnetosomes were added, and cells were incubated until they reach 90-100% confluency. Cells were detached from the flask using 1-3 ml of trypsin/EDTA. Cells were transferred to a 50 ml falcon tube and centrifuged at 4 000 rpm 4 C degree for 5 min. The supernatant was removed, and cells were washed with PBS 3 times every wash followed by centrifugation. Subsequently, cells were fixed in 2.5% glutaraldehyde/PBS overnight in 4 C degree . Rest of sample preparation was performed by Christopher J. Hill and Svetomir B. Tzokov - Electron Microscopy Service Department of Biomedical Science, C29 Firth Court, Sheffield University, Sheffield, S10 2TN, England

2.8 Imaging

2.8.1 Particles

Images of nanoparticles and functionalised nanoparticles were taken with a Zeiss observer microscope (5x,20x 40x 100x). For the evaluation of the magnetic properties of particles 10μl of the solution was placed on the coverslip. Particles sediment on the glass were used for functionalisation efficiency. The floating fraction was used in experiments to calculate magnetic force applied images were taken for 2 min with 0.5 sec intervals.

2.8.2 Cell cultures

Cells incubated with magnetic particles were imagined with Z1 observer microscope (5x,40x 100x) magnetic force was applied from 0.5 to 2cm distance for 15 min images were taken with 0.5 sec intervals.

2.8.3 TEM

The TEM images were taken in the Department of Biomedical Science with FEI Tecnai Biotwin operated at 120kv with an Orius 1000 camera and images were captured by Gatan Digital Micrograph

2.8.4 Magnetic nanoparticles injected into the zebrafish embryo

The movement of particles was recorded with Zeiss Z1 Observer (x5, x20,0. x40) and QuantEM:512SC camera. Once embryos formed the first somite, with correctly orientated body axis and containing particles were identified, time lapse was set up. Images were taken for 30 min with 30 sec intervals, without applying the force as a control, then force was applied from directions perpendicular to the body axis 30 min each. In the last set movement of cells without applying force was obtained.

2.8.5 Confocal Microscopy

Confocal images were taken with an Olympus FV1000 confocal microscope (10x,20x,60x oil lenses). Immunostained whole embryos images were collected using the Olympus FV1000 confocal microscope with either 40x or 60x water dipping lens.

2.8.6 Imaging of Zebrafish zebrafish larvae

Zebrafish larvae (1dpf-5dpf) were anaesthetised with 2.4% tricaine. Once larvae stop moving, they were aligned in 2% methylcellulose and imaged with Zeiss AXIO Zoom.V16. After those larvae were put back to E3 media.

2.9 Data analysis

2.9.1 Fiji (ImageJ)

2.9.1.1 Angle of cell migration

The MIC of time lapse of migrating cells was created. Tracks of migrating cells (centrosomes, nuclei) and particles were measured in Fiji. The line representing body axis was drawn as a reference point followed by lines following tracks were drawn. The angle of migration was calculated by subtracting the value of body axis angle from the values of angle for each of the track. In the case when the body axis was on the bottom

of the images, 180 degrees was subtracted, and the modulus of the result was calculated.

The change in angle was calculated by subtracting the average value of cells migration at t0 from values for t0,0. t1,t2 and t3 subsequently modulus of results was calculated.

2.9.1.2 Cilia length, particles diameter, heart and yolk size.

A line was drawn across lengthwise cilium and across the diameter of particles, hear or yolk, then measured with ImageJ.

2.9.1.3 Binding of magnetosomes to actin.

The line was drawn across red signal of magnetosome and pasted on green actin channel. Fluorescence signal was measured with Fiji and graphs were created in Excel.

2.9.2 Matlab R2016a - Angle histogram plot

Angle histogram plots showing angles of migration were plotted in Matlab R2016a.

2.9.3 GraphPad Prism version 7.00 – statistics and graphs

Graphs were plotted, and statistical significance (t.test) were performed using GraphPad Prism version 7.00 for Windows, GraphPad Software, La Jolla California USA, www.graphpad.com".

2.9.4 Blender 2.78 - 3D models

3D models of aims of the project were made in Blender 2.78.

2.9.5 FEMM 4.0 – Modeling electromagnet.

FEMM 4.0 software was used to model the electromagnetic flux of electromagnetic tweezers and optimising amount of coils and current.

Chapter 3. Functionalisation of magnetic particles.

3.1 Introduction

Rapid development in the last three decades within the field of nanotechnology has provided new approaches to deal with scientific problems. Nanotechnology focuses on material properties at the nanoscale level, such as optical, electrical and magnetic, as well as its size, surface area, shape, and surface chemistry (Alivisatos, 2008; Burda et al., 2005). Nanoparticles have emerged as promising tools in a range of scientific applications ranging from protein purification to innovative cancer treatments, drug delivery and induction of signalling cascades in neurons or differentiating cells. (Desprat et al., 2008; Henstock et al., 2014; Markides et al., 2012; Master et al., 2015; Wheeler et al., 2016).

In this work, both commercially available, as well as biogenic magnetic particles, were used. The commercial particles, ADEMETECH MasterBeads Streptavidin (ADEMTECH particles), were monodispersed, superparamagnetic particles of iron oxide coated with streptavidin (~500nm). The biogenic particles were magnetosomes, which are organelle-like structures produced by magnetotactic bacteria (Blakemore, 1975; Komeili et al., 2006; Staniland et al., 2010). Magnetosomes are composed of a magnetic core (either greigite (Fe_3S_4) or magnetite (Fe_3O_4) surrounded by a phospholipid

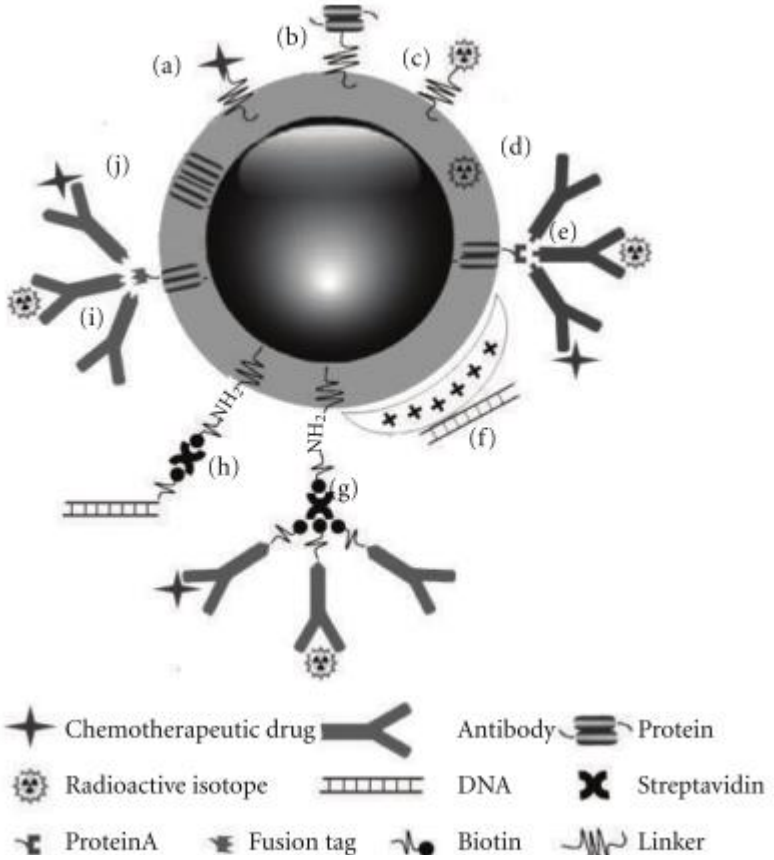

Fig. 3 Schematic diagram of multifunctional BMs. Chemotherapeutic drug (a), protein drug (b), and radioactive isotope (c) could be loaded onto BMs by cross linkers or chelators. Radioactive isotopes could be incorporated in the membrane of BMs during the formation of BMs (d). Antibodies modified with or without radioactive isotopes or chemotherapeutic drugs could be loaded onto BMs by immunoconjugating the genetic engineering expressed Protein A (e) or fusion protein tag (i) or by streptavidin-mediated conjugation with the biotin-streptavidin-biotin (g). DNA drugs could be absorbed onto BMs modified with cationic silanes (f) or linked to BMs with biotin-streptavidin-biotin (h). Specific protein drug could be expressed in BMs membrane by genetic fusion to BMs membrane protein (j) (Sun et al., 2011).

bilayer containing glycolipids, sulpholipids, phospholipids (in weight ratio of 1:4:6), free fatty acids such as palmitoleic acid and oleic acid, and unique membrane proteins (Gorby, et al., 1988; Komeili et al.,2006; Uebe et al., 2016). This membrane can be modified to functionalised the core particle, including attachment of chemotherapeutic drugs, proteins, isotopes, specific DNA sequences etc. (Fig.5) (Sun et al., 2011). The highly uniform size and shape of magnetosome particles is an additional advantage (Lee et al., 2011) for biomedical applications.

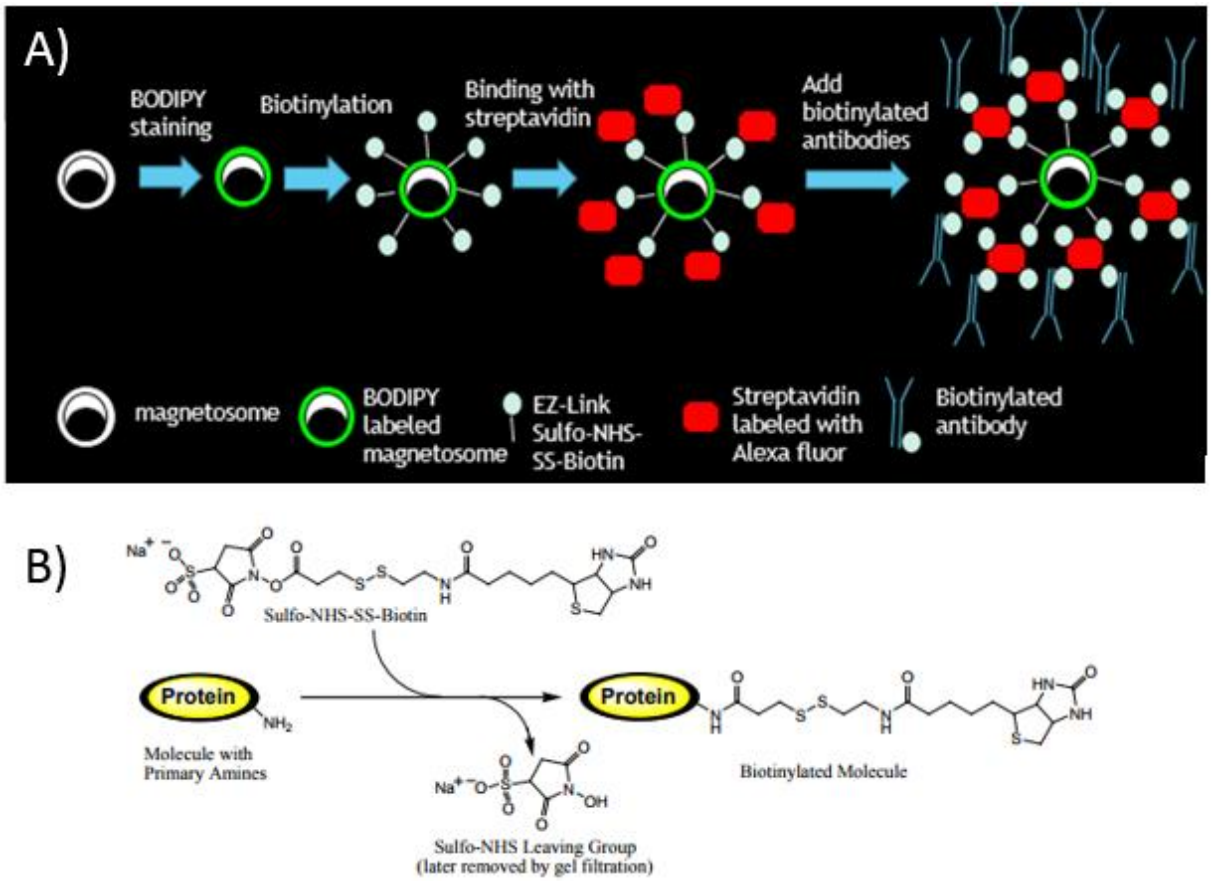

Fig. 4 Schematic representation of magnetosomes functionalisation. Panel A) shows the general approach to functionalize magnetosomes. Panel B) shows the reaction of Sulfo-NHS-SS-Biotin with a primary amine (from product website).

The surface of purified magnetosomes from *Magnetospirillum magneticum* AMB-1 was biotinylated with EZ-Link™ Sulfo-NHS-SS-Biotin, which creates a covalent bond between primary amines (-NH2), such as those found on lysine side-chains, or the amino-termini of polypeptides, and the reactive group of biotin Sulfo-NHS-SS-Biotin (Fig.6b). Then I used fluorescently labelled streptavidin (AlexaFluor488 or AlexaFluor594), which has four biotin binding sites. Alternatively, I used hydrophobic fluorescent dye BODIPY FL that enabled staining membranes and visualise particles using fluorescence microscopy. The final step in functionalisation was to add biotinylated anti-GFP antibodies or/and biotinylated ATTO560 fluorescent dye (Fig.6)

to complex with the streptavidin on the surface of the magnetosomes. ADEMTECH beads were purchased pre-conjugated with streptavidin, and for this reason, they were treated only with ATTO560 and/or biotinylated Anti-GFP antibodies. Despite many advantages, working with magnetic particles creates some problems such as clumping, due to their magnetic nature. Magnetotactic bacteria divide every 9 hours and live at low oxygen concentration, which makes them prone to various contaminations. These problems are addressed in this part of this work.

3.2 Experimental work

3.2.1 Purification of particles

The first step was to obtain a contamination-free culture of *Magnetospirillum magneticum* AMB-1. Cultivation began from a 1 ml frozen glycerol stock of strain AMB-1 in gas Whitley VA 500 workstation cabinet, which provided 1% oxygen gas and 99% nitrogen ratio - optimal for *Magnetospirillum magneticum* AMB-1 growth. Contaminations are one of the biggest challenges in the cultivation of *Magnetospirillum magneticum* AMB-1, due to its slow division rate. These cells divide once per 12 hours (Staniland et al., 2010), making them susceptible to being overgrown by other kinds of bacteria and fungi. The growth of magnetotactic bacteria can be noticed as medium changes its colour from blue to steel grey.

Contaminated bottles usually have a slightly yellowish colour. The response of magnetotactic bacteria growing in bottles with media was checked on a magnetic stirrer. Subsequently, bacteria were collected with a neodymium magnet attached to the bottle overnight (Fig.7).

To release magnetosomes from bacteria, cells were subjected to sonication. It was essential to maintain the magnetosome membrane surrounding the particles intact to facilitate later functionalisation, as well as to avoid excessive clumping. Therefore, a range of different lysis methods was tested to find a suitable condition. Lysis buffer containing 1% sodium N-Lauroylsarcosine, a mild detergent, led to rapid clumping of particles, as visualised by TEM (Fig.8a).

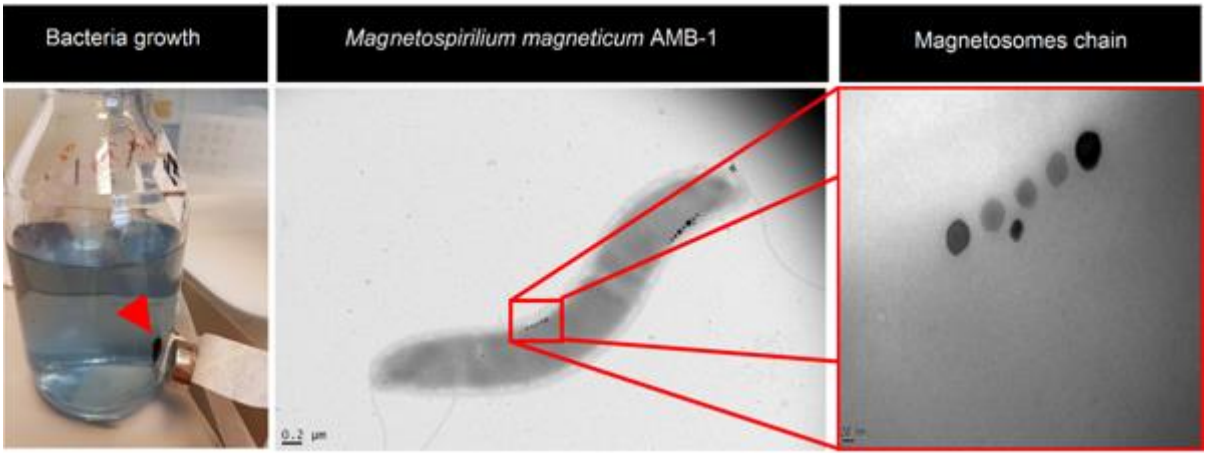

Fig. 5 Cultivation of *Magnetospirillium magneticum* AMB-1. A) Bacteria gathered on the wall of the bottle by the neodymium magnet (indicated with the red arrowhead). B) The TEM image of *Magnetospirillum magneticum* bacterium containing magnetosome chains. C) Magnetosome chain inside the bacterium. Scale bars 200 and 20 nm.

Only when the viscosity of the solution was increased with dextran did the particle dispersal improve slightly but the difference was not significant.

Closer inspection of TEM images revealed that the 1% sodium N-Lauroylsarcosine – a detergent, had removed the membrane from magnetosomes, causing them to clump over time. An alternative buffer Tris-HCl (10mM, pH=7.4) was tested.

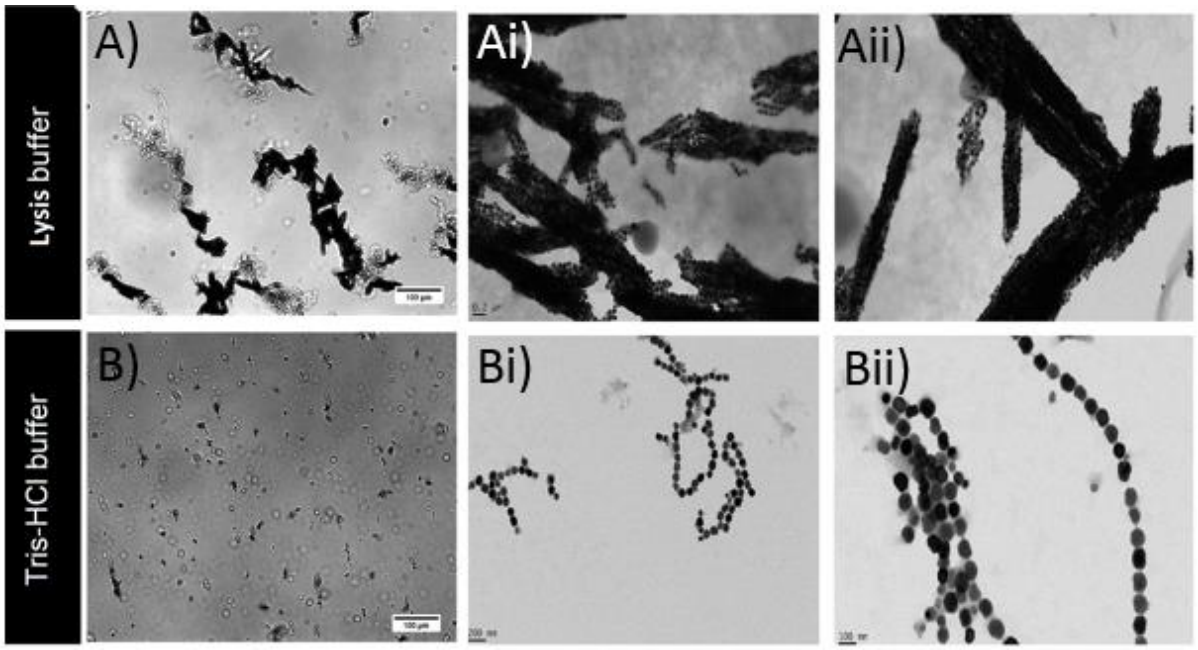

Fig. 6 Isolation of magnetosomes using the lysis buffer and Tris-HCl buffer. Panel A) shows magnetosomes isolated in lysis buffer containing 1% sodium N-Lauroylsarcosine. Panel B) shows magnetosomes isolated in Tris-HCl buffer – images A) and B) were taken with a Zeiss Observer Z1 microscope. Panels Ai), Aii), Bi) and Bii) show images taken with Transmission Electron Microscope. Scale bars- A) and B) 100µm, Ai) and Bi) 200nm, Aii) and Bii) 100nm.

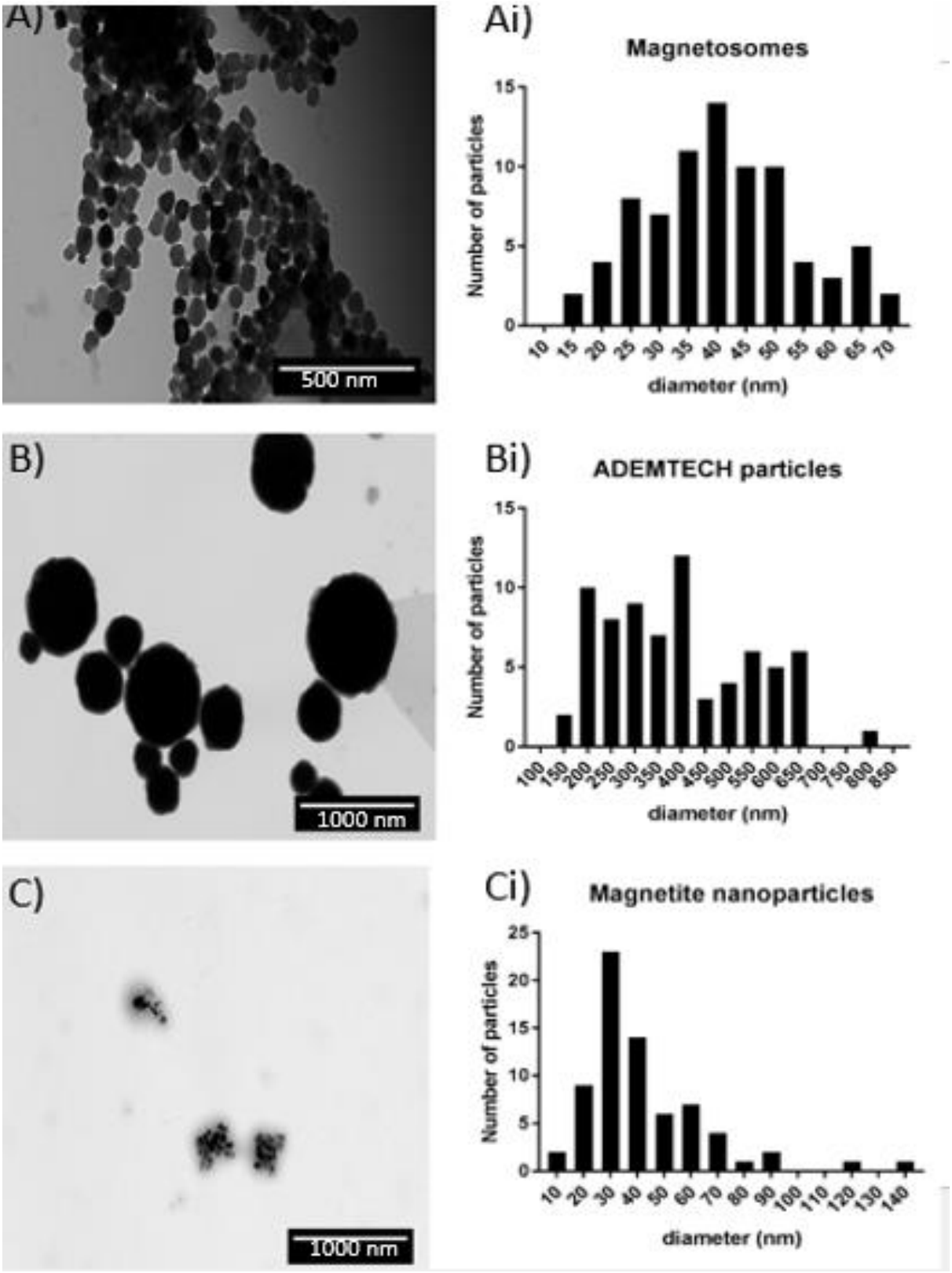

Fig. 7 Size distribution of magnetic particles. Panels A), B) and C) show a TEM image of A) magnetomes B) ADEMTECH particles and C) synthetized magetite nanoparticles. Panels Ai), Bi) and Ci) show the size distribution of Ai) magnetosomes, Bi) ADEMTECH particles and Ci) synthetized magetite nanoparticles. Scale bars A) 500nm, B) and C) 1000nm.

TEM images showed that using Tris-HCl alone resulted in discrete chains of magnetosomes that were surrounded by a membrane (Fig.8).

Using TEM the size of magnetosomes, ADEMTECH particles and synthesised magnetite was calculated (Fig.9). That revealed the diameter of magnetite inside magnetosomes is 41.1 ± 13 nm, inside ADEMTECH particles 390 ± 157 and inside synthesised magnetite particles is 42.6 ± 23 nm.

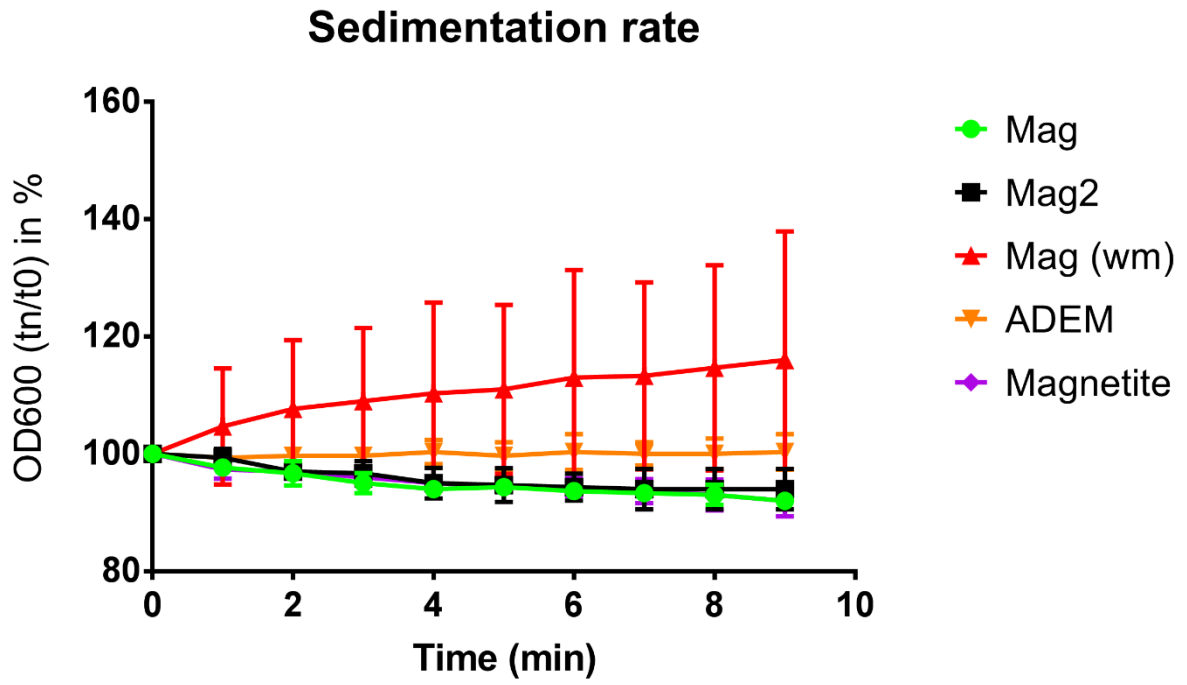

Fig. 8 Impact of the membrane removal on magnetic particles clumping. The graph shows the percentage value of OD600 calculated by dividing the value of each time point by OD600 of t0. Mean with 95% CI of n=3.

It is suggested that the membrane prevents magnetosomes from collapsing and agglomerating through maintaining their chain arrangement (Huízar-Félix et al., 2016). To confirm this the sedimentation of magnetosomes with the membrane (Mag+) and without membrane (Mag-), ADEMTECH particles (ADEM), and synthetic uncoated magnetite nanoparticles of comparable size to the magnetosomes were investigated using a simple turbidity assay. The premise for this experiment was that fast clumping particles create bigger conglomerates which sunk faster-covering bottom of the well and as a result increasing OD600 value. To do that, I measured the change in OD600 value over 10 minutes (tn/t0) for magnetosomes (Mag), functionalised magnetosomes

(Mag2), magnetosomes without membranes (Mag wm), ADEMTECH particles (ADEM) and magnetite (magnetite). This experiment showed that magnetosomes extracted with detergent sediment at the same rate as synthetic magnetite nanoparticles, indicating that the magnetosomes were without a membrane. The Tris-HCl extracted magnetosomes did not sediment over the course of the experiment and behaved in a similar way to the ADEMTECH coated nanoparticles, indicating that these particles had their membrane intact. (Fig.10).

3.2.2 Labeling of the magnetosomes with BODIPY FL dye

The ultimate goal of the project was to use magnetic particles *in vivo*, requiring methods to visualise them within cells and embryos and to attach them to intracellular targets.

At first, magnetosomes were labelled with BODIPY FL dye, which, due to its hydrophobic properties, intercalates in magnetosome membranes. Using fluorescence microscopy to detect labelled magnetosomes, green clusters are visible. When an external magnetic field is applied, and moved, green clusters follow the direction of the field source (Fig.11). This observation indicates that the Tris-HCl extracted magnetosomes still contained membranes after the process of purification and staining.

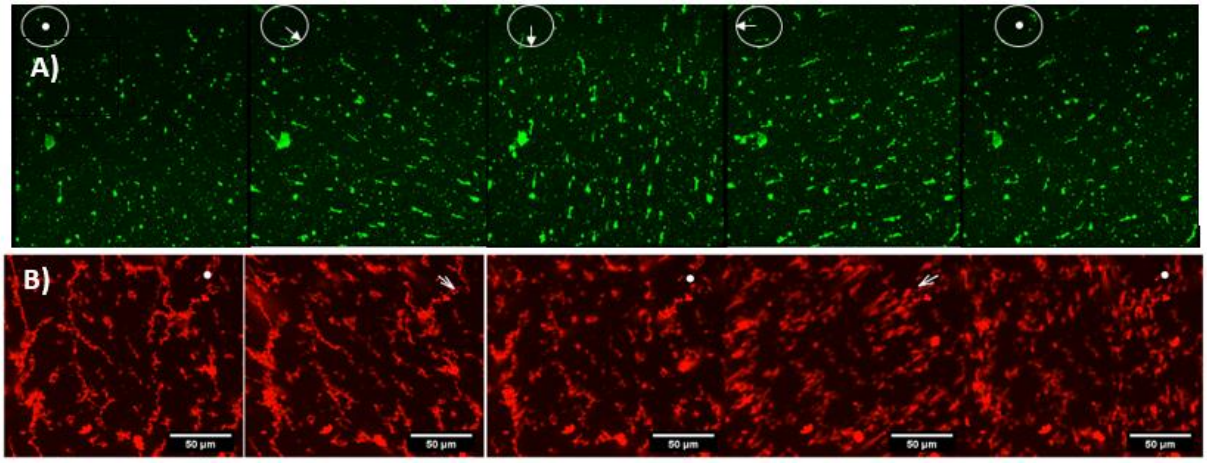

Fig. 9 Labelled magnetosomes under magnetic force. Panel A) BODIPY FL labelled magnetosomes showed in green. Panel B) shows biotinylated magnetosomes labelled with streptavidin conjugated with Alexafluor594 White arrows indicates directions from which the magnetic force was applied, the dot indicates lack of the force.

3.4 Functionalisation of magnetosomes with biotin.

To provide a flexible conjugation method to link a variety of molecules to the magnetosome surface EZ-Link™ Sulfo-NHS-SS-Biotin was used. After incubation of the membrane intact magnetosomes with the labelling reagent, excess biotin was removed via magnetic washing. Streptavidin has four biotin binding sites (Freitag et al., 1997), and for this reason further washes with 1% bovine albumin and excess streptavidin were performed to prevent magnetosomes from binding one to another through a crosslinking interaction between biotin and streptavidin. Next, Streptavidin Alexafluor594 functionalised particles were mixed with biotinylated anti-GFP antibodies, and subsequently with biotin labelled GFP. Co-localisation of green and red signals from the AlexaFluor dye and the GFP, respectively, suggests that my approach works *in vitro* and functionalised magnetosomes can recognise their biotinylated targets (Fig.12). To check, if the fluorescent signals were in fact labelled magnetosomes, they were exposed to an external magnetic force (Fig.11b).

Commercially available ADEMTECH beads were purchased with streptavidin already attached to their surface. For this reason, ATTO560 biotinylated dye and biotinylated anti-GFP antibodies were linked to the particles surface in order to make them recognise their targets (Fig.13). Finally, magnetic force was used to confirm the attachment of particles to GFP by coordinated displacement.

Prior to *in vivo* studies, it is necessary to calculate the amount of force applied to the particles using a bar magnet. To do so, Stokes law was used, which describes the force of viscosity acting on a small sphere moving through a viscous fluid. It is given by the equation:

$$F_d = 6\pi\eta R v$$

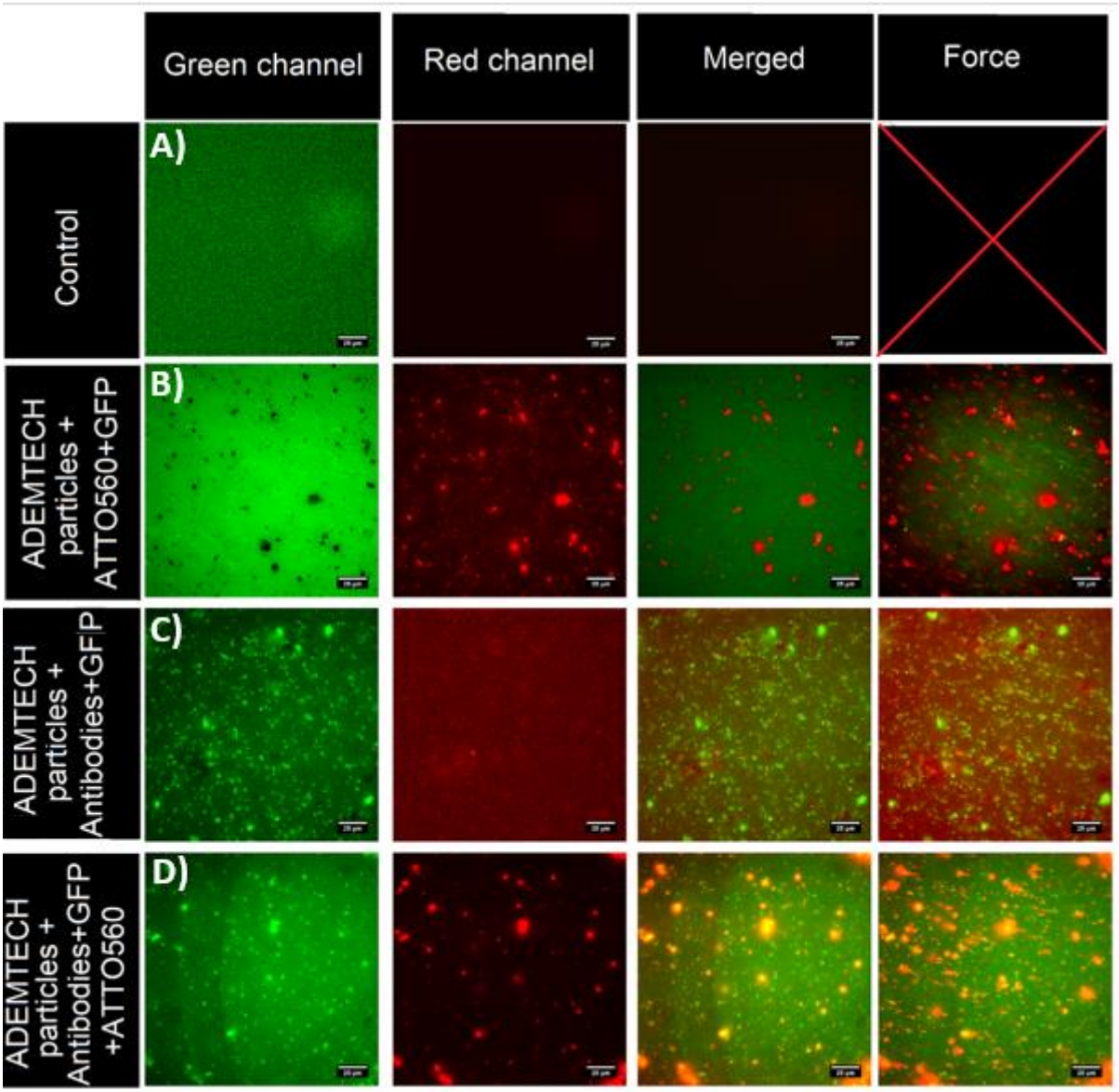

Fig. 10 Functionalisation of magnetosomes. Panel A) shows non-biotinylated magnetosomes control which was incubated with streptavidin conjugated to AlexaFluor594. Panel B) shows biotinylated magnetosomes which were incubated with streptavidin conjugated with AlexaFluor594. Panel C) shows biotinylated magnetosomes which were incubated with streptavidin conjugated with AlexaFluor594 and GFP. Panel D) shows biotinylated magnetosomes which were incubated with streptavidin conjugated with AlexaFluor594 then incubated with biotinylated anti-GFP antibodies and GFP. Scale bar= 50 µm. n=3.

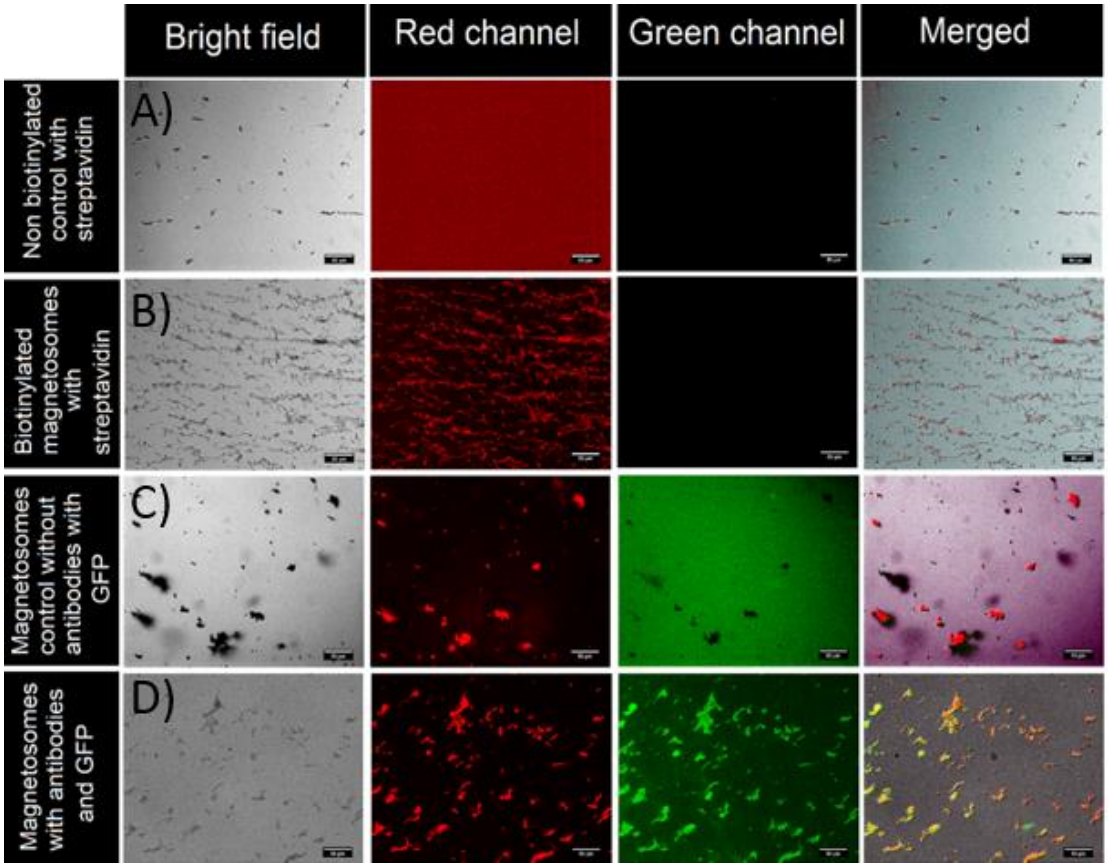

Fig. 11 Functionalisation of ADEMTECH particles. Panel A) shows non-functionalised ADEMTECH particles. Panel B) ADEMTECH particles incubated with biotinylated ATTO560 and GFP. Panel C) ADEMTECH particles incubated with anti-GFP antibodies and GFP. Panel D) incubated with biotinylated ATTO560 and anti-GFP antibodies in ratio 1:100 and GFP. Force was applied for 30 sec from the right. The MIP was created to show tracks.

Where Fd is the frictional force known as Stokes' drag acting on the interface between the particle and the fluid, η is the dynamic viscosity, R is the radius of the spherical object and v is the flow velocity relative to the object. To perform these tests, ADEMTECH particles were suspended in 0%, 25% and 75% glycerol (comparable to the viscosity of the cytoplasm) (Etoc et al., 2013; Shah et al., 2017; Steketee et al., 2011). These particles were chosen over magnetosomes because they do not form chains. Because their shape is mostly spherical, their behaviours can be approximated using this equation. I imaged their motility under magnetic force to determine their velocity, and their radius was determined using ImageJ (Fig.14). My calculations show that 4pN of force was being applied from a distance of 1.6 cm. The distance that I apply magnetic field from is determined by the radius of the μdishes used for later *in vivo* studies.

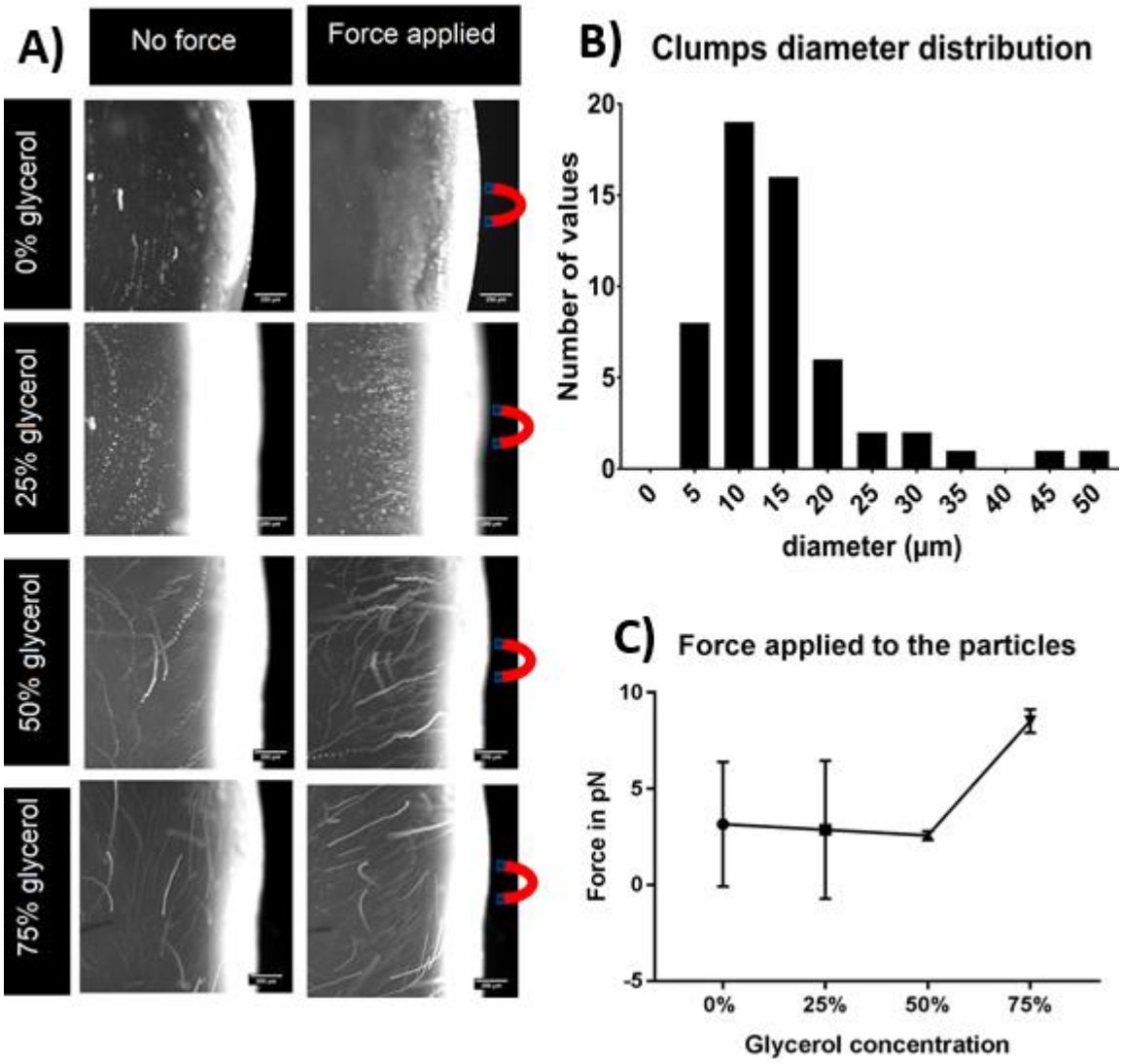

Fig. 12 Calculating force applied to the particles. Panel A) shows the MIP of a reaction of particles to the magnetic force for 2 min. The direction of the force is indicated by red magnet icons. Panel B) shows clumps the diameter of magnetic particles used in calculations. Panel C) shows average force calculated for four different glycerol concentrations 0% and 25% n=3 50% and 75% n=2. Scale bar – 250 µm.

3.3 Discussion

The data shows that magnetosome chains from *Magnetospirillum magneticum* AMB-1 strain could be successfully extracted. Furthermore, the membranes can either be removed or maintained through the addition of detergent. Solving this issue was crucial, due to the problems caused by magnetosomes clumps during the microinjection of particles into zebrafish embryos, which will be discussed later in this work. Previous studies have reported that chains of magnetosomes, unlike clumps, can be internalised by MDA-MB-231 and HeLa cells (Alphandéry et al., 2012). Using

TEM imaging the presence of single chains of magnetosomes is clearly visible. This indicates that magnetosomes, prepared in the way described in this chapter, may be suitable for cell uptake and *in vivo* experiments.

Magnetosomes could be successfully labelled using either BODIPY FL, ATTO560 dyes, or fluorescently labelled streptavidin. However, experiments performed later have shown that staining of magnetosomes with BODIPY FL leads to leaking of the dye and staining of cell membranes. Functionalisation of particles using biotinylated anti-GFP antibodies has proven that particles decorated with the antibody are able to recognise their target in solution. Magnetic nanoparticles are reported to be useful in manipulating extracellular targets. However, the question remains whether this is the case inside a living cell (Vagida et al., 2016). Lastly, particles were suspended in high viscosity solutions to calculate the force that is exerted on particles during the experiments.

For this reason, Stoke's Law was used which describes the behaviour of small spherical objects in solutions. Calculations for ADEMTECH particles have shown that the force experienced by the particles is approximately 4 pN. Variations in measurements can be the result of either movement of fluid or distance of the magnetic force source from the sample. It has been reported that a force of ~1 pN is enough to dislocate magnetic nanoparticles within cells, yet it usually takes several minutes and force of 4 pN to induce the response in mechanically gated channels in mesenchymal cells (Etoc et al., 2015; Henstock et al., 2014).

These experiments opened the door for further investigation to understand the behaviour of magnetic particles in cell cultures.

Chapter 4. Delivery of nanoparticles to HeLa cells and their interaction with actin.

4.1 Introduction

A growing number of successful usage of magnetic nanoparticles *in vitro* has revealed further possible applications to study biological processes employing them (Alphandéry et al., 2017; Cho et al., 2012; Yoshino et al., 2008). However, data obtained from these experiments vary and sometimes contradict each other. For example, it has been shown by one group that nanoparticles interact with microtubule cytoskeleton, disrupting it and as a result, increasing tension within a cell and impairing its ability to migrate (Tay et al., 2014). Meanwhile, another study has shown that applying magnetic force on magnetic nanoparticles taken up by cells accelerates the velocity of their migration towards the source of the magnetic force (Shen et al.,2014). It has been shown that magnetic nanoparticles introduced to cells *in vitro* are stored in lysosomes, and a connection between lysosome and the actin cytoskeleton immobilises them (Master et al., 2015). Contrastingly, there is also evidence suggesting that magnetic nanoparticles inside lysosomes can relocate them under the influence of magnetic force (Shen et al.,2014). It has been suggested that magnetic particles ~500nm in diameter can be immobilised within a cell due to entanglement with the cytoskeleton network. This makes particles ~50 nm in diameter the most suitable for relocating them inside cells (Etoc et al., 2015).

The initial question was whether either type of nanoparticles used in this work, (magnetosomes (~50nm) or ADEMTECH particles (~500nm)) could be internalised by the cells. To answer this question, HeLa cells were used. Next, we asked if it was possible to relocate the magnetic particles within the HeLa cells. Finally, will the particles in question interact with the actin cytoskeleton, as indicated by potential interactions between nanoparticles and the microtubule cytoskeleton, in previous studies (Tay et al., 2014). Furthermore, magnetosomes are aligned into chains by the interaction between actin-like protein MamK and magnetosome membrane protein MamJ (Komeili et al., 2006; Rioux et al., 2010). MamK shares 42% positive hits and 22% identical scores with actin-related protein 2-B isoform X1 from *Danio rerio*, which supports the idea of possible direct interaction between the actin and magnetosomes.

4.2 Results

4.2.1 Uptake of particles by HeLa cells

My initial aim was to prove that functionalised magnetic nanoparticles can be internalised by living cells. To investigate this, I incubated HeLa cells overnight with magnetosomes labelled with streptavidin conjugated with AlexaFluor594 or ADEMTECH particles labelled with ATTO594. This experiment showed that signals from both magnetosomes and ADEMTECH particles correlate with positions of cells (Fig.15 b,c). However, there is the possibility that magnetic particles are bound on cell membranes. To investigate whether magnetosomes are internalised within cells, cells were incubated overnight with magnetosomes functionalised with streptavidin labelled with AlexaFluor594, fixed and stained with anti-tubulin antibodies and counterstained with DAPI (to visualise nuclei). Subsequently, Z-stacks were taken, and 3D projections were generated using a Zeiss Observer Z1 microscope (Fig.16).

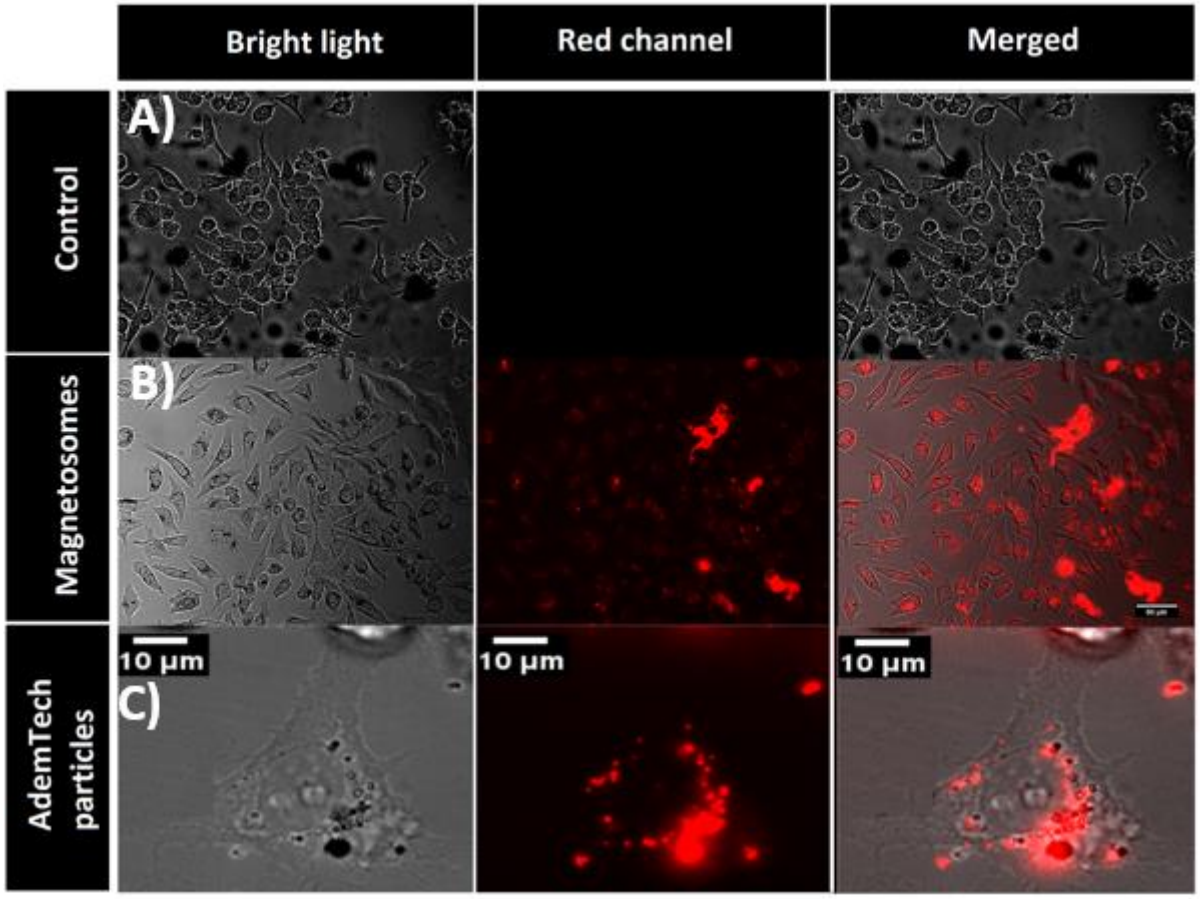

Fig. 13 Uptake of magnetic nanoparticles by HeLa cells. Panel A) HeLa cell growing without particles. HeLa cells incubated with B) magnetosomes and C) ADEMTECH particles. Magnetic nanoparticles are shown in red. Scale bar - 200 µm for A) and B), 10 µm for C).

These data proved the presence of magnetosomes within the cells. The next step was to check whether magnetosomes are free to attach to cytoplasmic targets or if they are stored in lysosomes, as previously suggested (Alphandéry, 2014; Master et al., 2015; Shen et al., 2014). This question could be addressed in a several ways for example by using LysoTracer dye or CD68 or CXCR4 enabling visualisation of lysomes. Another way could be over expression of GFP in the cytoplasm and checking colocalistion between signals of functionalised particles and GFP. I decided to use the TEM. Sections of cells incubated with magnetosomes demonstrate that magnetosomes are found both in the cytoplasm and within vesicles (Fig.17). The next step was to induce the movement of magnetic particles within the cells using a magnetic field. As calculated previously, approximately 4 pN of force was used to induce magnetosome movement within HeLa cells (Fig.18,). Application of force allows relocating magnetosomes within the media towards the magnet (Fig.18a). However, inside cells, magnetic particles responded just by aligning with magnetic field lines, without any apparent signs of coordinated displacement (Fig.18c).

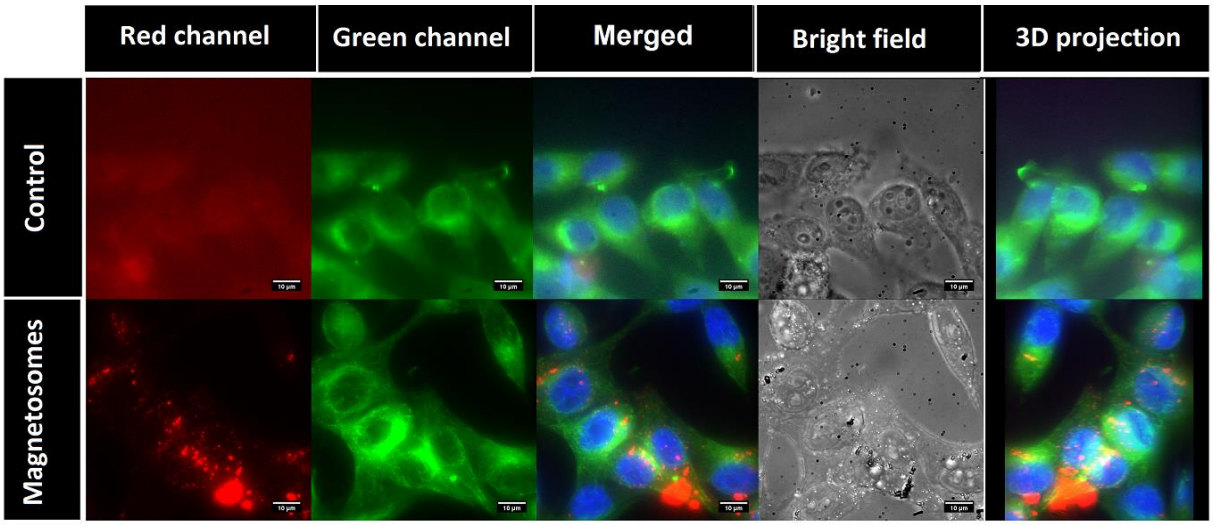

Fig. 14 Magnetosomes uptake. Red channel shows magnetosomes labelled with streptavidin conjugated with AlexaFluor594. Green channel shows immunostaining of tubulin cytoskeleton with antibodies conjugated with AlexaFluor488. Projection of ZStack showing the presence of magnetosomes within the cells. Scale bar – 10 µm.

Finally, I decided to check if ADEMTECH particles functionalised with antiGFP antibodies are able to bind to GFP labelled centrosomes *in vitro*. To answer this question, particles conjugated with ATTO594 and antiGFP antibodies were incubated with MDCK cells in which NPHP6 was fused with GFP resulting in green fluorescent

signal marking basal bodies positions (Fig.19a). I noticed that in 3 out of 65 cells the red signal of ADEMTECH particles correlated with basal body positions (Fig.19b).

To ensure that the correlation between these signals is not accidental I decided to record their behaviour over a period of 30 sec (Fig.19c). This recording revealed the overlapping coordinated movement of both signals for the entire duration of the time-lapse. This proves that an interaction between antibodies and GFP was stable within the cells.

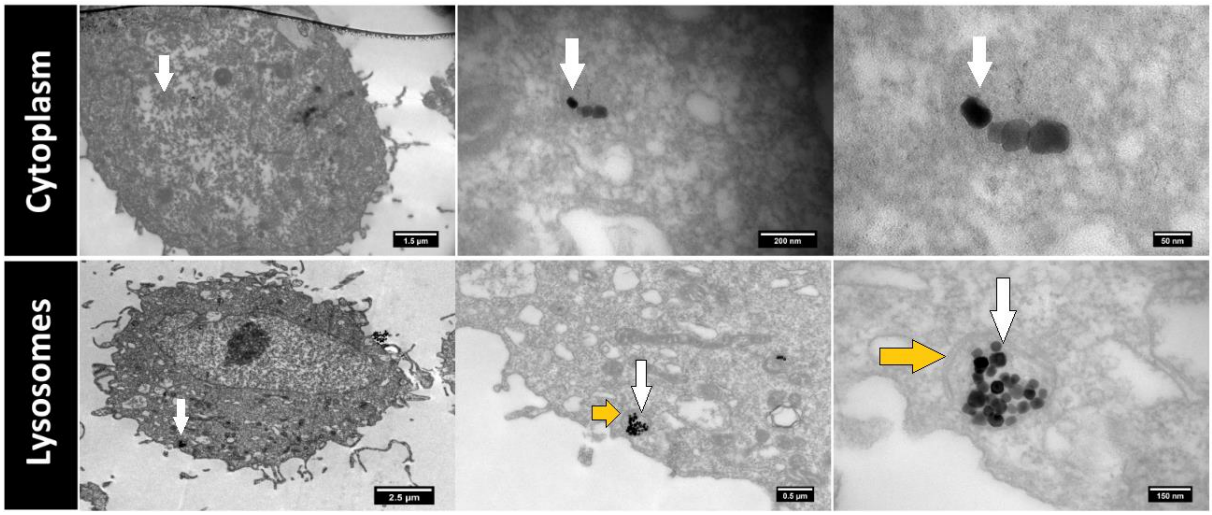

Fig. 15 The intercellular localisation of magnetosomes. TEM images are showing two ways of storing magnetosomes (indicated with white arrows) by HeLa cells. Panel A) shows magnetosomes localised in the cytoplasm. Panel B) shows magnetosomes segregated from the cytoplasm by membrane vesicle (indicated with yellow arrows).

These data confirm that both magnetosomes (~40nm) and ADEMTECH particles (~400nm) can be internalised by the HeLa cells. These particles can be stored either in vesicles (presumably lysosomes), and the cytoplasm. The fraction of particles that are stored in the cytoplasm can be attached to intracellular targets. However, the efficiency of this process is low (only 5% of the cells have shown a positive correlation for particles and centrosome signal). Lastly, under the magnetic force particles responded by aligning themselves with the lines of magnetic flux, created by the bar magnet, but particles remained unmoved. This behaviour suggests that the magnetic particles were either trapped between cell compartments, the cytoskeleton or were immobilised due to internalisation into lysosomes (Etoc et al., 2015; Master et al., 2015). Another possible explanation was direct interaction between particles and tubulin cytoskeleton (Tay et al., 2014; Tay et al., 2014; Tay & Leong, 2014) or magnetosome membrane proteins with actin.

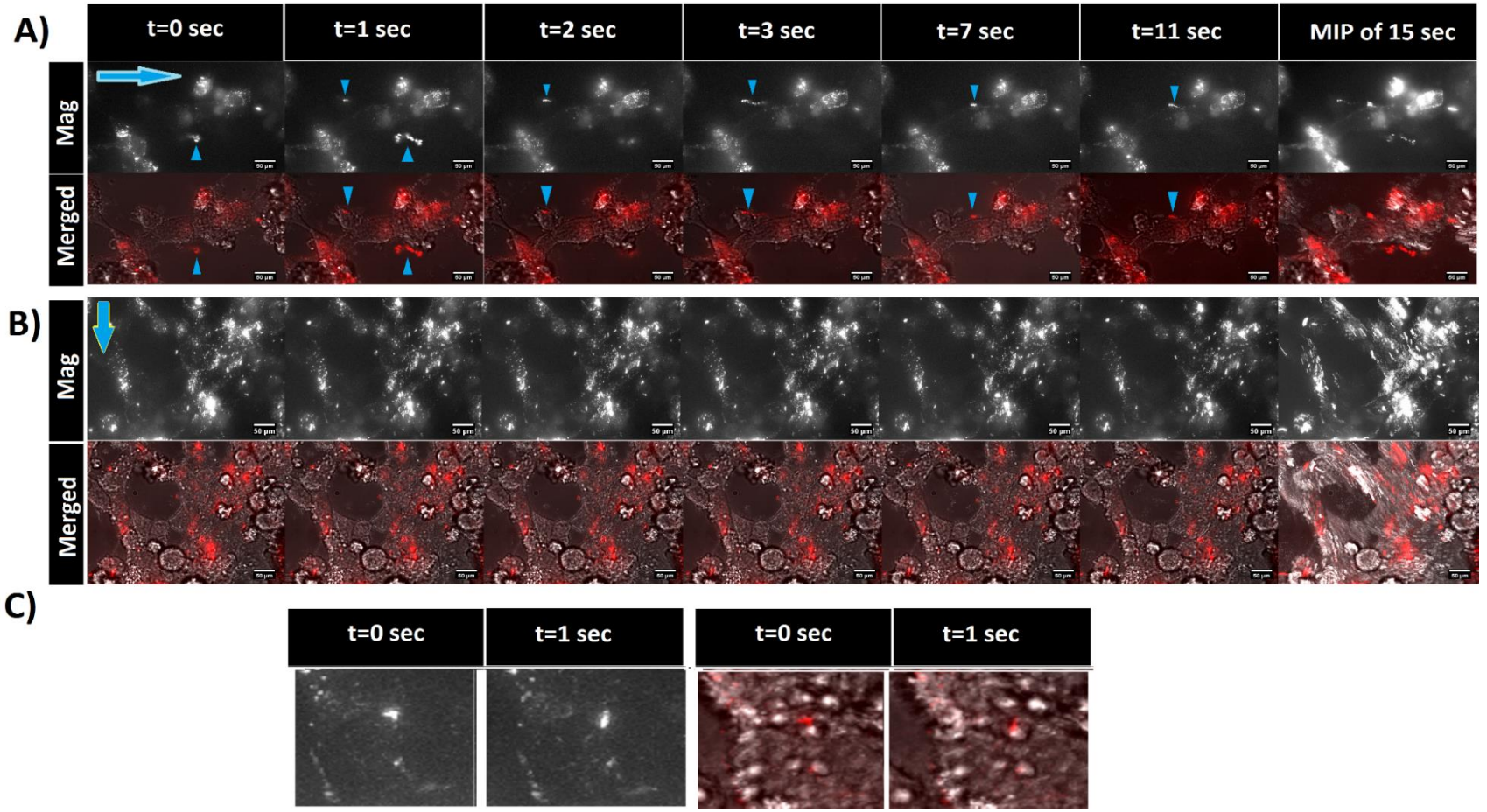

Fig. 16 The response of magnetosomes to the magnetic force. Panel A) shows the response of magnetic particles to the force applied from the right side (indicated with the big blue arrow). Arrowheads show magnetosomes which were not uptaken by HeLa cells, therefore free to move in media solution towards the magnet. Panel B) shows the results of applying the magnetic force from the top (indicated with the big blue arrow). Panel C) shows enlargement of the area marked in panel B) with red the square and rotation of magnetic particles under the magnetic force. Scale bar – 50 µm.

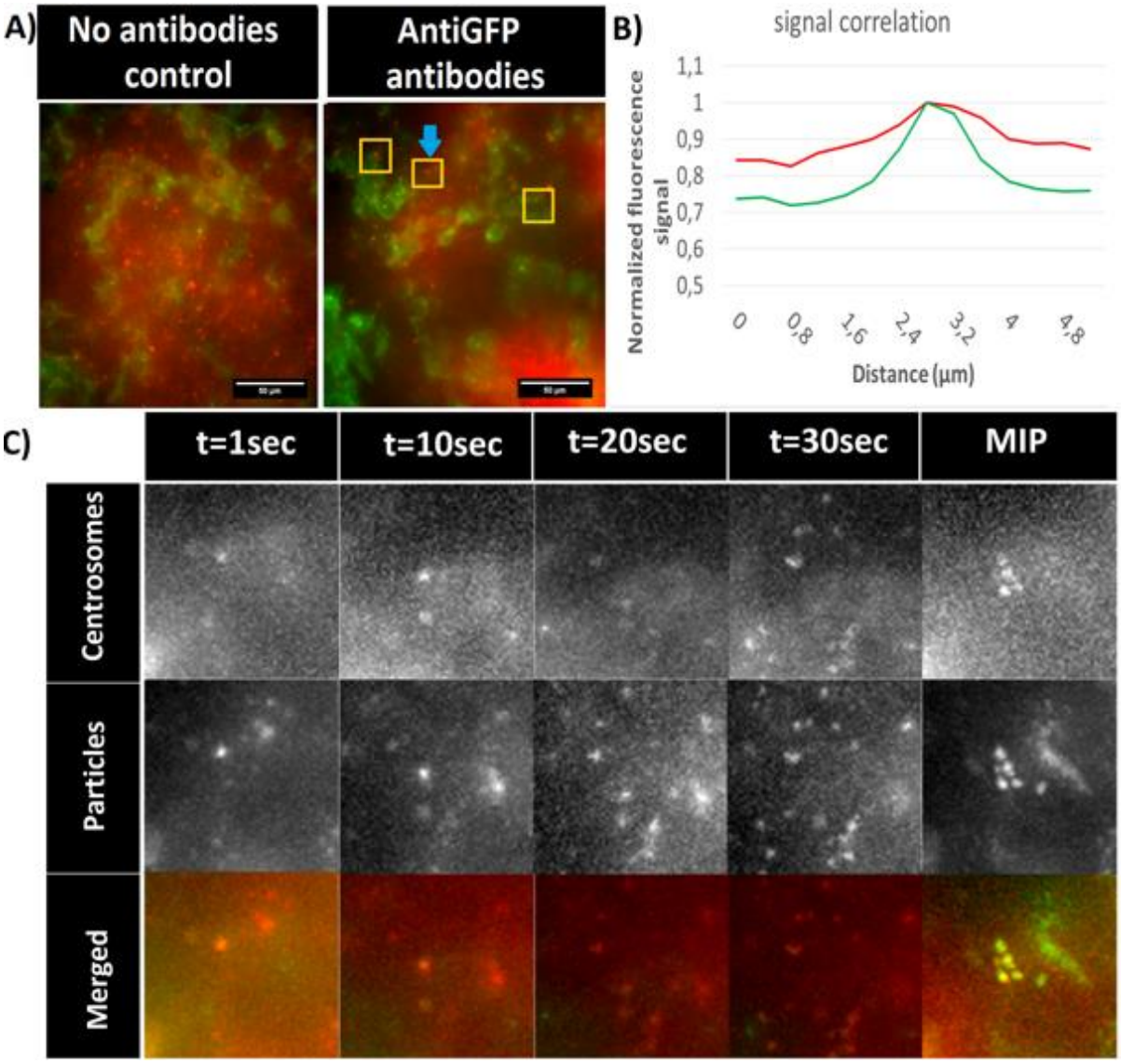

Fig. 17 Attachment of functionalised ADEMTECH particles to GFP labelled centrosomes. Panel A) shows MDCK cells incubated overnight with both ADEMTECH particles labelled with ATTO594 and ADEMTECH particles labelled with ATTO594 and antiGFP antibodies. Yellow squares show areas where red and green signal correlated. Panel B) shows correlating peaks of ADEMTECH particles and centrosomes fluorescence signals. Panel C) shows the behaviour of attached particles and centrosomes over 30sec in the area marked with the blue arrow on panel A). Blue arrowheads mark correlating signals. MIP (maximum intensity projection of 30 sec time lapse. Scale bar - 50 µm.

4.2.2 Interaction of magnetic particles with the actin

To investigate the possible spontaneous attachment of magnetic particles to actin via direct or protein-mediated interaction, I took three separate approaches. First, I incubated magnetosomes labelled with streptavidin conjugated with AlexaFluor594 with filamentous actin labelled with AlexaFluor 488. Samples were observed under the microscope directly after adding magnetosomes and after 30 min of incubation. Then, I measured the correlation between green and red signal (Fig.20). Measurements of a correlation in fluorescence signal have not shown correlating peaks for magnetosomes and actin signals. This experiment suggests that magnetosomes do not interact directly with actin. To confirm this finding, magnetite, magnetosomes without membranes, magnetosomes with membranes and ADEMTECH particles were incubated with filamentous actin for 2 hours on the ice. Then magnetic particles were washed twice, and the amount of remaining actin on particles was checked on the SDS-PAGE gel (Fig.21). This data further proves that neither magnetosomes nor other magnetic particles interact directly with the actin as the correlation of signals were not seen.

Previously, in this chapter, I have confirmed that magnetic nanoparticles can be internalised by HeLa cells. As an additional step, HeLa cells were incubated with functionalised magnetosomes and later stained for actin using phalloidin. This experiment revealed that 33.5 ± 20.5% of signals from magnetosomes, within cells, correlated with peaks of fluorescence for the stained actin (Fig.22). It is possible that correlating peaks are a subfraction of particles encapsulated within vesicles that are surrounded by actin (Master et al., 2015). This explanation is supported by my observations using TEM.

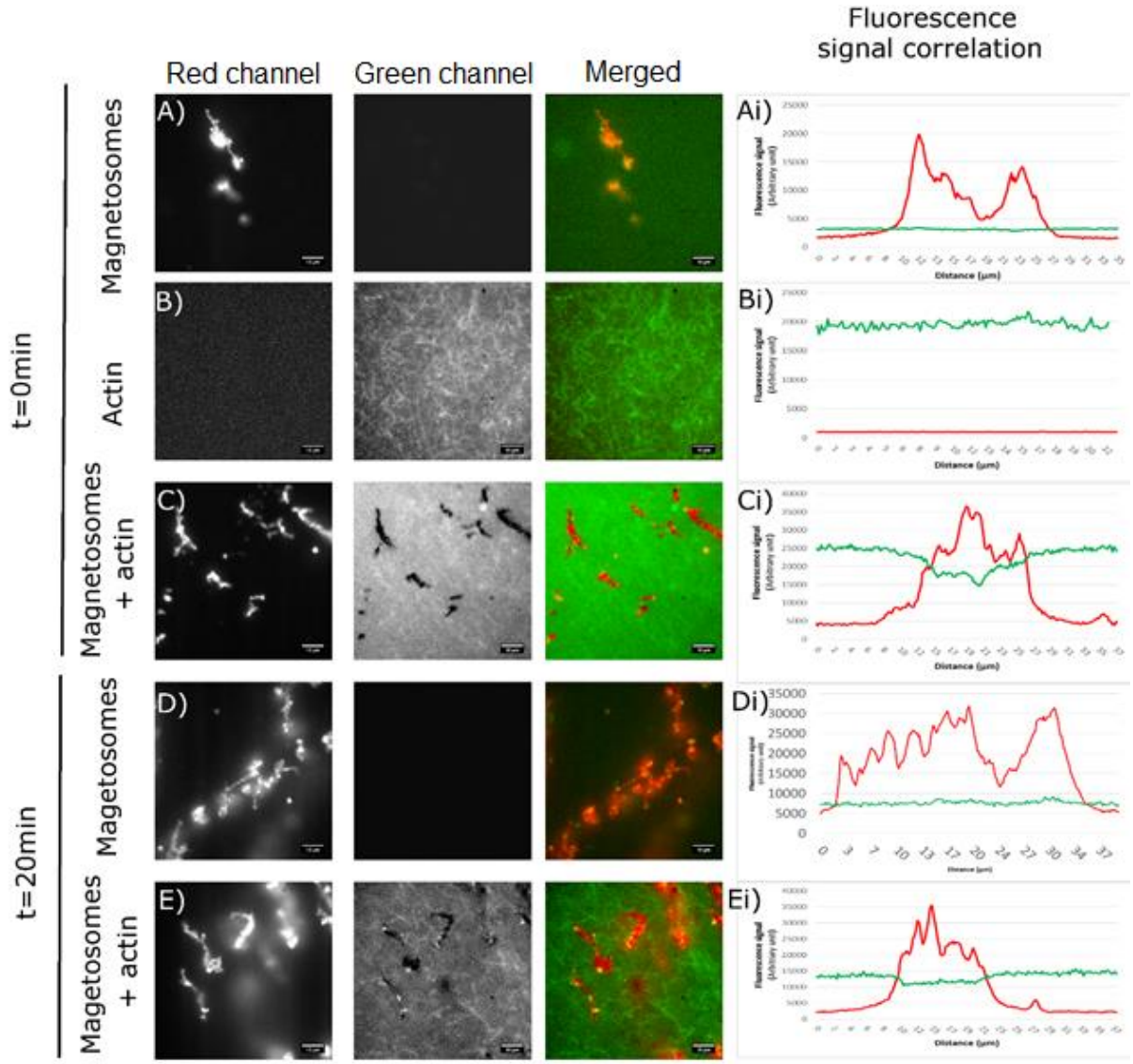

Fig. 18 The interaction of magnetosomes with actin. Magnetosomes were labelled with streptavidin conjugated with AlexaFluor594 (red), and actin was labelled wit Alexafluor488 (green). A) The control sample containing labelled magnetosomes at time 0. A') measurement of correlation between the red and green signal for magnetosomes at time 0 B) Control containing filamentous actin labelled with Alexafluor488 at time 0. B') measurement of correlation between the red and green signal for filamentous actin at time 0. C) The mixture of magnetosomes and filamentous actin at time 0. C') measurement of correlation between red and green signal for magnetosomes incubated with filamentous actin at time 0. D) The control sample containing labelled magnetosomes after 30 min incubation D') measurement of correlation between the red and green signal for magnetosomes after 30 min. E) The mixture of magnetosomes and filamentous actin after 30 min incubation. E') measurement of correlation between the red and green signal for magnetosomes incubated with filamentous actin after 30 min incubation. Y-axis arbitrary units for fluorescence signal strength, X-axis length in µm. Scale bar - 10 µm.

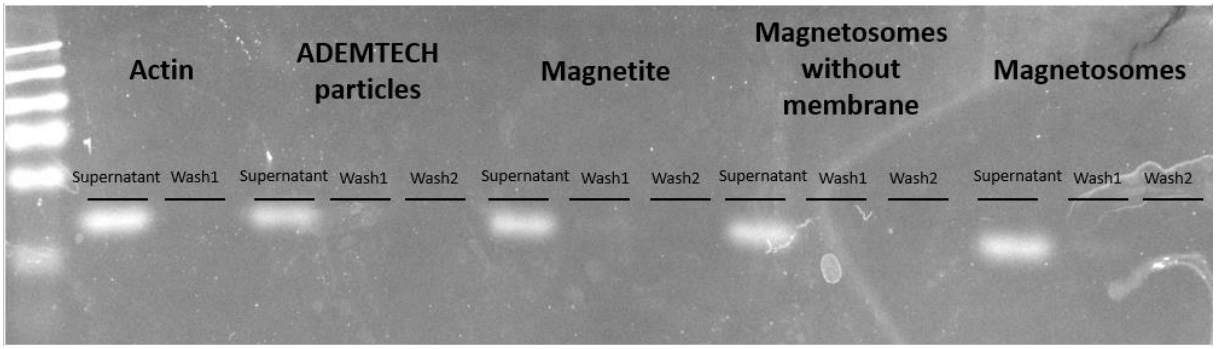

Fig. 19 The SDS-PAGE has shown that the actin does not remain attached to the magnetic particles.

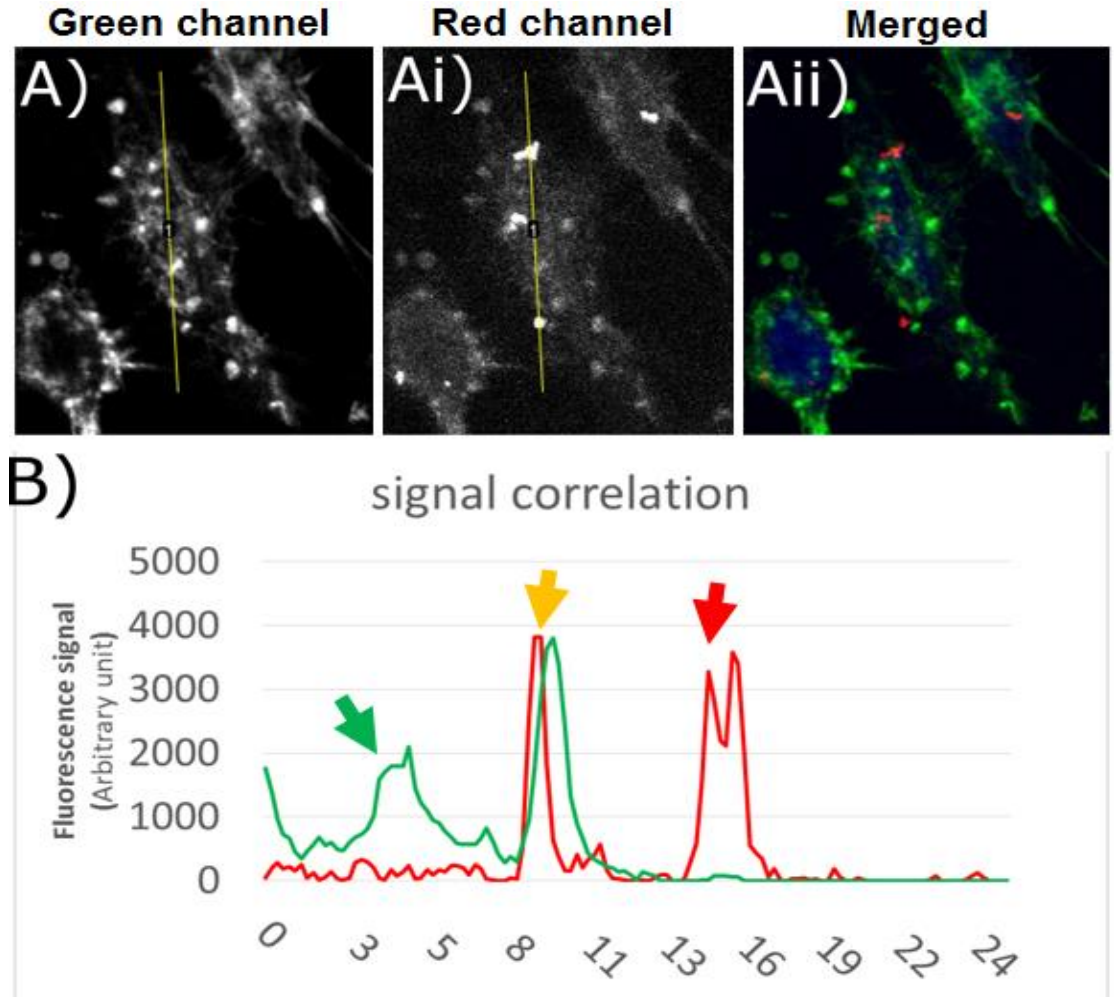

Fig. 20 Actin accumulation around magnetosomes in HeLa cells. A) image of an actin cytoskeleton with a phalloidin staining. Ai) image of magnetosomes labelled with streptavidin AlexaFluor594. Aii) composite of magnetosomes and the actin stainings. The yellow line shows the area of fluorescence measurement. B) Example of correlation of an actin and magnetosomes signals across the range of measurement. The green arrow indicates peak for the actin signal, and the orange arrow shows correlating peaks for actin and magnetosomes signals, the red arrow shows the peak for the magnetosomes signal, x axis shows length in um.

4.3 Discussion

These data show that both magnetosome and ADEMTECH particles can be taken up by cells, which is consistent with research conducted on the other magnetic nanoparticles (Alphandéry, 2014; Markides et al., 2012; Steketee et al., 2011). Furthermore, I confirmed that biotinylated particles labelled with the fluorescent streptavidin remain stable after being delivered to the cells, and thus allow one to track their position over time. Immunofluorescence staining against tubulin cytoskeleton and TEM have revealed intracellular localisation of particles. Moreover, DAPI counterstaining in tubulin and phalloidin stained cells suggest that uptake of particles do not cause apoptotic or necrotic cell death, which is observed by nucleus fragmentation (Elmore, 2007). TEM revealed that nanoparticles could be found both in the cytoplasm and isolated from the intracellular environment by membrane vesicles, which according to literature, are most probably lysosomes (Shen et al., 2014). During the use of magnetic force, I was able to rotate clumps of magnetic particles, but I was unable to relocate them within the cells. In literature, this problem is associated mostly with 3 factors; high viscosity level of the cytoplasm, a web-like network of the cytoskeleton, and the connection of lysosomes to the actin cytoskeleton (Etoc et al., 2013; Etoc et al., 2015; Master et al., 2015; Tay et al., 2014; Tay et al., 2014). However, it has been reported that the relocation of magnetic particles within the cell is possible with the use of magnetic force (Etoc et al., 2015). This could be due to a different method of delivery of nanoparticles to the cells, wherein they were injected in comparison to the incubation of cells with magnetic particles.

Additionally, interactions of the membrane protein MamK of magnetosomes with the actin-like protein MamJ increased chances of direct interactions between magnetosomes and actin (Rioux et al., 2010). To check this possibility, I took three independent approaches; (i) Incubation of filamentous actin with magnetite (~50nm), (ii) magnetosomes without membranes (~50nm), and (iii) magnetosomes (~50nm) or ADEMTECH particles (~500nm) for 30 min. This did not show binding of actin to any of these particles. A similar result was observed by incubating magnetosomes with fluorescently labelled actin and measuring the signal correlation of magnetosomes and the actin. Finally, I investigated whether actin accumulated around magnetosomes within living cells. My experiments suggested that 33.5 ± 20.5% of magnetosomes were surrounded by actin. Combined with previous observations of magnetosomes are

not interacting directly with actin and that they are stored within membrane vesicles these results support existing literature that suggests lysosomes are anchored to microtubule highways and are tightly associated with actin filaments (Master et al., 2015). The Results from these experiments enabled a better understanding of data obtained from zebrafish described below.

Chapter 5. Influence of magnetic particles on Zebrafish (*Danio rerio*) embryo migrating cells.

5.1 Introduction

Zebrafish have become an important model organism in research in the last 20 years. Their small size, transparent larvae, high fertility, rapid and precisely described development make them the perfect model organism for studies involve microscopy techniques (Kimmel et al.,1995; Topczewski et al., 2001). An additional advantage is a fully sequenced genome and relatively easy methods of genetic modification of this animal model (Malicki, 2000). These features make zebrafish embryos the perfect model for research about cells migration patterns during early development. Tools of genetic modification allow for the creation and use of various transgenic lines in which proteins are fused with fluorescent proteins and can be observed in a living organism. In this part of my work I used three transgenic lines- centrin2: GFP, H2B: RFP centrin2: GFP and 4xGTIIC:eGFP transgenic line in which eGFP is driven by the 4xGTIIC promotor and can be used to monitor the activation of the Hippo pathway (Miesfeld et al., 2014).

Cell migration is an extremely complex process involving the rearrangement of the actin and tubulin cytoskeleton and the position of organelles (Blaser et al., 2006; Hassan, 2016; Mayor & Etienne-Manneville, 2016; Norden et al., 2009; Solnica-Krezel & Sepich, 2012). It has been documented among various cell types to orientate centrosomes with respect to the direction of cell migration, which also orchestrates in tubulin cytoskeleton reorganisation (Dupin et al., 2009; Elric et al., 2014; Tang et al., 2012). Rearrangement of the actin cytoskeleton leads to formation of filopodia, lamellipodia or bleb expansions and establishes lead and rear edges (Charras et al., 2008; Dang et al., 2013; Krause et al., 2014; Nobes at al., 1995; Paluch et al., 2013; Thiam et al., 2016). Cell migration can be induced, orchestrated and modulated as a result of different types of taxis such as chemotaxis (response to chemoattractant or chemorepellents), durotaxis (response to the stiffness of surface), thermotaxis (response to temperature) etc. Cell migration can also be modulated in response to mechanical stimuli (Ruprecht et al., 2015; Weber et al., 2012), such as the role a friction force as it was described for anlage positioning in zebrafish embryos (Smutny et al., 2017). These cellular reactions can be mediated by the activation of Ca2+ influx or the activation of mechanosensitive pathways such as the Hippo pathway (Codelia et

al., 2013; Kim et al., 2015). Cells can migrate singly or collectively. In collective movement three types of cells are distinguished; leader, follower and side cells (Etienne-Manneville, 2014; Mayor et al., 2016). It has been shown that that in the wild-type zebrafish embryo, the convergence of the notochord-forming mesoderm occurs at about the same rate as the adjacent somitic mesoderm. This finding suggests that during gastrulation, all of the dorsal trunk mesoderms behaves as a single unit with respect to axis narrowing (Glickman et al., 2003). Zebrafish has been successfully used in research evaluating the usefulness of magnetic particles in the activation of the apoptosis cascade, through activation of an extrinsic apoptosis receptor (OTR) (Cho et al., 2012).

In this work, I asked whether functionalised magnetic particles, both, magnetosomes and ADEMTECH particles, can be used to change the migration pattern during zebrafish gastrulation (Fig.23). To accomplish that delivery of the magnetic particles into the zebrafish embryo at one cell stage was accomplished via microinjection.

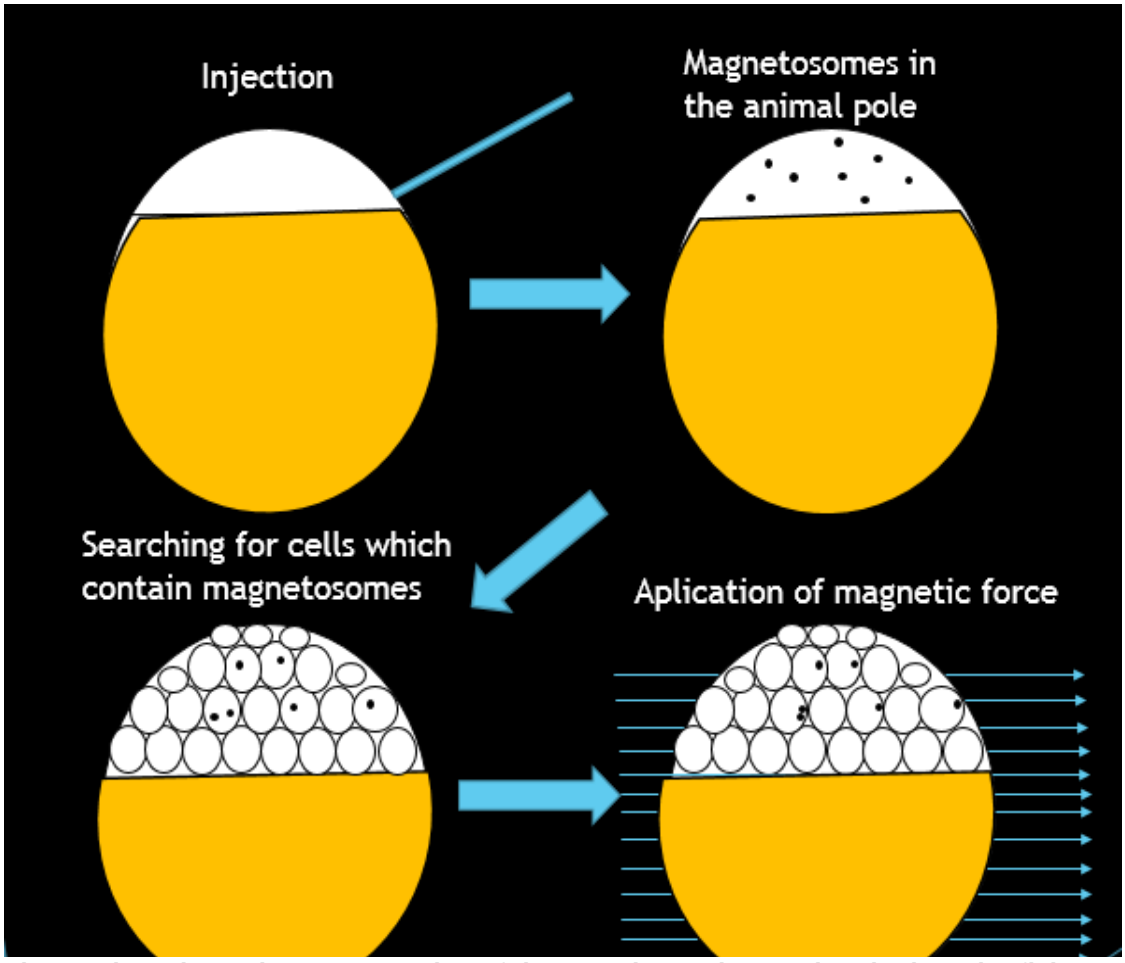

Fig. 21 The schematic representation of the experimental procedure in the zebrafish embryo. Black dots represent magnetic nanoparticles.

Then, a stage during which cells are migrating the longest distance towards the body axis was determined. By virtue of this, small differences in migration under the application of magnetic force should be visible. I checked if the functionalised particles are delivered to migrating cells of the developing embryo, and if they remain stable. Following this, the response of magnetic particles to the magnetic force in 8-10 hours old embryos were checked. The cell membrane was labelled with BODIPY FL and used as a reference point for the particles' movement. Lastly, I exposed migrating cells containing functionalised particles to magnetic force and evaluated if the application of the force changed cell behaviour.

5.2 Results

The first step which I took was the optimisation of a method to deliver particles into the zebrafish embryo. I started with microinjection of magnetosomes functionalized with BODIPY FL.

Trying to overcome a problem of particles internalising within membraned vesicles I injected particles at the one cell stage embryos. However, I had to resign from using BODIPY FL functionalized particles due to the dye leakage to surrounding cell membranes (Fig.24). This initial difficulty, overcome by usage of biotinylated magnetosomes labelled with streptavidin conjugated with AlexaFluor594. These particles were injected in Claudin: GFP zebrafish embryos. Claudin is a tight junction protein and fusing it with GFP results in membranes being labelled with GFP.

That allowed me to localise particles better and showed presentence of functionalised particles within cells of the embryo (Fig.25a). That was the first step in proving that it is possible to successfully deliver magnetic particles to the cells of the developing embryo. The second proof was cryosections of 8-hour old embryos, which showed particles signal in cells surrounding the yolk. (Fig.25b).

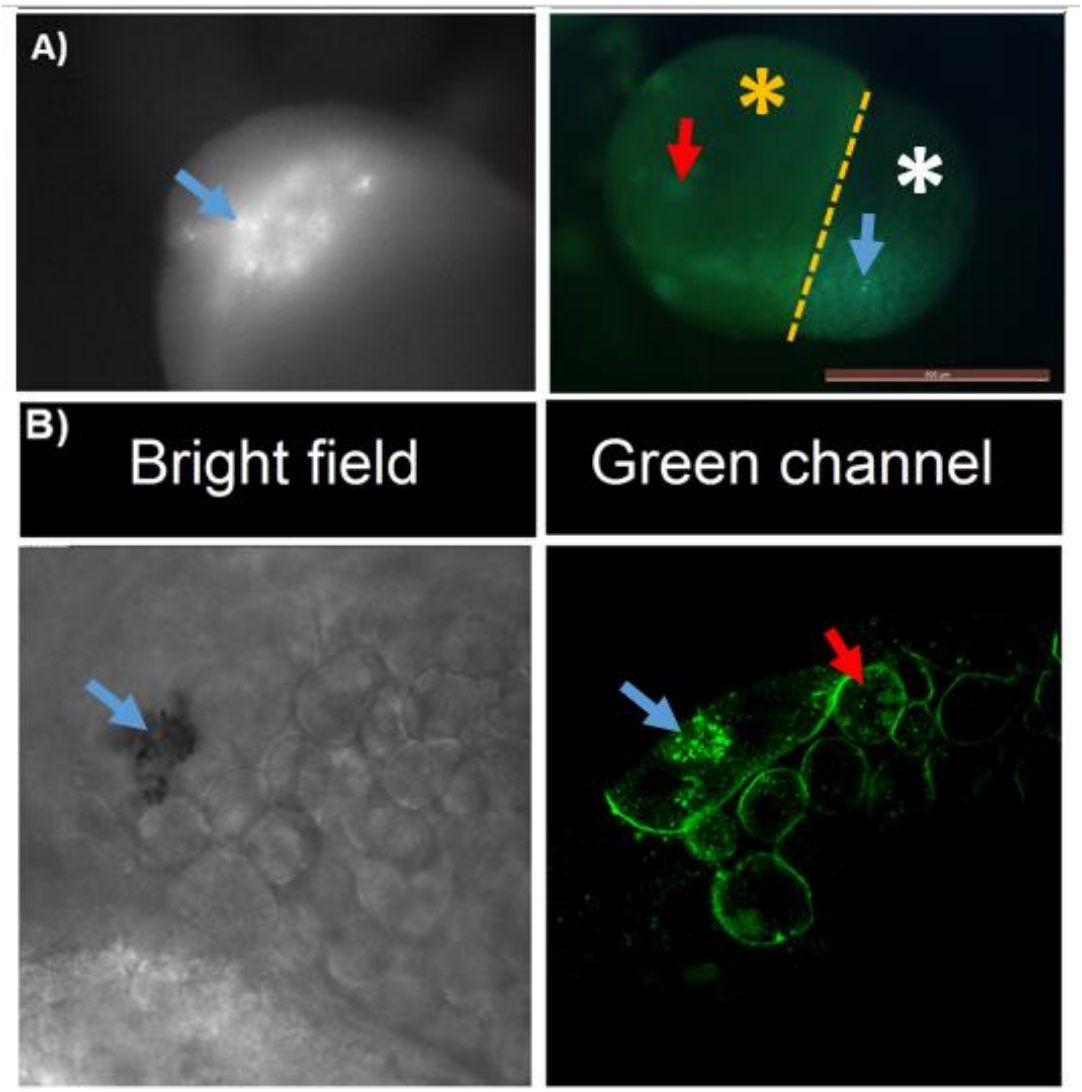

Fig. 22 The position of BODIPY FL labeled magnetosomes without membranes within zebrafish embryo 5hpf. Panel A) pictures of the whole embryo orange line marks boarder between yolk (orange asterix) and anime pole (white asterix) of developing embryo, blue arrows show magnetomes, red arrows show BODIPY FL leakage. Panel B) shows confocal pictures of magnetosomes within the zebrafish embryo and leakage of BODIPY FL to surrounding cell membranes. Pictures were taken with the confocal microscope water dipping lens.

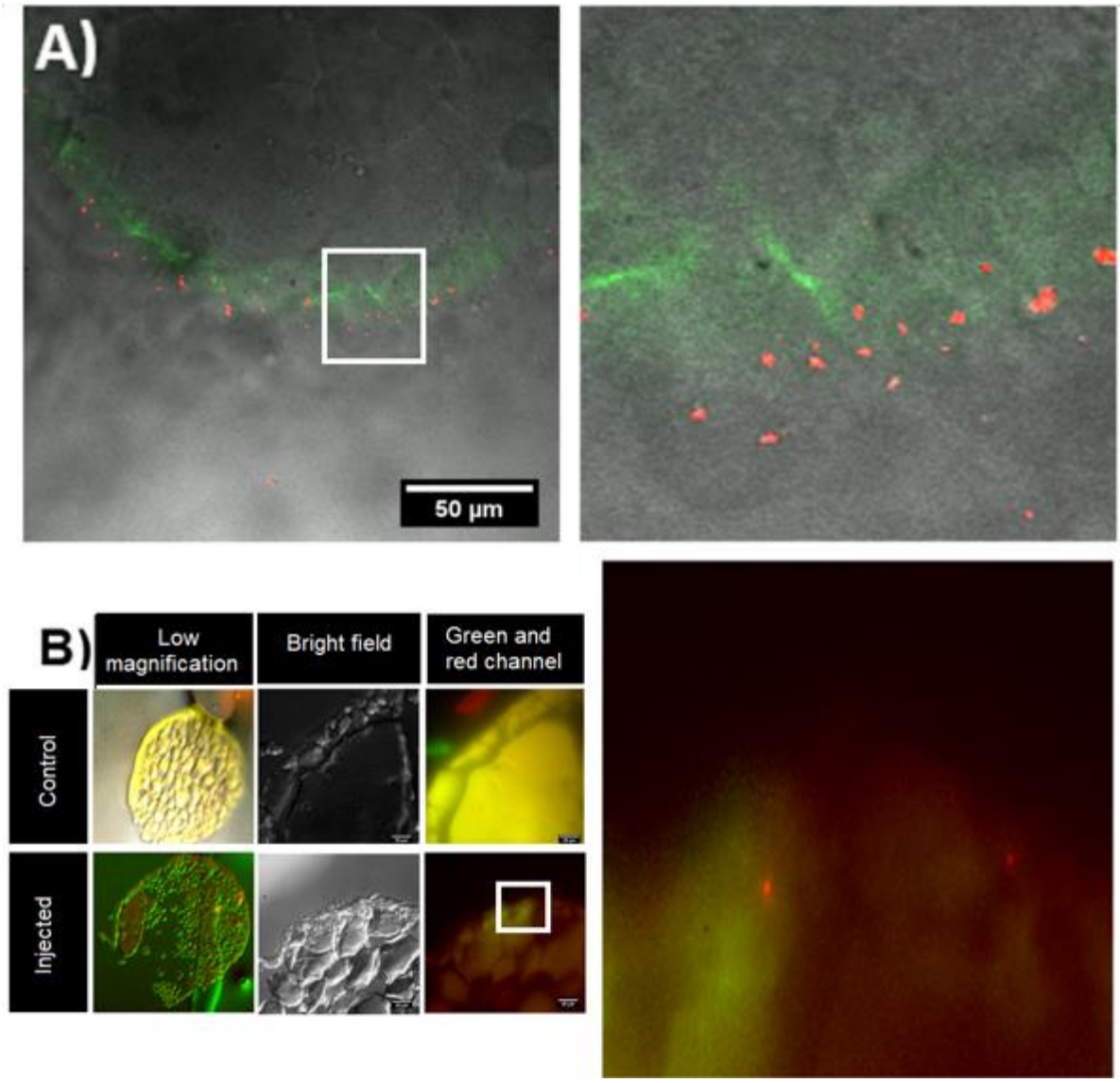

Fig. 23 Localization of magnetic particles within the zebrafish embryos. Panel A) shows localisation of magnetosomes in chain form, functionalised with fluorescently labelled streptavidin in the Claudin: GFP embryo. Panel B) shows the localisation of ADEMTECH particles within cells in 8hpf embryos.

Example of magnetosomes labelled with BODIPY FL shows the effect of injecting aggregated magnetosomes into one cell stage embryos (Fig.24) in comparison to particles dispersed and not aggregated which were labelled with streptavidin (Fig.25). These data show the role of aggregation of magnetosomes in internalisation of the particles by zebrafish embryo cells.

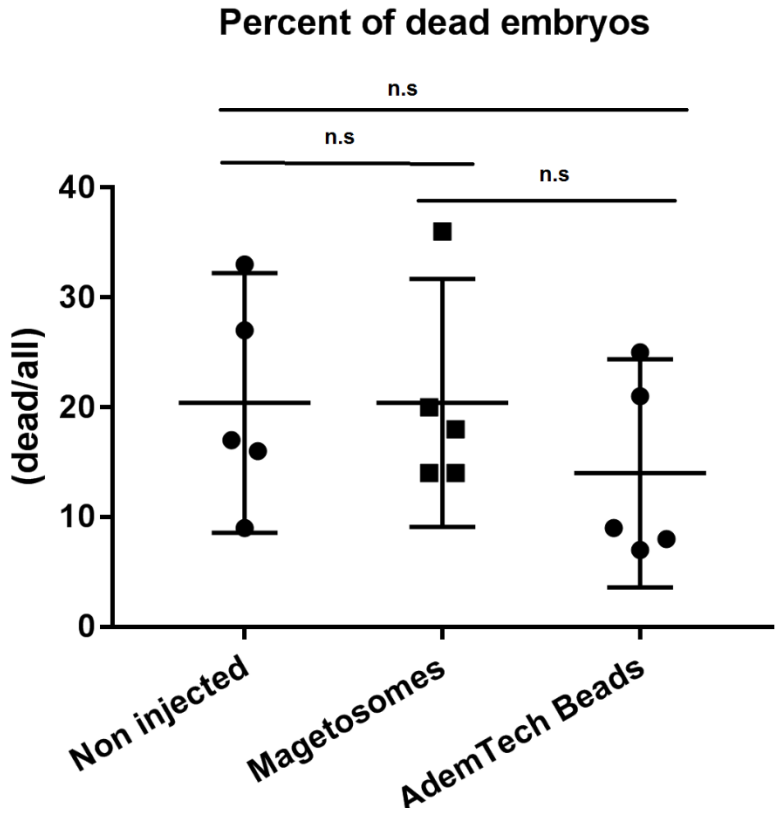

Fig. 24 Percentage of dead embryos after magnetic particles injection. Embryos were injected at the one-cell stage with magnetic particles, and mortality of embryos was assessed at 8hpf. n=5, mean with 95% CI, p>0.05.

Once presentence of magnetic nanoparticles within cells of the developing embryo was confirmed, I tracked migrating cells and centrosomes. For this purpose transgenic centrin2: GFP line, which marks centrosomes with GFP signal, was crossed with H2B: RFP line, which allows tracking nuclei. This process created a line, which allows for the relatively easy following of cell migration and centrosome position process of migration. As the next step, I had to evaluate if the injection of magnetic particles has an impact on embryo survival ratio. The embryos were injected with 0.2 µl of the solution. What in ADEMTECH (10 mg/ml) particles case corresponds, after 100x dilution, to approximately 0.02 µg of particles and 0.014 µg of iron oxide. 1ml of ADEMTECH solution contains around 10^{11} particles (statement of the maufacturer) what should result in approximately ~500 000 particles being injected into the embryo. I calculated the percentage of dead embryos after 8h post-injection particles in comparison to the non-injected control group. Injection of the particles did not cause any significant differences in mortality between samples injected with magnetosomes, ADEMTECH magnetic particles compared to non-injected control (Fig.26).

Then I optimised techniques for preparing embryos for imaging. Initially, the Olympus FV1000 Confocal microscope was used to establish if it is possible to deliver magnetic particles to the cells of the developing embryo. However, limitations of this system such as the speed with which images can be collected and difficulties with mounting the embryo made the usage of Zeiss Observer1 inverted microscope with QuantEM:512SC camera much more suitable. That allowed me for a much faster collection of images and was essential for the recording of the particles react to the magnetic force and possible changes in the cell migration.

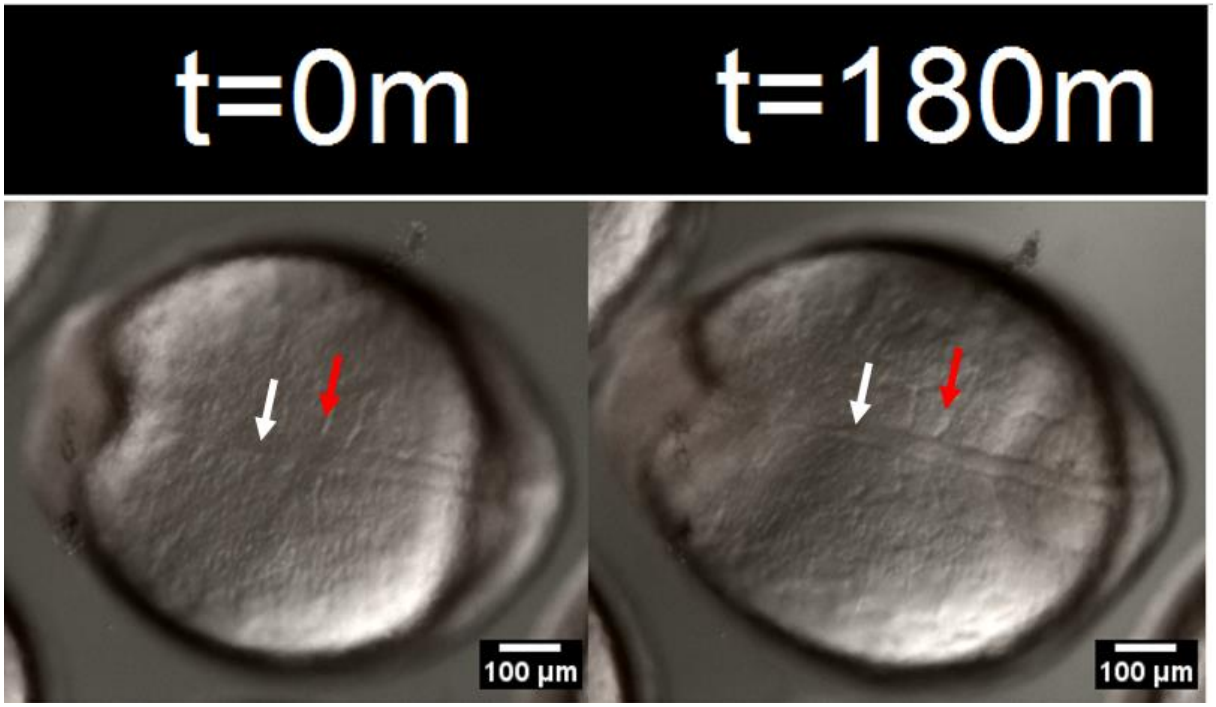

Fig. 25 Embryo immobilisation. Embryos were immobilised in 1% low melting point agarose after dechorionation. Panel A) shows the embryo at the one-somite stage at the beginning of the experiment. Panel B) shows the same embryo after 3 hours of recording. Red arrows show somite, and white arrows show the body axis. Scale bar - 100 µm.

Another obstacle which had to be overcome was devising a way to immobilise the embryo. 0-24 hpf embryos are very fragile and prone to bursting. To prevent embryos from rotation within the chorion and to decrease the distance of the migrating cells sheet from the microscope lens I removed their chorions. This made them even more prone to damage during mounting and positioning. I used 2% methylcellulose to immobilise samples, but this method turned out to be unsuccessful due to the embryo drifting in the viscous media. Then, low melting point agarose was used as

it polymerase creates the gel, not the high viscosity liquid. After optimisation, it was established that 1% agarose was most efficient in the immobilisation of embryo and still letting for putting the sample in the desired position before gel solidify (Fig.27).

To have a clear reference to monitor the migration of the cells, I focused on the body axis during first somite formation (Fig.27) (Glickman et al., 2003; Kimmel et al., 1995). Next thing which had to be established was the description of how particles react to the magnetic force in the zebrafish embryo. Initial experiments confirmed my data from *in vitro* work. Magnetic particles under the magnetic force were rotating, but I was not able to see clear displacement (Fig.28). For this reason, I co-injected functionalised ADEMTECH particles with BODIPY FL which allowed to visualise the cell membrane as a reference point for particles displacement within cell boundaries. To make displacement more clear the force was applied from right, left and up for 60 seconds each direction with 60 seconds intervals between. Then I calculated the angle of particles displacement. During these experiments, the majority of the particles reminded unresponsive, only 6,5±2,5% of particles responded to magnetic force (Fig 30a). Then I compared the number of particles moving inside cells with and without applying force (Fig.30a). This has shown that the application of the magnetic force results in a 58% increase in the movement of particles in comparison to samples not treated with the magnetic force (Fig.30).

Fig. 26 Response to the magnetic force by functionalized magnetosomes in the zebrafish embryo. Arrows indicate the direction from which magnetic force was applied. Scale bar - 20 µm.

However, the movement of particles was not organised towards magnetic force (Fig.30). The particles displacement could be the result of Brownian motion, a random movement of particles in gas or liquid. Some of the particles moved in organised matter towards each other and clumped together. That suggested an idea that even though I could not pull magnetic particles towards the magnet, particles responded to the magnetic field by aligning with magnetic flux lines generated by the magnet. To test this possibility, I suspended ADEMTECH particles in HEPES buffer and applied magnetic force. All particles localised to lines ~2,5 μm apparat without clear movement toward the magnet. This observation strengthened the idea that the seemingly random movement of particles reflects positioning along the magnetic flux lines (Fig.32).

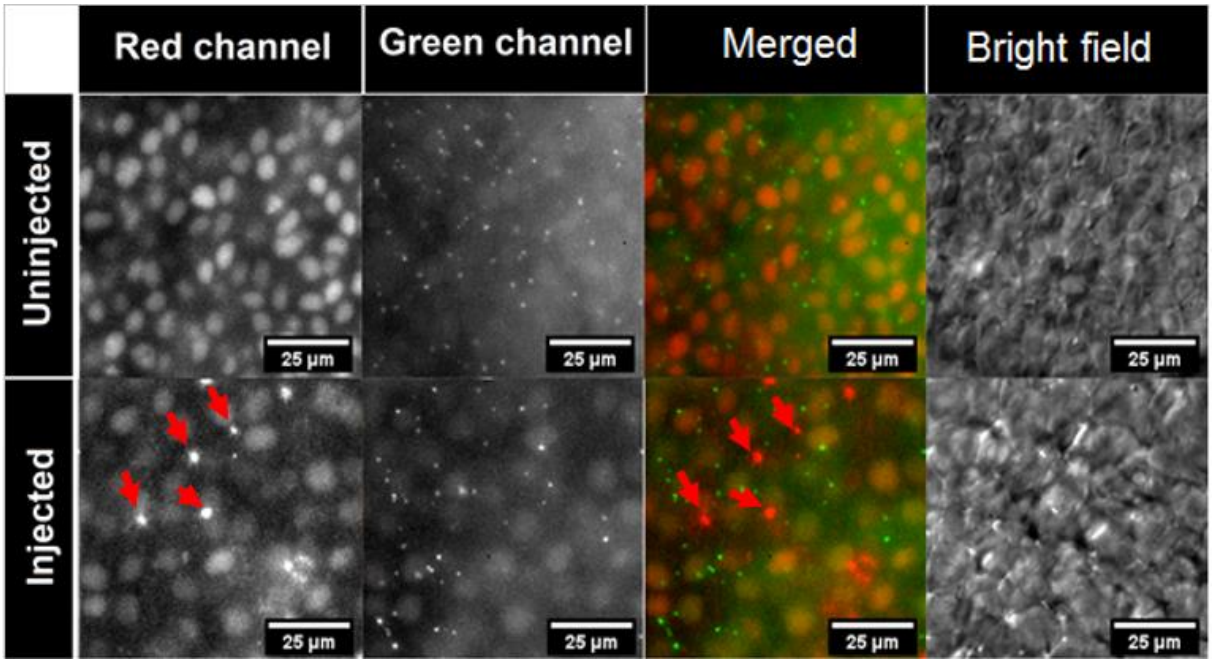

Fig. 27 Centrin2: GFP and H2B: RFP double transgenic line. Panel A) shows the uninjected control embryo. In the red channel nuclei and green centrosomes. Panel B) shows an injected embryo. Red arrows pointing functionalized with ATTO594 ADEMTECH particles.

After I established that particles could be found in cells of the zebrafish embryo, the area and stage of embryo providing me with the explicit reference point, I created double transgenic line containing centrin2: GFP and H2B: RFP transgenes. This line allowed me to track centrosomes and nuclei (Fig.29a). Double transgenic embryos were injected with ADEMTECH particles functionalised with anti-GFP antibodies but interaction with GFP tagged centrin2 was not seen (Fig. 29b). Even though I could not

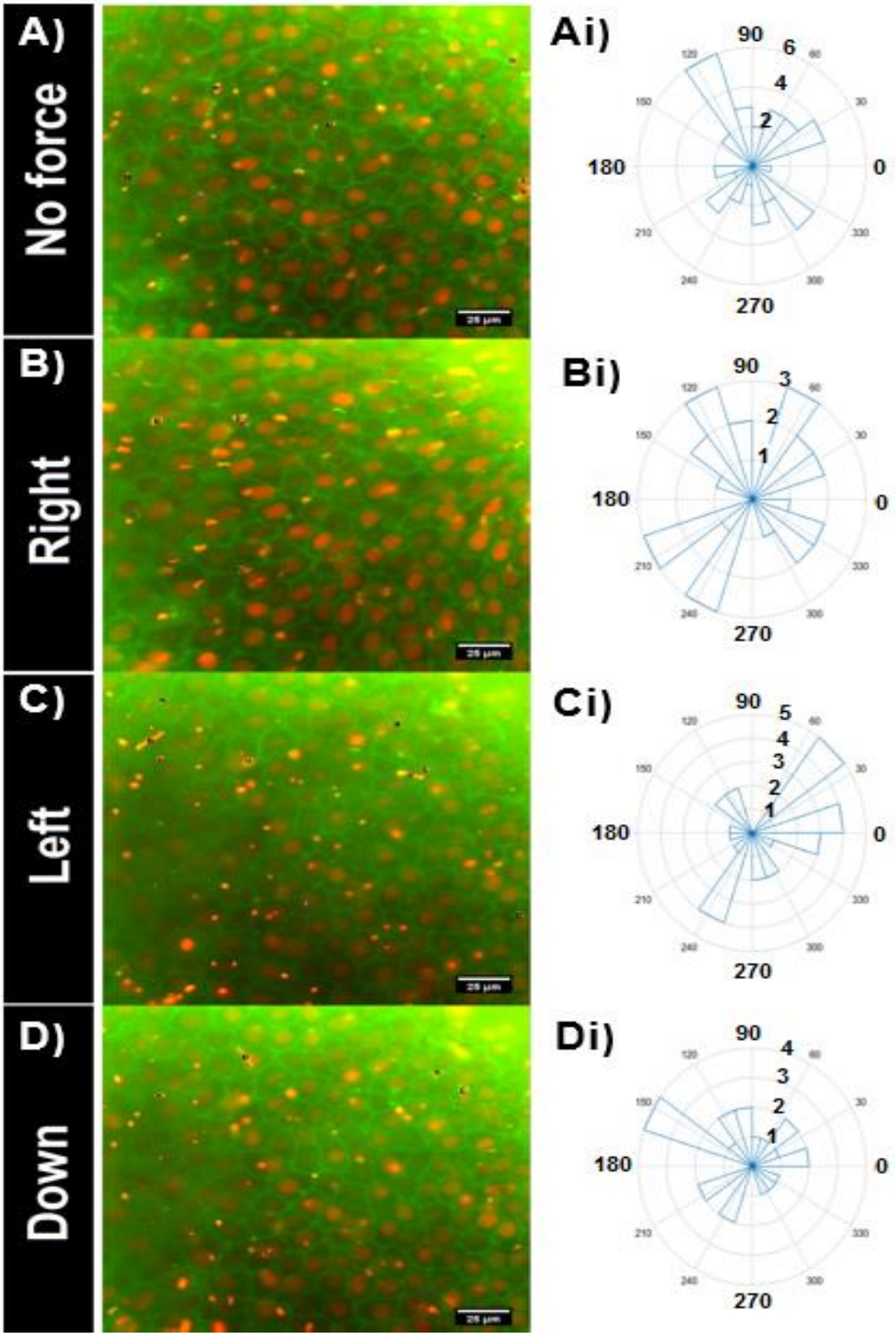
A)
No force
B)
Right
C)
Left
D)
Down
Ai)
Bi)
Ci)
Di)
90
180
0
270
25 µm

Fig. 29 Tracking movement of ADEMTECH magnetic nanoparticles within the zebrafish embryo. Panels A), B), C) and D) show magnetic particles (bright red dots) within cells with membranes labelled with BODIPY FL (green) when magnetic force is applied from 3 different directions; right B), left C), down D) and control without the force A) Particles were observed for 60 seconds then MIP were compared with time lapse to define direction of movements. Panels Ai), Bi), Ci) and Di) show angle of particles movent calculated from MIP of corresponding images. Numbers associated with circles indicate the number of particles. n=4. Scale bar - 25 µm.

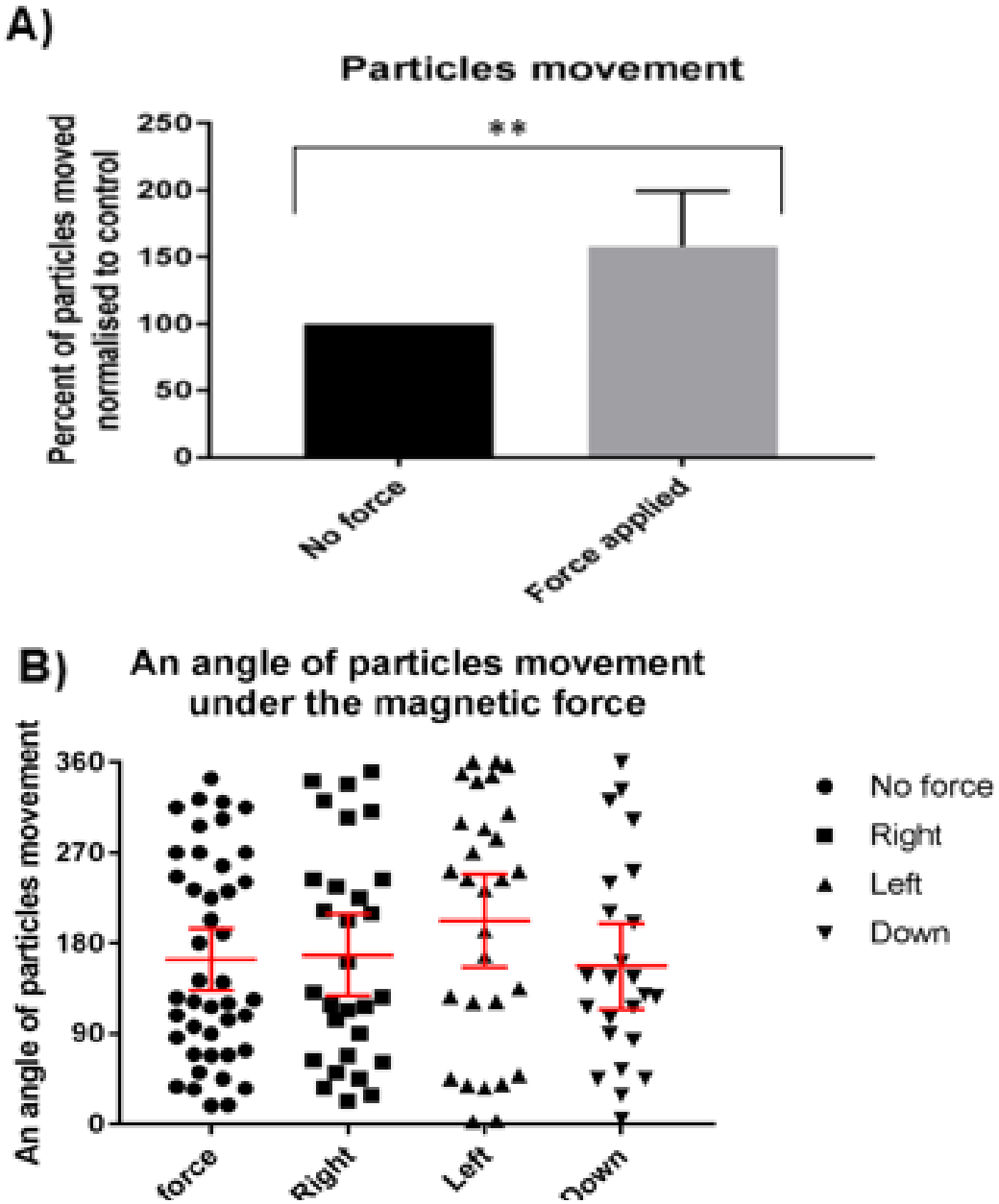

Fig. 28 The response of magnetic particles to the magnetic force and angle of movement. Panel A) compares the percentage of particles which moved inside the cells of the developing embryo without applying magnetic force and under magnetic force calculated from MIP from Fig.30 (p=<0.01). Panel B) shows data from panels Ai), Bi), Ci) and Di) from Fig.30 plotted into a scatter plot showing that applying that magnetic force did not affect the direction of particles moving in the statistically significant way. n=4 mean with 95% CI.

pull particles towards the magnet, it was suggested in the literature that immobilised particles still can exert the force on the cytoskeleton and trigger a response (Master et al., 2015). To establish control values I started with the recording of non-injected migrating cells.

I recorded 30 min of cell migration without applying magnetic force, then 30 min when force was applied from right, then 30 min from the left and last 30 min when the force was not applied. Then the angle of movement of 18 cells per embryo in each experiment was measured. Both GFP signal of centrin2 and RFP signal of H2B were tracked to show centrosome and nucleus movement during the cells' migration (Fig.33). The experiment has shown that without magnetic force nuclei migrates 104.8 ± 10.15, (n=6) degree toward the body axis and value for centrosomes was 100.9 ± 8.575, (n=5). The same values were measured with magnetic force applied from right, left and without magnetic force and results were for nuclei 97.41 ± 9.739, (n=6), 98.58 ± 6.679, (n=6) and 92.03 ± 8.316, (n=3) and for centrosomes 92.05 ± 13.51, (n=5), 97.31 ± 10.19, (n=5) and 91.55 ± 5.765, (n=3) (Fig.33. E,F,G,H). That showed that centrosomes could be used as a reference for a direction of cell migration due to lack of statistically significant difference in nuclei and centrosomes pattern of migration over 2 hours when measurements were taken. Once the migration of control sample was described; fluorescently labelled ADEMTECH particles were injected into one cell stage embryos. Embryos were kept for 8 hours at 27 Celsius until they develop a body axis. Once the area of the first somite formation, was identified, and the presence of particles was confirmed, the movement of cells was recorded for half hour without applying the magnetic force. The migration pattern of these cells was not significantly different from the movement of uninjected cells. Then a force of 4 pN was applied for 30 min twice by placing the bar magnet from the direction of either head or the tail of embryos. The position of the magnet bar should orientate magnetic flux lines to parallel to the body axis. Last 30 min of the recording was taken again without the magnetic force. Then the change in migration pattern was calculated. To do that first I normalised cell migration angle to the body axis position using the following formula:

$$A=|(X-Y)| \text{ or } A=|(X-Y)-180|$$

Where A= relative angle of cell migration to the body axis, X= angle of migration and Y= angle of the body axis. 180 degrees were subtracted when the body axis was at

the bottom to unify measurements. As the last step, the mean of 18 measurements per the embryo was calculated. Then to calculate if the magnetic force had an impact on the cells' migration, mean of the angle of migration from the first time point was subtracted from every measurement.

$$A=|(X-Y)-R| \text{ or } A=|[|(X-Y)-180|-R]|$$

Where R= means of the angle from the first time point.

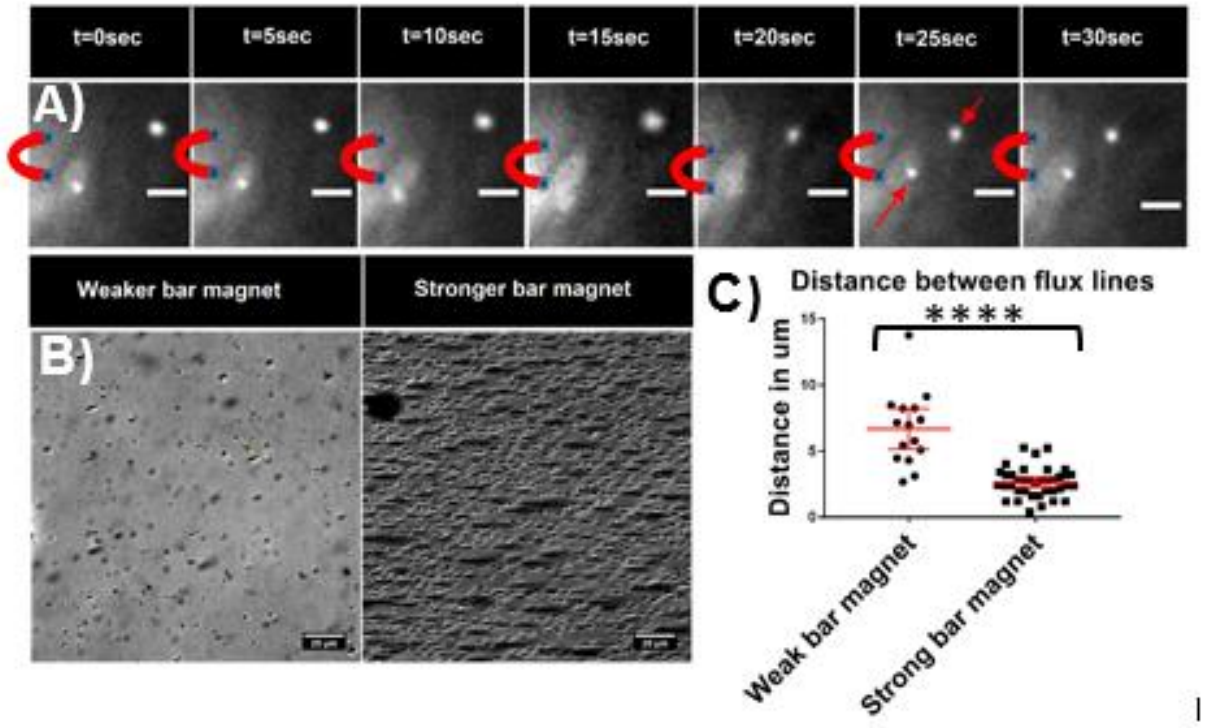

Fig. 30 Alignment of particles along magnetic flux lines. Panel A) shows the movement of two ADEMTECH magnetic particles within zebrafish embryo cells magnetic force was applied from left, as indicated by magnet icons, for 30 sec. Red arrows show the direction of movement of particles toward each other under the magnetic force, scale bar - 5 µm. Panel B) shows the alignment of magnetic particles when an iron magnet bar (weak) and a neodymium magnet bar (strong) were used scale bar = 25 µm, mean with 95% CI, P value<0.0001.

This experiment showed that in uninjected embryos, on the average, cells migration differ in the range of angles 16.82 ± 2.456, (n=8) without applying force, 21.07 ± 2.109, (n=13) when force is applied and 20.15 ± 2.406, (n=9) when the bar magnet was removed (Fig.34a). None of these differences was statistically significant one from the another (Fig.34c). Showing that the magnetic force does not alter the angle of the migration of the cells. From the other hand in cells containing fluorescently labelled magnetic particles change in the angle of migration was 17.57 ± 1.842, (n=11) without the magnetic force, 27.6 ± 2.151, (n=19) when the force was applied and 19.77 ± 1.581, (n=10) when the source of force was removed. Application of the magnetic force had

the significant impact of cells migration pattern when compared to both before and after force application (Fig.34b.c). What is a more important change in the migration pattern without magnetic force wasn't different in not injected control and injected samples, when the magnetic force wasn't applied but significantly changed in the injected sample when force was applied (Fig.34c).

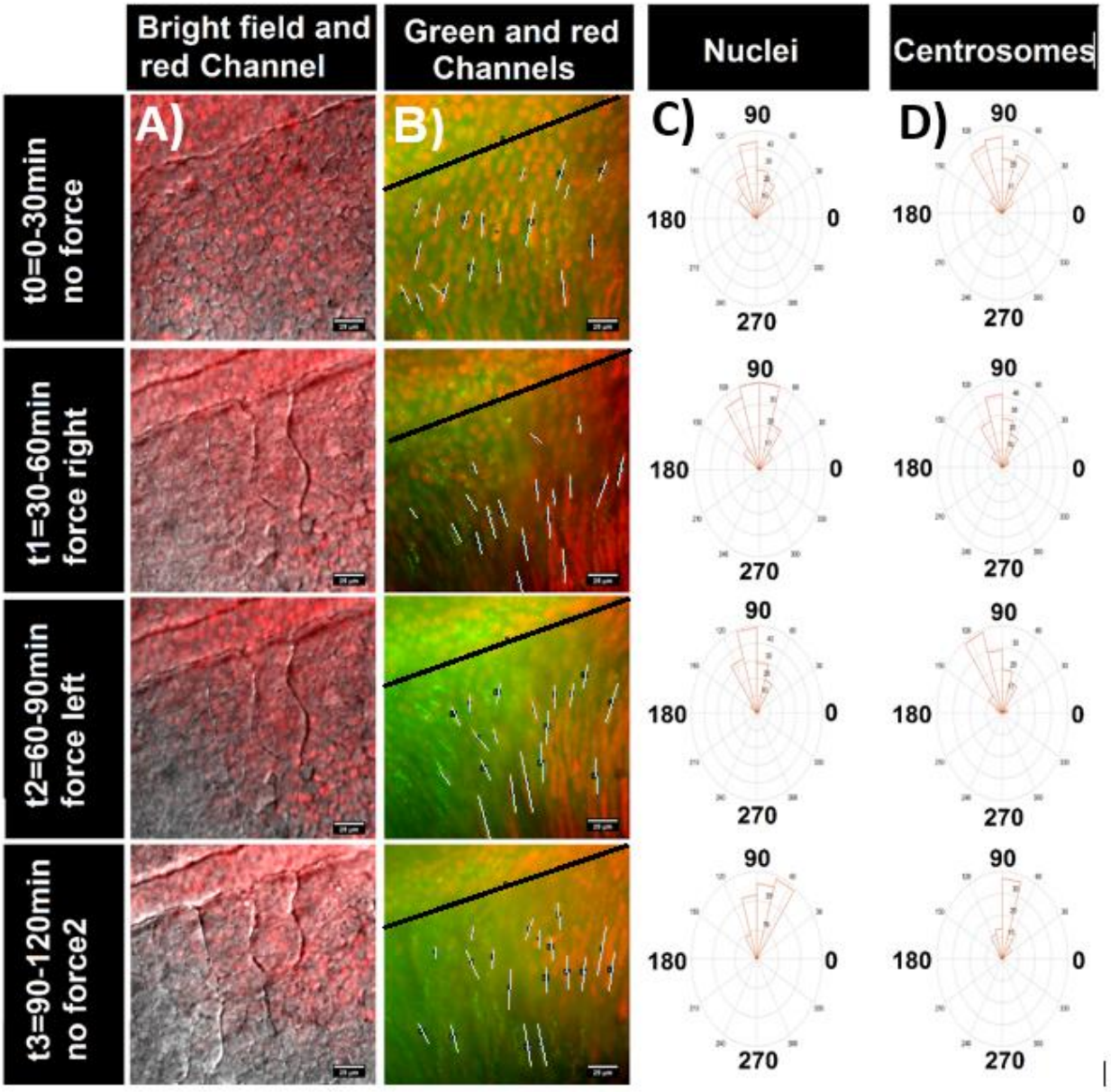

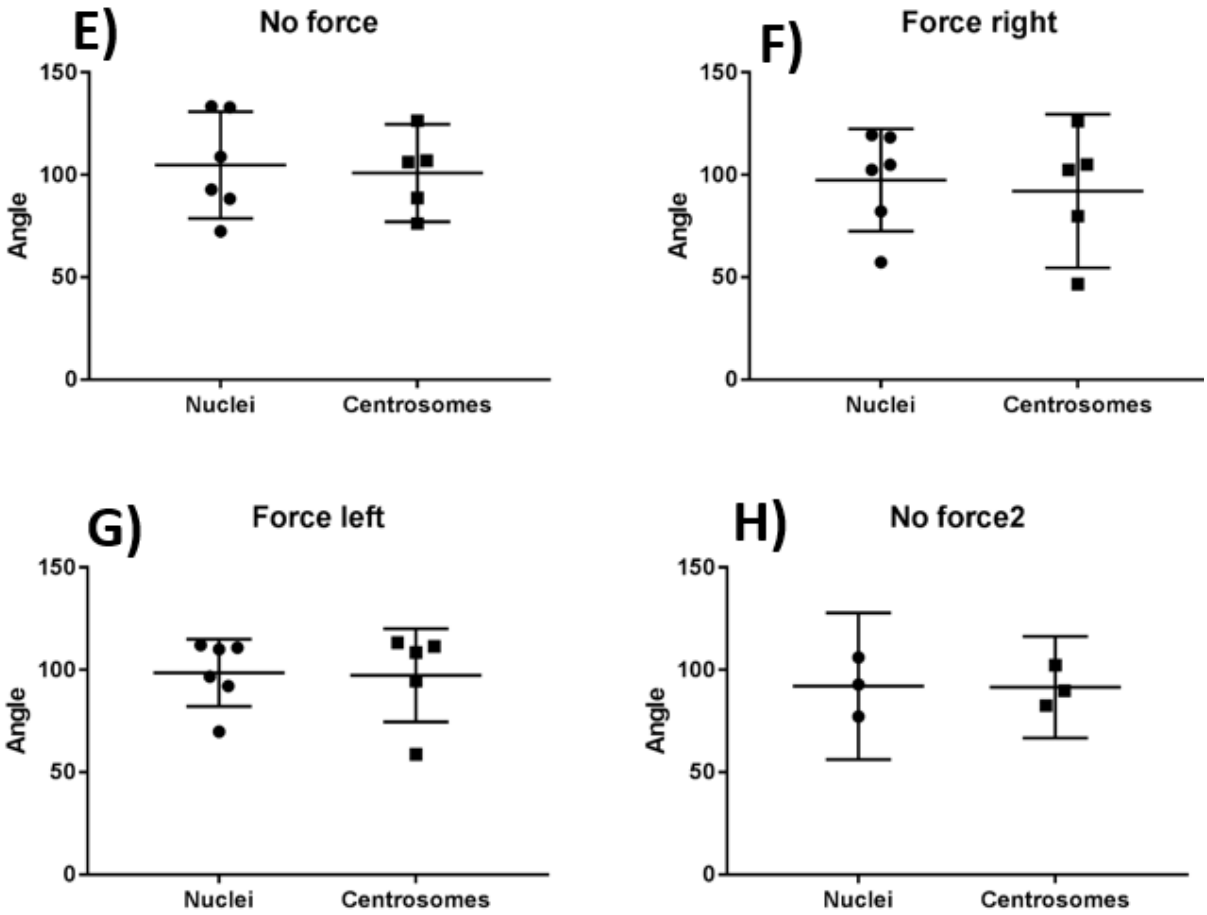

Fig. 31 Comparison of an angle of migration for nuclei (red) and centrosomes (green). Column A) shows the position of the body axis and the first somite. Column B) Shows MIP of a 30 min time-lapse recording of nuclei (red) and centrosomes (green) migration. The black line (1) shows the position of the body axis and icy blue lines show the example of measurements of nuclei migration angle. Column C) and D) shows rose plots of migration angle for nuclei C) and centrosomes D) standardised to the body axis position. Figures E), F), G) and H) show averages for the angle of migration per embryo for nuclei and centrosomes n=6 mean with 95% CI, scale bars - 25 µm.

This experiment showed that magnetic particles have the potential to affect cells migration during early development of the zebrafish embryo. Trying to find a mechanism through which it can happen I injected functionalised particles into Hippo pathway reporter zebrafish transgenic line (Miesfeld & Link, 2014). However, there was no a visible difference in GFP signal between cells containing magnetic particles and these which did not (data not shown).

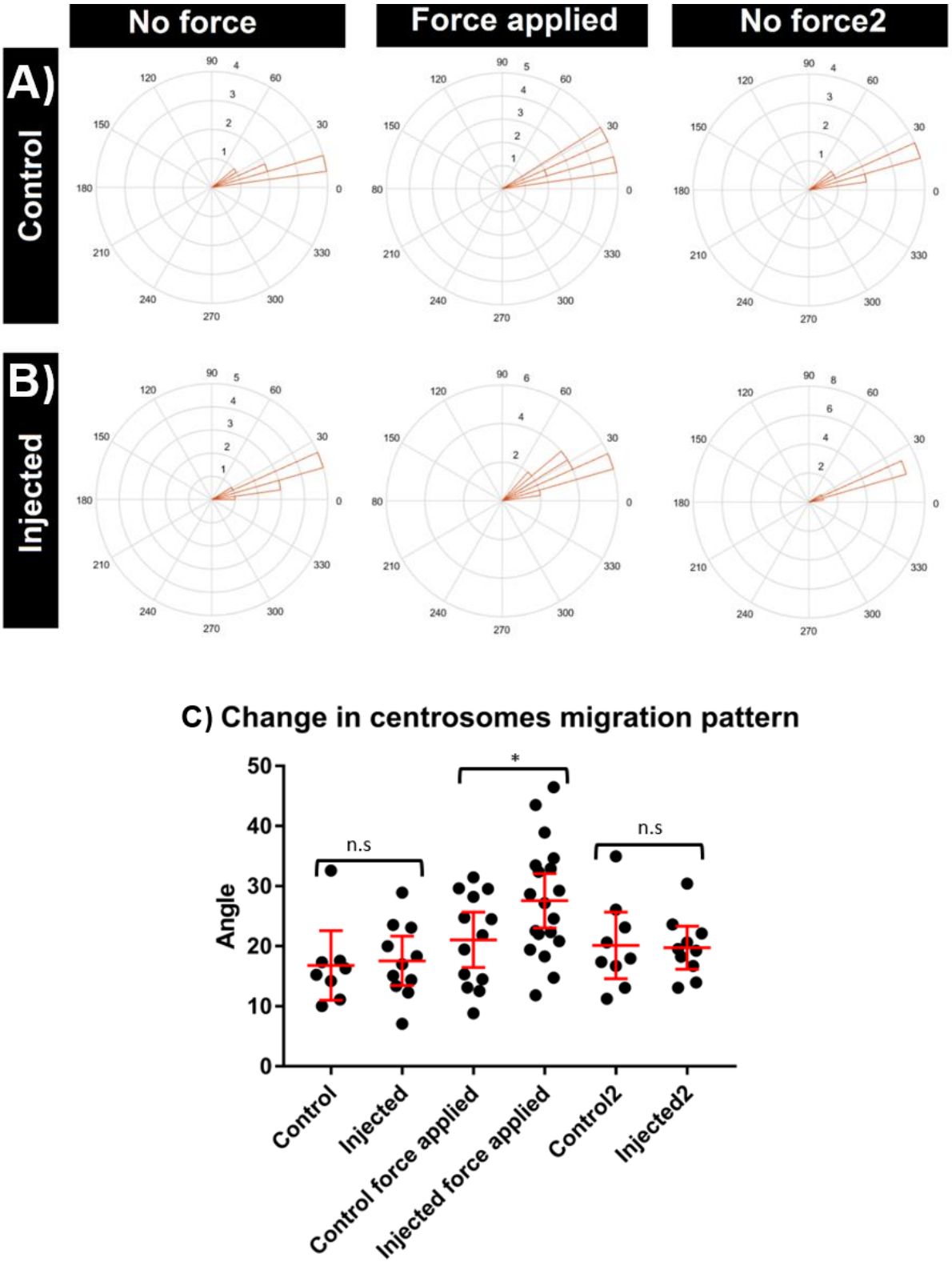

Fig. 32 A change in cells migration pattern under the magnetic force. Panel A) shows the angular change in a migration of cells (standardised to the migration when force was not applied) without application of the force (30min), with force (1 h) and again without the force (30min) for not injected samples. Panel B) shows results of the same experiment for injected samples (numbers above circles indicate the number of samples migrating in the specific range of angles). Panel C) shows plotted values for results from the experiment. P>0.05 control n=8 injected n=11 mean with 95% CI.

5.3 Discussion

Growing interest in an impact of mechanical forces in shaping life leads to constant discovery and development of scientific approaches. Using magnetism and magnetic particles gained a lot of attention in recent years (Desprat et al., 2008; Etoc et al., 2015; Master et al., 2015; Rotherham et al., 2017; Shah et al., 2017; Novakova et al., 2017; Wheeler et al., 2016). Previous research has shown that magnetic particles can be both assimilated by cells (Lee et al., 2011; Master et al., 2015; Shen et al., 2014; Steketee et al., 2011) or injected into cells *in vitro* (Etoc et al., 2013; Etoc et al., 2015) and successfully delivered to the higher organisms such as mice or chicken embryos (Kolosnjaj-Tabi, et al., 2013; Rotherham et al., 2017). In my research presented in this chapter both magnetic particles magnetosomes and ADEMTECH particles were shown to be successfully delivered to the developing zebrafish embryo and reminded within it until the first somite formation. Injection of particles did not cause higher mortality in zebrafish embryos what suggest that obtained data are not result of potential toxic effects of particles. Next, I have shown that exerting the force of 4pN on the particles is enough to cause rotation and “random” movement. It is possible that immobile particles were entangled in the cytoskeleton network or encapsulated within vesicles as it was shown in chapter 4 and literature (Apopa et al., 2009; Etoc et al., 2015; Master et al., 2015; Tay & Leong, 2014). However, the movement looks random, both without and with the application of the magnetic force, and most probably is caused by on rearrangement of organelles and cytoplasm within cells. My measurements showed however that movement happens much more often when the magnetic force is applied. It can be explained by that, and however particles aligned themselves with magnetic flux lines created by the magnet, a magnetic field gradient and force were not strong enough to pull particles toward the magnet (the role of the magnetic gradient will be discussed further in next chapter). Then I obtained a double transgenic line which nuclei was labelled in red by H2B fused with RFP and centrosomes labelled in green by GFP fused to centrin2. This line allowed me to track the cell movement during experiments and to measure the angle of their migration. Even I was not able to pull magnetic particles toward the source of the magnetic field within living cells it was reported that particles can still affect cells without visible movement of the particles (Master et al., 2015). Exerting the magnetic force on the magnetic particles was shown to have the impact on the cell migration *in vitro* (Shen

et al., 2014; Steketee et al., 2011). My observations confirm that cells migration angle change when the magnetic force is applied to zebrafish embryo cells containing magnetic particles. It is possible that my observations are a result of particles interacting with the cytoskeleton or activating a mechanosensing pathway such as the twist expression in Drosophila, but the mechanism is yet to be found (Apopa et al., 2009; Desprat et al., 2008; Master et al., 2015; Tay & Leong, 2014).

The interesting explanation arose from experiments conducted by Oster group in the 1990s on Fundulus epiboly (Weliky & Oster, 1990). In this research through mathematical modelling, they simplified the 2 dimensional model of Fundulus epiboly in silico. The authors showed that cell rearrangement during this stage of the development could be seen as a result of two forces: 1) mechanical stress resulting stretching or deformation of the cell sheet by external forces and (2) internally generated protrusive forces generated by an individually activated cell subpopulation (Weliky & Oster, 1990). In this model, the cell was simplified to contain only half of dozen contractile microfilaments, which when stretched beyond certain critical length respond by contracting too much shorter length than the equilibrium. Then cell were cloned into a blastula shape and one cell was contracted what triggered gastrulation of the model. What was even more amazing by changing “firing threshold” of the contractile filaments model run in the same fashion as the previous model, predicted creation of neural tube (Weliky & Oster, 1990). It is possible that migrating cells forming somite in my experiments reacted in a similar way to the exerted force as in the model prediction. That would highlight the importance of the mechanical forces I development even further.

Chapter 6. Electromagnetic tweezers set up

6.1 Introduction

Usage of an external magnetic force in biological research has become more popular and proved itself useful in various experiments investigating mechanical properties of cell and tissues (Bryan et al., 2010; Desprat et al., 2008; Etoc et al., 2015; Shen et al., 2014). Most of the research using magnetic particles uses bar magnets or a magnetic needle to elicit a response (Desprat et al., 2008; Etoc et al., 2013; Master et al., 2015; Shen et al., 2014). This is not the optimal method for high magnification imaging due to the micro-movements of the microscope stage when the magnet bar moved. I decided to develop an electromagnetic tweezer set up.

Electromagnets create a magnetic field due to electricity flow through solenoid made from electric conductor wrapped around an iron core. The first electromagnet was built by William Sturgeon in 1825. It was built from copper coil wired around an iron core through which electric current was passed. A long thin solenoid carrying an electric current generates a magnetic field very much like that of the bar magnet. The strength of the magnetic field depends on the number of coils and the electric current and is called e.m.f (electromotive force), and this relationship is shown by the formula:

$$e.m.f = IxN$$

Where I is the current in amperes and N is the number of coil turns. The magnetic field can be either uniform or have a gradient. In the uniform magnetic field, particles orientate themselves relative to North and South poles, whereas the gradient field can exert the translational force on the dipole (Fig.35).

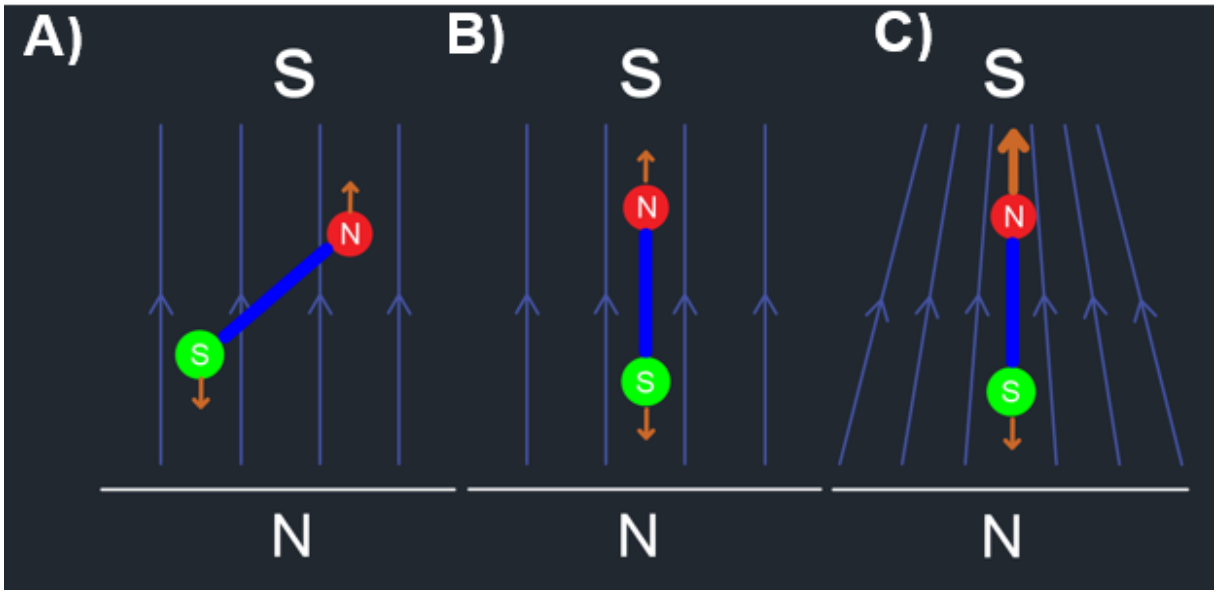

Fig. 33 The behaviour of a magnetic dipole in uniform and gradient magnetic fields. A) Uniform magnetic field is orientating the magnetic dipole. B) Forces on North and South pole balance. C) Gradient magnetic field is exerting the translational force on dipole with a stronger force on the North pole.

6.2 Design

The design of the electromagnetic tweezers contained two soft iron cores wrapped in two sets of solenoids. It allowed passage of current in two directions in a single magnet (Fig.36). This was necessary to generate creation both gradient and uniform magnetic fields. To design the electromagnetic tweezers, FEMM 4.2 software was used. To simulate experimental conditions, I measured dimensions of the Zeiss observer microscope were taken and applied to the model (Fig.36).

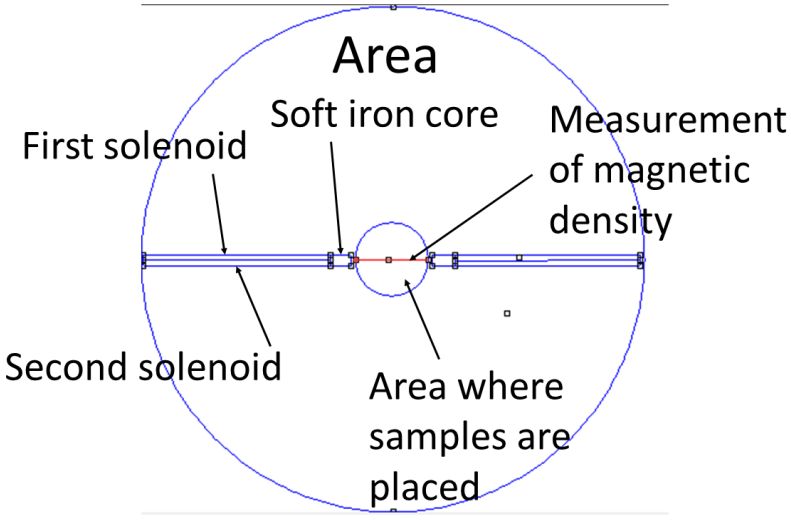

Fig. 34 The description of FEMM 4.0 simulated magnetic tweezers.

To fit on a microscope stage, magnets had to be 10 cm long, 3,5 cm apart where a µ-Dish can be placed. These dimensions were used in the simulation. I ran four separate scenarios with 200 coils per solenoid. Situation 1 - control without current (Fig.37), scenario 2 - one magnet on with 2 amps (Fig.37a), scenario 3 - two magnets with 2 amps current running in the same direction (Fig.37c), and scenario 4 - with two magnets with current running in opposite directions (Fig.37c). Then I measured the magnitude of magnetic flux density per each situation (Fig.37a,b,c). Estimates from simulations gave me magnetic flux density varying at peaks from 2 to 3 mT.

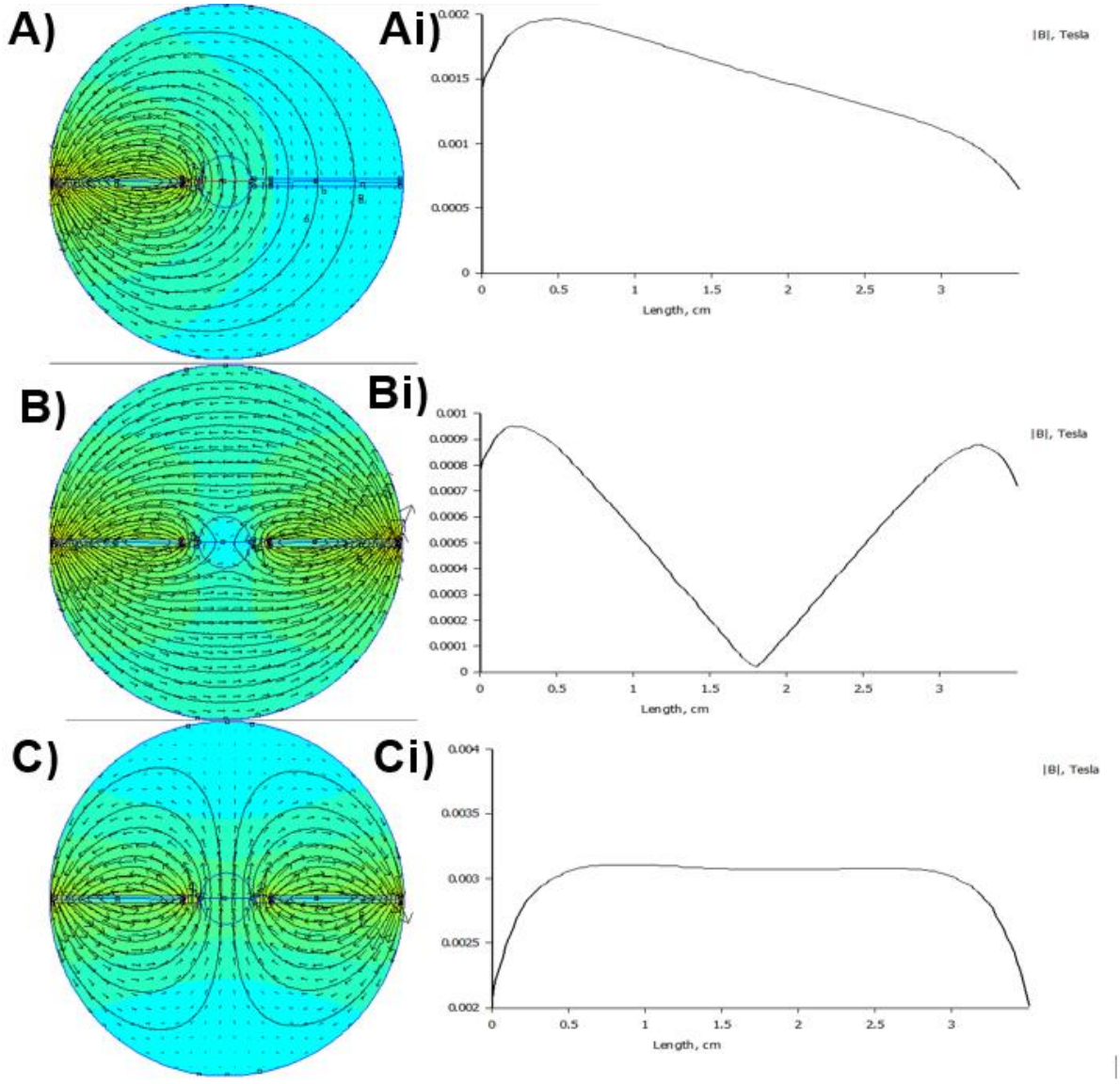

Fig. 35 FEMM 4.2 magnetic fields simulations. A) shows magnetic flux density when 2 amps current was run through the left magnet. B) shows magnetic flux density when 2 amps current was run through the left and right magnet in the same direction. C) shows magnetic flux density when 2 amps current was run through the left and right magnet in the opposite directions. Ai), Bi) and Ci) magnetic flux density in the are between magnets where samples are placed.

6.3 Results

Electromagnetic tweezers were constructed by Garry Turner, Chemistry Workshop Manager. The first test was to prove predictions from FEMM 4.2 simulation. For this purpose, I used a gaussmeter which allows for the magnetic flux density to be measured. The measurements were made next to the magnet and 3.5 cm away, which covers the distance in which samples could be placed.

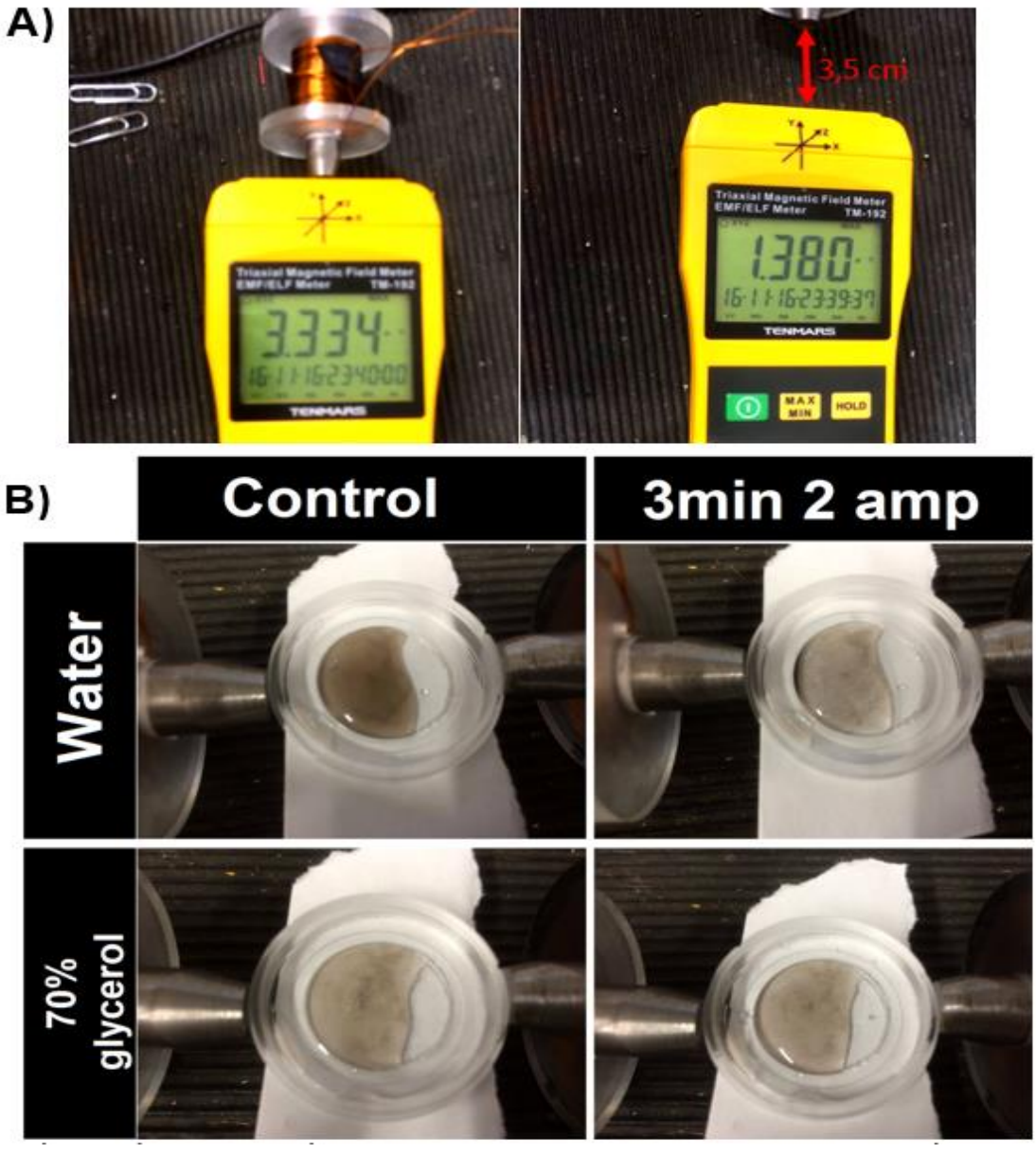

Fig. 36 Testing the electromagnetic tweezers prototype. Panel A) shows measurements of a magnetic flux density with a gaussmeter. Panel B) shows the reaction of magnetic nanoparticles suspended both in water and 70% glycerol in the magnetic field created with 2 amps running for 3 minutes through the electromagnet.

In agreement with the expectations of magnetic density flux next to the magnet was 3.33 mT and 3.5 cm away was 1.38 mT (Fig.38a). The behaviour of magnetic particles in macro-scale was observed both in water and 70% glycerol with 2 amp current over 3 minutes. Particles suspended in the water moved quickly towards the magnet, whereas particles suspended in 70% glycerol did not make any observable movements (Fig.38b). Subsequently, electromagnetic tweezers were installed on the Zeiss Observer microscope, and the reaction of the magnetic nanoparticles suspended both in water and glycerol was observed (Fig.39). Using current of 2 amps in the left magnet and 0.5 amp in the right I was able to move magnetic particles in 70% glycerol solution.

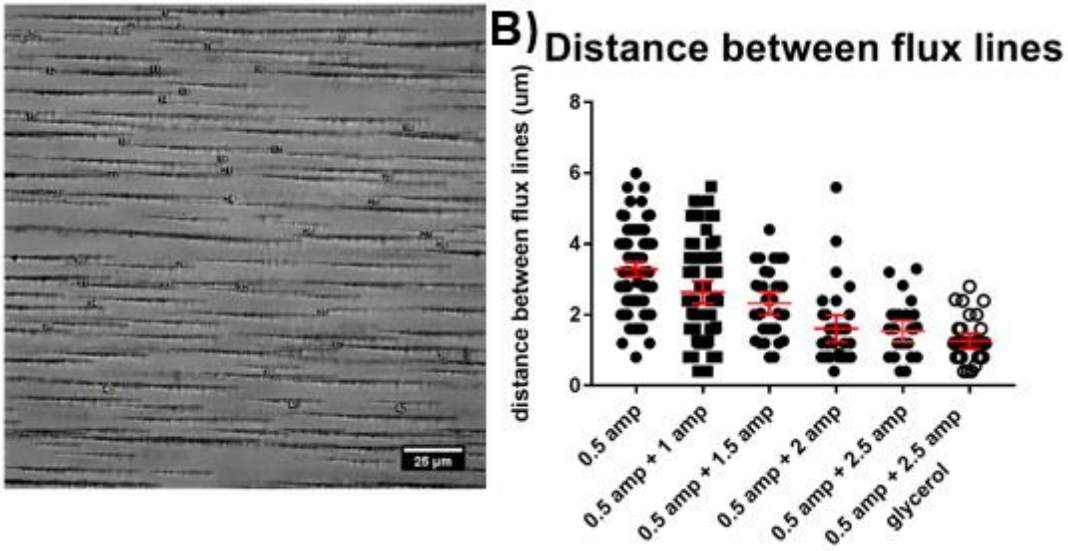

Fig. 37 Testing the magnetic tweezers on the microscope Panel A) shows the example of measurements using 0.5 and 1 amp setting. Panel B) shows distance measurement between magnetic flux lines created by different settings on the electromagnetic tweezers. Scale bar =25µm mean with 95% CI.

Experiments involving zebrafish embryos demand exposure to the magnetic field for a period of 30 to 60 minutes, which created a problem of overheating of the solenoids depending on the current running through them due to Joule heating. This is the heat released as a result of electrons passing through a conductor and is described with the formula:

$$P = (Va - V\mathrm{b})\mathrm{I}$$

Where P is power, (Va-Vb) is the voltage drop across the element, and I is the current travelling through the resistors or the other components. The temperature at 1 amp has risen to 35 Celsius degree in 79 minutes, at 1,25 amp in 22 minutes at 1,5 amp in 12 minutes and at 3 amp in 3,5 minutes. Cool down from 35 Celsius degree to room temperature took 49 minutes.

6.3 Discussion

In this chapter, I presented a process of developing of developing electromagnetic setup. The most significant advantage of this system is it's it customisation, which allows for adjustment of components and its strength. Additionally, this system would allow for turn on/off Application of magnetic force without inconveniences created by the placement of bar magnet such as small variability in distance of the sample from a source of the magnetic field and distortions in the plane of focus. Model created with FEMM 4.0 allows for prediction of system features and provides an easy way for alternating them, Generation of both uniform and gradient fields by two sets of solenoids generates a stronger field with the steeper gradient. It should allow forcing magnetic particles to move particles in high viscosity fluids mimicking the cytoplasmic environment. Usage of 2 amp with the right solenoid and 0.5 amp with the left caused particles to align with the magnetic field in 75% glycerol, but particles were pulled toward magnet until they formed long spikes, This could be solved by usage higher current as it directly translates to the strength of the electromagnet. It is possible to wire up more coils however space limitations created by microscope makes this solution less desirable.

On the other hand, increasing current leads to overheating of solenoids. The main concern is that a change in temperature affects the development of the embryo. The rapid increase in temperature caused by the rising current makes impossible to run these experiments for 1 hour. In literature, it is suggested that this problem can be overcome by installation air cooling system, but it would introduce the additional level of complexity to the system which is limited by the size of the microscope. Next proposed method is an instalment of a crowbar circuit (Cao et al., 2015). Crowbar circuit works like a fuse and reduces the oversupply of power. Further development of

electromagnetic tweezers is essential for establishing the system which will allow for obtaining more reproducible and quantifiable data.

Chapter 7 HDACs

7.1 Introduction

Cytoskeleton takes part in the vast amount of cellular events including adhesion, morphogenesis, migration, metabolism, apoptosis, division and differentiation. Core proteins of cytoskeleton such as actin and tubulin are some of the most conserved proteins across eukaryotic species. Yeast and human tubulin are 75% identical. Proteins of the cytoskeleton are divided into three main categories: microtubules (23nm diameter) composed of α- and β-tubulin; intermediate filaments (10nm diameter) including keratin, desmin, vimentin, lamin, synapsin and glial fibrillary acidic protein (GFAP) and microfilaments (6 nm diameter) which are composed of actin.

Tubulin microtubules play a crucial role in various cellular processes. To be able to to carry out multiple tasks, tubulin undergoes highly conserved posttranscriptional modifications which modify its properties and functions. To such modifications belong for example acetylation, deacetylation, detyrosination, glycylation or glutamination.

Acetylation of tubulin lysine 40 was shown to increase microtubule stability and their resistance to mechanical stress (Sadoul et al., 2016; Szyk et al., 2014). Acetylation and deacetylation of microtubules are suggested to have an impact on cell motility including migration in healthy cells and pathological ones (Westermann et al., 2003; Zuo et al., 2012). HDAC6 and Sirt2 are two well-known proteins responsible for microtubule deacetylation. What more both were localised in centrosomes as well as other proteins from HDAC family including HDAC1 and HDAC10 (Ling et al., 2012). Proteins from HDAC family are divided into four classes. Classes 1, 2, and 4 have a well-conserved zinc-dependent catalytic domain and less conserved accessory domains, with regulatory functions. Class 2 and 4 are tissue-specific while class 1 is expressed in a non-tissue specific manner. Class 1 and 4 HDACs are localised in the nucleus, while class 2 and 3 HDACs function both in the nucleus and in the cytoplasm (Menegola et al., 2006; Tong et al., 2002). Activity of HDAC proteins can be inhibited with non-specific inhibitors such as trichostatin A (TSA) or can be selectively inhibited with for example Cay-10603 for HDAC6 or AK-2 for Sirt2 (Bitler et al., 2017; Bobrowska et al, 2012; Dhanyamraju et al., 2015; Finnin et al., 1999).

HDAC1 belongs to class 1 HDACs and is localised in nucleus and centrosomes (Ling et al., 2012; Magnaghi-Jaulin et al., 1998). HDAC1 is an epigenetic regulator which through modulation of a chromatin plays role in development of tissues including for example the retina, central neuronal system and the ear (Dovey et al., 2010; Guo et al., 2007; Harrison et al., 2011; He et al., 2016; Magnaghi-Jaulin et al., 1998). Homozygotes of *hdac1*$^{-/-}$ in which protein is absent or dysfunctional are lethal in mice before day 10.5 of embryonic development and before day 5 of development in zebrafish (Harrison et al., 2011; He et al., 2016). Furthermore, *hdac1*$^{-/-}$ zebrafish larvae resemble ciliary zebrafish phenotype which is characteristic body curvature. What more it was reported to impair the development of hair cells in zebrafish ear as well as lead to the creation of smaller otoliths (He et al., 2016).

HDAC6 and HDAC10 belong to class 2b of HDACs. HDAC6 is a well-described deacetylase. Unlike other HADC proteins HDAC6 forms complexes with the proteins involved in transcription (Tat, β-catenin, p300), cell signaling (GRK2, GSK3β,PCKα), inflammation (Foxp3, NF-kappaB), protein degradation (VCP, PLAP, Hsp90. HIF1α, TRIM50), cell survival (Ku70. Bax, CYLD, PP1, G3BP1, surviving), angiogenesis (Hsp90. HIF1α, EB1), cell motility (tubulin, contractin, dynein) and cilia reabsorption (AuroraA) (Aoyagi & Archer, 2005; Hook et al., 2002; Kaluza et al., 2011; Li et al., 2013; Matsuyama et al., 2002; Pugacheva et al., 2007; Riolo et al., 2012; Tang et al., 2007; Zhang et al., 2007; Zhang et al., 2008). HDAC6 contains three domains: catalytic domain 1, catalytic domain 2 and C-terminal Zinc-finger domain (ZnF-UBP). The first catalytic domain was shown to have low enzymatic activity in deacetylation of acetylated tubulin and the second domain to has been proved to be the key player in the process (Miyake et al., 2016). Loss of catalytic activity of HDAC6 was shown to affect mouse behaviour. The behaviour was resembling one caused by anti-depressants (Fukada et al., 2012).

Even though little was known about HDAC10 function, this protein was connected with poor prognosis of lung cancer (Pang et al., 2010). HDAC10 is lacking the second of catalytic domains with the first one being almost identical with the catalytic domain of HDAC6 what made it a good candidate for being possibly redundant with HDAC6 (Tong et al., 2002). Recently it was shown that HDAC10 is polyamine deacetylase (PDAC) and acetylated tubulin isn't its subtract (Hai et al., 2017).

Sirt2 - NAD+-Dependent Tubulin Deacetylase is the second, other than HDAC6, a well-described protein able to deacetylase microtubules and belongs to class 3 HDACs

(North et al., 2003). This protein is a homolog of yeast Sir2 protein (North et al., 2003). Sirt2 has been shown to be present in the centrosome and affect its duplication cycle as well as to play a role in cilia maintenance (Forcioli-Conti et al., 2016; Zhou et al., 2014). Furthermore, dysfunction of this protein is affecting neuronal growth and is suggested to have an impact on the development of neurodegenerative diseases such as Parkinson's disease (Outeiro et al., 2007). This protein has also been shown to have a role in metabolism as it deacetylases Glucose-6-phosphate dehydrogenase (G6PD) which is a key enzyme in the pentose phosphate pathway (PPP). Its function is crucial in the oxidative stress response as it produces NADPH, the main intracellular reductant (Wang et al., 2014).

7.2 Results

*Hdac*6 mutants were created with TALEN, and three alleles were identified *Hdac6*^{sh398}: 2bp deletion, Hdac6^{sh399}: 8bp deletion and *Hdac6*^{sh400}: 14bp deletion. Homozygotes were viable and upon rising to adulthood did not display any obvious phenotypes (Fig.40a). *Hdac6* 14 bp deletion caused frameshift and occurrence of the stop codon in first domain at position 94aa of 1081aa (Fig.40c). HDAC6 and HDAC10 proteins share almost identical catalytic domain 1 what made it possible that HDAC10 can deacetylase tubulin (Hai et al., 2017). Thus to assumed redundancy with HDAC10. *Hdac10* mutated fish were generated with CRISPR technology. Introduced deletion of an 11 bp caused the frameshift and stop codon in first domain at position 147/676aa (Fig.40c). Homozygotes of these fish were viable and not affected by mutation as well (Fig.40a). Through crossing *hdac6*$^{-/-}$ with *hdac10*$^{-/-}$ fish double heterozygotes and later double homozygotes were obtained and identified. Double homozygotes did not display any abnormalities as well (Fig.40a). Therefore it was decided to inject CRISPRs for the *sirt2* gene in double homozygote background to create triple mutants. The introduced mutation included a 24 bp addition and a deletion of 2 bp causing the appearance of a stop codon at position 43 aa of 379 aa (Fig.40c). The work introduced in this paragraph has been done by Dr Niedharsan Pooranachandran.

Then triple heterozygote was identified and outcrossed with double homozygote of *hdac6* and *hdac10*. Their offspring were screened for *sirt*2$^{+/-}$ *hdac6*$^{-/-}$ and *hdac10*$^{-/-}$. Once found in crossed what let to the generation of triple mutant. They did not display any obvious phenotype either was fertile and survived to adulthood (Fig.40a).

Hdac1$^{+/-}$ fish curly body phenotype is often seen in ciliary mutants and its presentence in centrosomes made this gene another candidate in the unrevealing role of Hdac6. The mutated fish were obtained from Dr Vincent Cunliffe (Harrison et al., 2011). They were outcrossed with double *hdac6*$^{-/-}$ *hdac10*$^{-/-}$. Since HDAC1 homozygotes display a clear phenotype in early development (Fig.41a) I identified offspring caring mutation in *hdac1* gene by in crossing them, and positive fish were screened for mutations in *hdac6* and *hdac10* genes.

Due to obvious phenotype displayed by *hdac1*$^{-/-}$ zebrafish larvae (Fig.41b) and presented evidence in the literature of HDAC1 being localised in centrosomes (Ling et al., 2012), identified *hdac1*$^{-/-}$ and their siblings were stained for acetylated tubulin and γ-tubulin. Staining of 3 dpf larvae revealed abundant ectopic cilia present around developing ear and cilia present in the lens of the mutant. These cilia rarely appeared in controls (Fig.41). However, there was a possibility that this phenotype is just a consequence of developmental retardation. Therefore, I stained *hdac1*$^{-/-}$ larvae at 1 and 2 dpf. Results of this staining strongly suggest that observed differences between mutants and the siblings were the consequence of slower development (Fig.41). Phenotypes at day 1 from *hdac1* mutants and wild-type did not differ and mutant embryos at day 2, and 3 resemble mutated samples from day 1 (Fig.41). This interpretation is further supported by clear underdevelopment of the whole ear, which remains an empty vesicle, does not develop columns that in wild-type delimit semi-circular canals and reabsorb cilia from the surface of epithelial cells. Development of eye is impaired as well what causes that cilia in lens remain (He et al., 2016; Yamaguchi, 2005). Given these observations, I conclude that presentence of cilia is also caused by the developmental delay.

Due to a lack of phenotype in *hdac6*$^{-/-}$, *hdac10*$^{-/-}$ and *hdac6*$^{-/-}$ *hdac10*$^{-/-}$ double mutant fish I checked possible redundancy between HDACs using Trichostatin A (TSA). This drug is well known for nonspecific inhibition of all HDACs (Brehm et al., 1998; Finnin et al., 1999; Miyake et al., 2016). High dose of the drug (200nM) results in blood circulation defects, abnormal tail curvature, heart oedemas and in the most severe cases embryonic death (He et al., 2016). These phenotypes were most

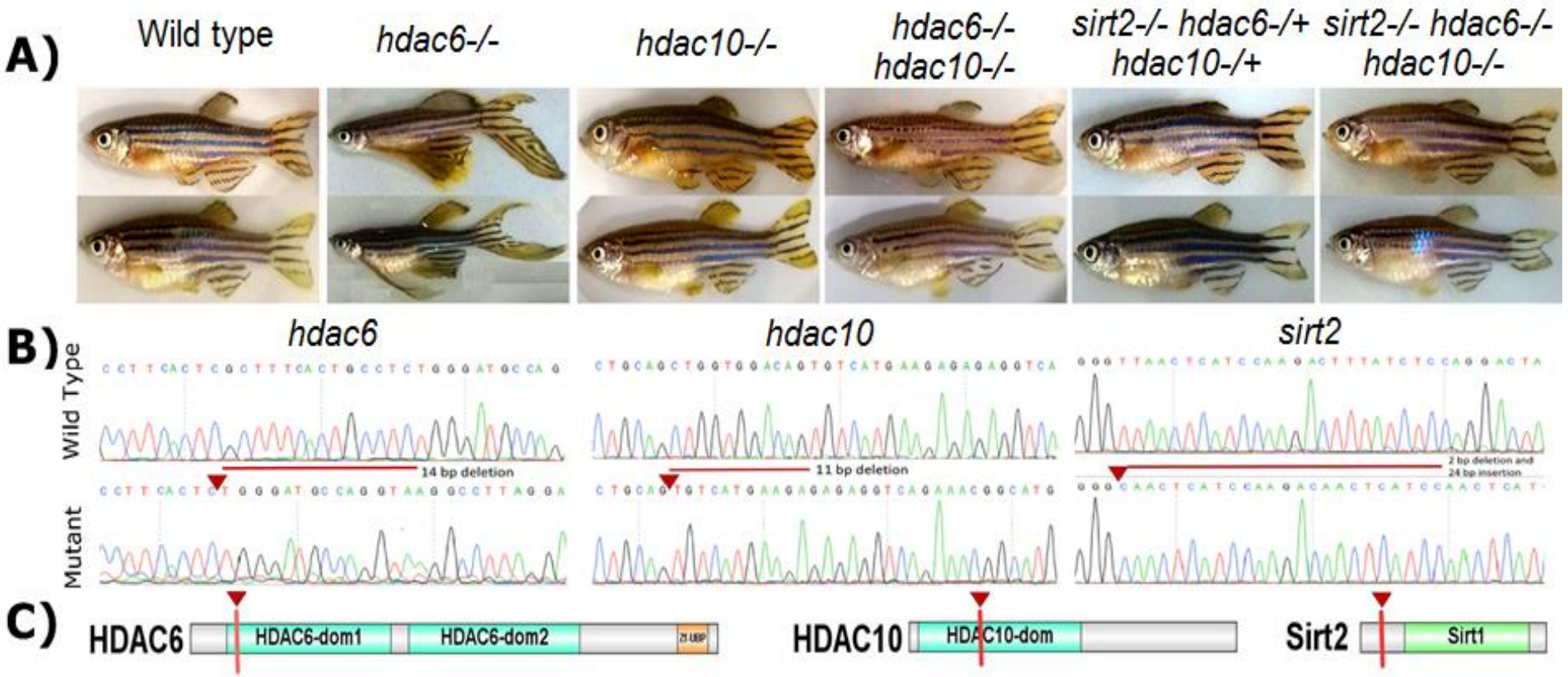

Fig. 38 Adult Zebrafish do not display any obvious external phenotype. A) Images of adult fish; neither single, double or triple mutants do display any abnormalities. Upper panel shows males lower females. B) Comparison of wild-type and mutated sequences for HDAC6, HDAC10 and Sirt2. Sirt2 and HDAC10 mutations were introduced with the CRISPR technique, HDAC6 with TALEN. Changes in original sequences are underlined C) Schematic representation of proteins of interest – red arrowhead shows premature stop codon caused by mutation.

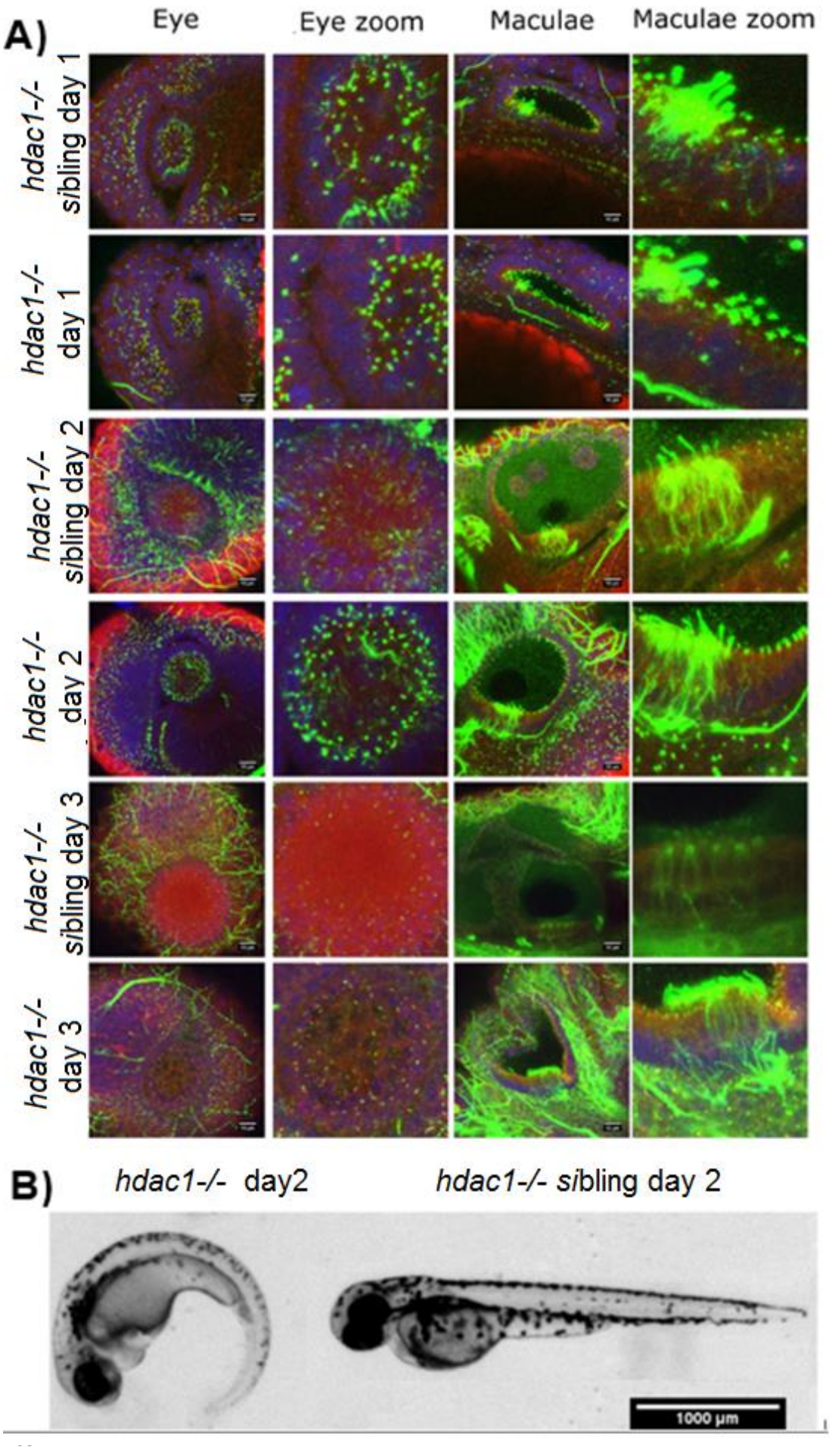
A)
Eye
Eye zoom
Maculae
Maculae zoom
hdac1-/- sibling day 1
hdac1-/- day 1
hdac1-/- sibling day 2
hdac1-/- day 2
hdac1-/- sibling day 3
hdac1-/- day 3
B)
hdac1-/- day2
hdac1-/- sibling day 2
1000 µm

Fig. 39 HDAC1 acetylated tubulin (green) and γ-tubulin (red) immunostaining. Panel A) shows 1,2 and 3 days old *hdac1*$^{-/-}$ and their siblings were stained for acetylated, γ-tubulin and DAPI (blue). The first column shows 12μm deep MIP of ZStack of the eye. The second column shows the lens. Third shows ear and surrounding tissues. Forth shows the zoomed area of the macula. Panel B) shows the external phenotype of *hdac1*$^{-/-}$ fish on day 2 on the left and control sibling on the right. Scale bar - 25 μm for panel A) and 1000 μm for panel B) n=3.

probably the result of HDAC1 inhibition (Fig.41). A dose of 50nM did not cause any visible differences including heart size (Fig.42).

I checked possible changes on the cellular level using immunostaining for acetylated tubulin in mutated fish. The expected outcome of these mutations increased in acetylated tubulin within the cells (Hubbert et al., 2002). Immunostaining confirmed that it is indeed the case, a however unexpected finding was made in triple mutant fish. I found that a subset of cilia in cristae and macula was hypoacetylated (Fig.43). This phenotype was never reported *in vivo* (Fukada et al., 2012; Zhang et al., 2008). To check the magnitude of change or if it is followed by any abnormalities in cilia I counterstained cilia with anti-glutaminated tubulin antibodies GT335 (Bobinnec et al., 1998) as a reference for changes in ciliary tubulin acetylation staining signal upon the absence of Hdac6, Hdac10 and Sirt2. This experiment has shown the significant drop in acetylation in cilia in the ear (cristae and maculae), but nasal cilia ware not affected (Fig.44a,b). With the data from the triple mutant, I decided to track down if double mutant of *hdac6*$^{-/-}$ and *hdac10*$^{-/-}$ and the single mutant of *hdac6*$^{-/-}$ will show the same drop in acetylation in cilia. Staining larvae of these genotypes have proven that loss of Hdac6 protein by itself is enough to cause hypoacetylation of cilia phenotype in the ear (Fig.44a,b). The next step was to check if this phenotype was observed due to the loss of deacetylase enzymatic activity and not other potential functions. For this reason, a specific HDAC6 inhibitor, CAY10603, was used on wild-type embryos (Bitler et al., 2017; Dhanyamraju et al., 2015). The phenotype recapitulated the mutant phenotype, hinting that the phenotype is strictly dependent on Hdac6's catalytic abilities and not due to other possible functions. To gain insight into the mechanism underlying this phenotype, I decided to treat larvae with the drug at days zero, one, and two dpf to check whether the phenotype depended on the timing of HDAC inhibition. The results have shown that only embryos treated from day 0 had the significant drop in acetylation of cristae cilia (Fig.45). CAY10603 data were obtained with Erasmus student - Katarzyna Zielonka.

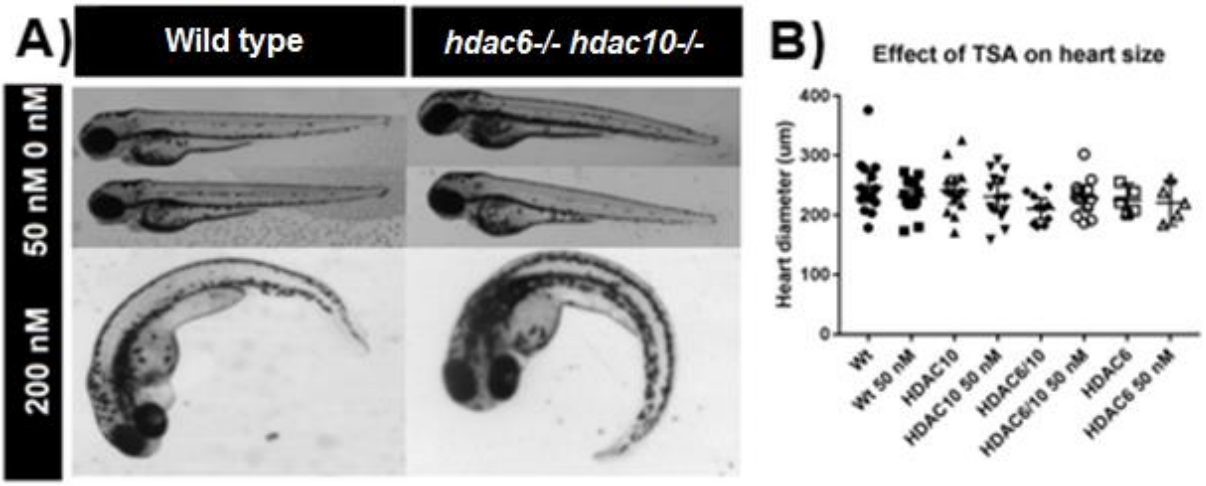

Fig. 40 Effect of TSA on HDACs mutant fish larvae. Panel A) shows zebrafish embryos phenotypes exposed to DMSO, 50 nM and 200nM concentration of TSA from both wild-type and double mutant *hdac6*$^{-/-}$ *hdac10*$^{-/-}$ background. Panel B) shows measurements of heart diameters for control and mutants fish. n=3 mean with 95% CI.

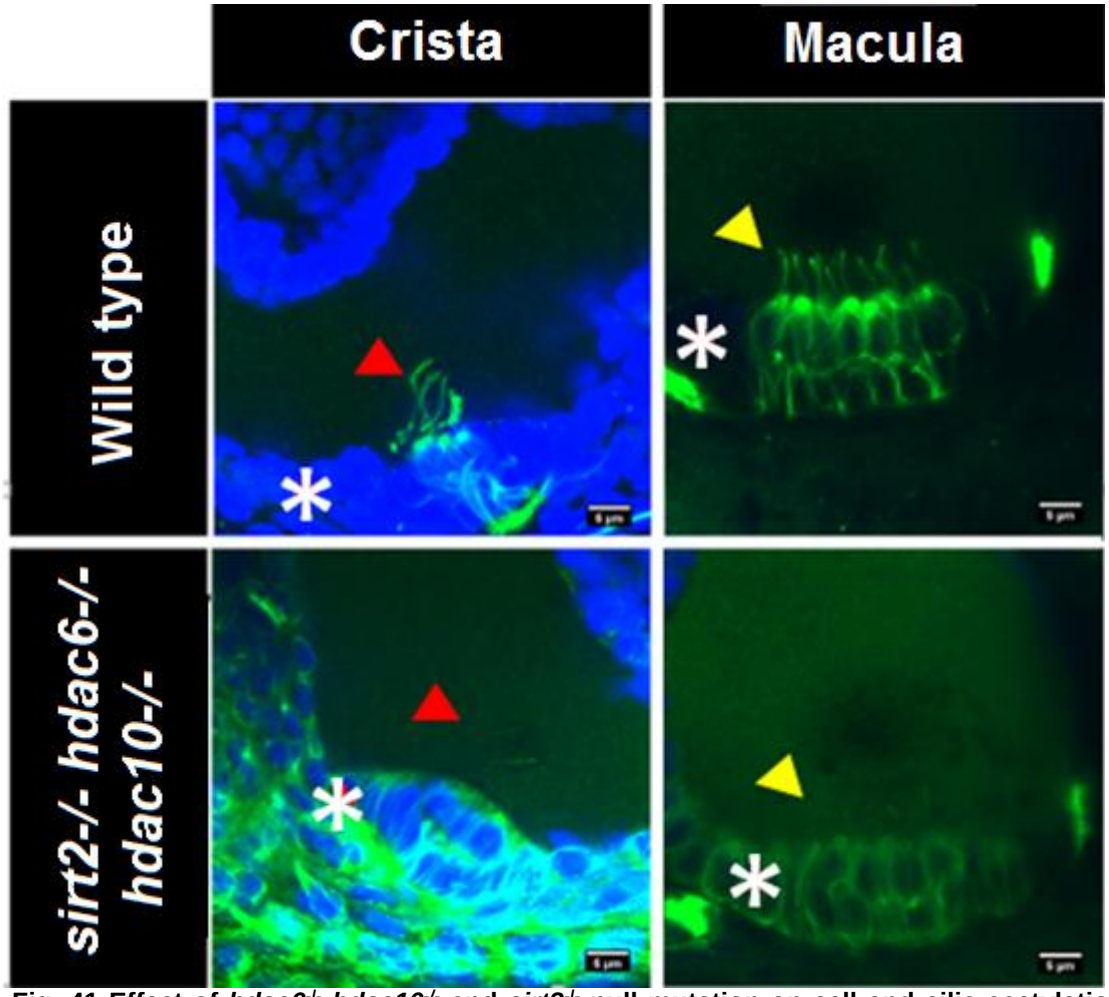

Fig. 41 Effect of *hdac6*$^{-/-}$ *hdac10*$^{-/-}$ and *sirt2*$^{-/-}$ null mutation on cell and cilia acetylation. Red arrowheads show cilia in criste in wild-type and hypoacetylation of tubulin (green) in cilia in triple mutant. Yellow arrowheads show cilia in the macula. Asterisks show increased acetylation in cells. DAPI nuclei counterstaining (blue). Scale bar - 5 µm.

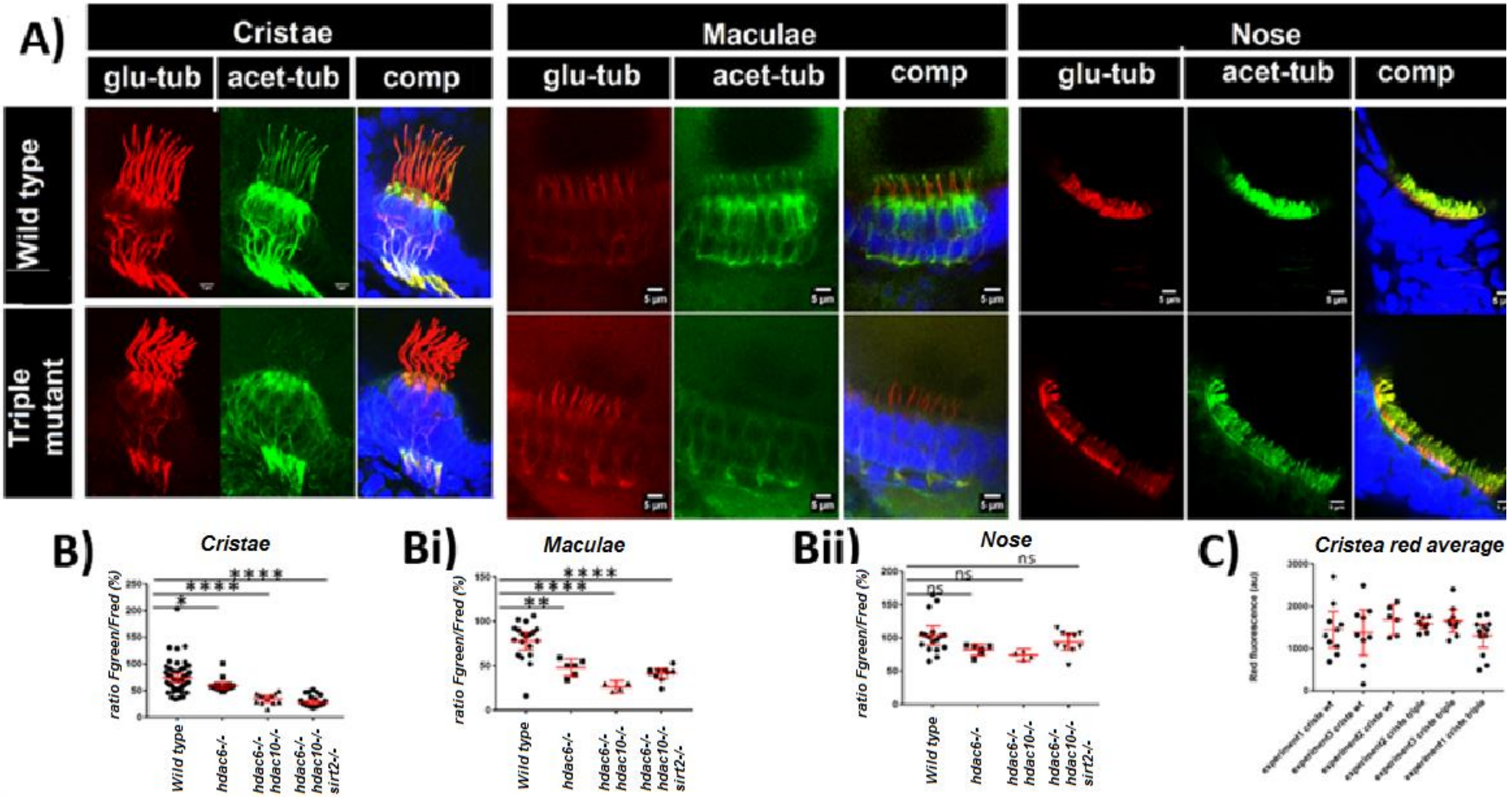
A)
Cristae
Maculae
Nose
glu-tub
acet-tub
comp
Wild type
Triple mutant
B)
Cristae
ratio Fgreen/Fred (%)
Wild type
hdac6-/-
hdac6-/- hdac10-/-
hdac6-/- hdac10-/- sirt2-/-
Bi)
Maculae
Bii)
Nose
ns
C)
Cristea red average
Red fluorescence (au)

Fig. 42 Fig. Role of HDACs in cilia acetylation. Panel A) shows cristae, maculae and nose cilia stained for glutaminated tubulin (red), acetylated tubulin (green) and nuclei (blue) for both wild-type and the triple mutant of *hdac6*$^{-/-}$, *hdac10*$^{-/-}$ and *sirt2*$^{-/-}$. Panel B) shows relative acetylation to the glutamination ratio of signal strength for *hdac6*$^{-/-}$ mutant, *hdac6*$^{-/-}$ *hdac10*$^{-/-}$ double mutant and *hdac6*$^{-/-}$ *hdac10*$^{-/-}$ *sirt2*$^{-/-}$ triple mutant in cristae, Bi) maculae, Bii) nose. Panel C shows the comparison of red signal strength across three experiments. Mean with 95% CI, P<0.05 and P<0.0001 statistical significance – student T.Test. Scale bar - 5 µm.

I tried to find if similar phenotype existed in nasal and retinal cilia. For this reason, 15 µm cryosections of 5 dpf embryos, treated with 0.1 mM PTU, were prepared and stained for acetylated tubulin and nuclei. This revealed that mutant cilia in the retina are hypoacetylated (Fig.47). Furthermore, staining of acetylated tubulin, Gfap and glutamine synthesise displayed abnormal morphology of glial cells in the retina. Images of stained cryosections of retina show lack of acetylation of tubulin in axons (Fig.47b). However, additional experiments are required to prove these suggestions as adult vision does not seem to be affected.

Lastly, I checked if hypoacetylation of cilia on hair cells in maculae and cristae have an impact on adult fish behaviour. Studies have shown that tubulin acetylation has serious implications for microtubules rigidity and endurance to mechanical stress. (Portran et al., 2017; Szyk et al., 2014). These studies suggested that hypoacetylated of microtubules in cilia, can lower their resistance to mechanical stress and make them more susceptible to damage upon the bending. Hair cells in cristae and maculae are responsible for both hearing and balance (Nicolson, 2005, 2017). Due to the presumed fragility of hypoacetylated cilia, I expected to see balance problems in the mutants. To check this possibility, I performed a drop test on 1,5 years old fish and recorded their swimming pattern for 10 minutes. This revealed that *sirt2*$^{-/-}$ zebrafish mutants exhibited different swimming patterns, namely they did not show exploratory behaviour which was demonstrated by other genetic backgrounds and control. *Sirt2*$^{-/-}$ mutated fish spend significantly more time on the bottom of the tank (Fig.49). However, measurements did not show significant differences in swimming speed (Fig.49c). What that may suggest that difference is not due to physical factors but rather neurological as Sirt2 was shown to effects neurons development (Melchor & Strickland, 2006; Satoh et al., 2017; Wang et al., 2017).

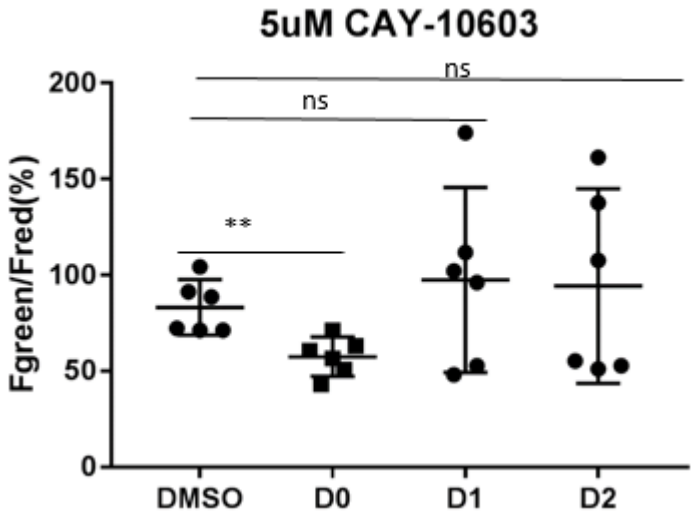

Fig. 43 Inhibition of HDAC6 with 5 uM CAY-10603 impact on the ratio between acetylation to glutamination in cristae in 3-day old embryos. Acetylation (green), glutamination (red) P<0.01 statistical significance – student T.Test n=6 mean with 95% CI.

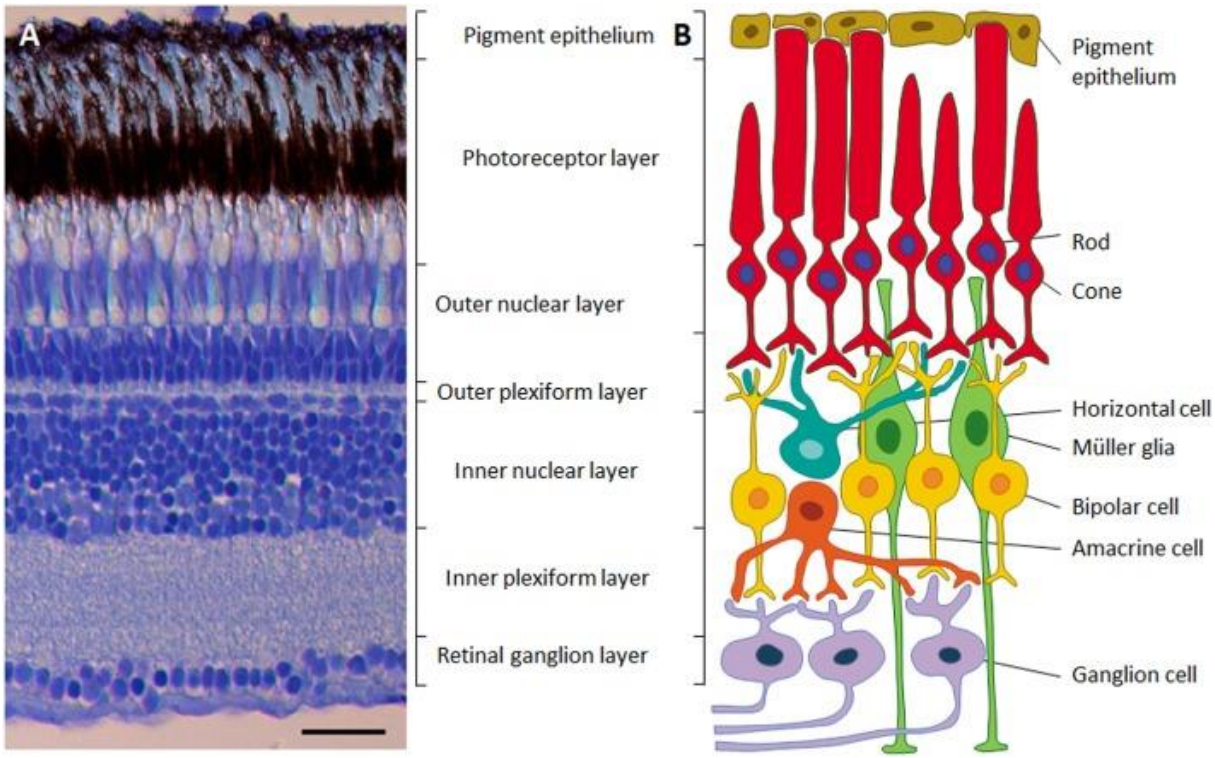

Fig. 44 Structure of the retina. A) Microphotograph of a cross-section through the retina of an adult zebrafish, showing the different cellular and synaptic retinal layers. B) Diagram of the neural circuit of the retina, showing the six neuronal cell types and the two supporting cell types (Müller glia and retinal pigmented epithelium). In A, the scale bar- 25µm (Gramage et al., 2014).

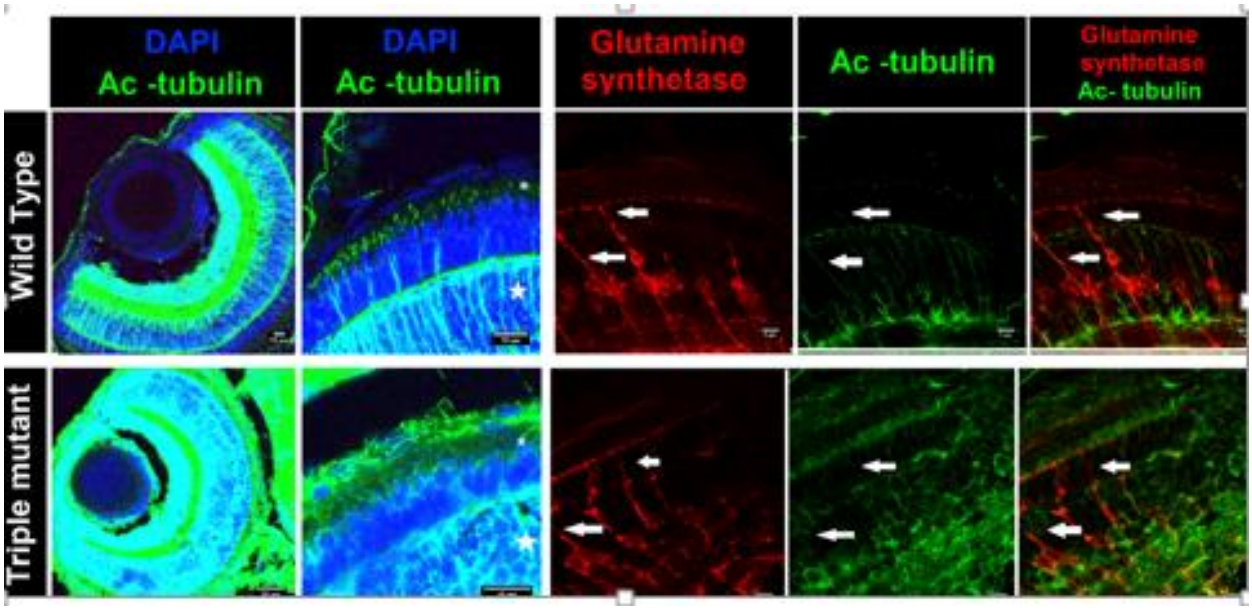

Fig. 45 Effect of mutation in *hdac6*$^{-/-}$ *hdac10*$^{-/-}$ and *sirt2*$^{-/-}$ on cilia in retina and axons acetylation in Muller glia. Panel A) shows double staining for acetylated tubulin (green) and nuclei (DAPI blue) in wild-type retina of 5 days old zebrafish embryos of wild-type and triple mutant. White asterisk shows the photoreceptor layer where cilia are present. White stars show Inner nuclear layer where Muller glia and bipolar cells axons are present. Panel B) shows staining for glutamine synthetase (red) and acetylated tubulin (green). White arrows show muller glia and corresponding tubulin acetylation.

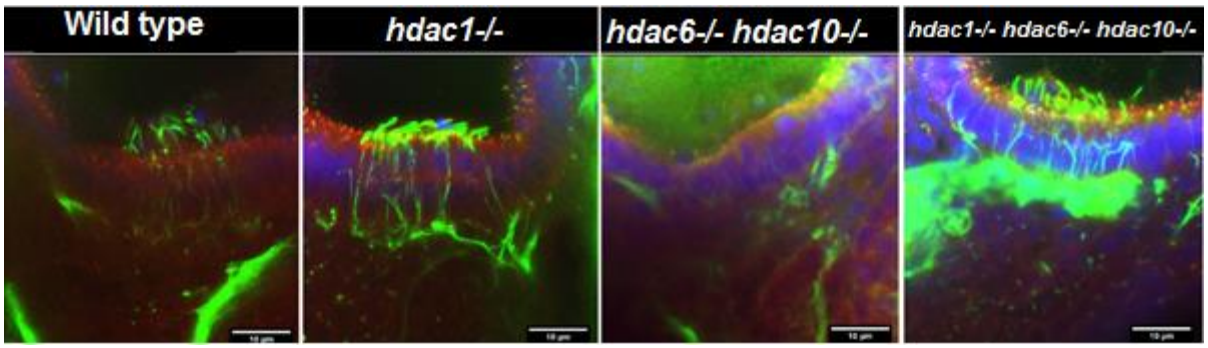

Fig. 46 Immunostaining for cilia and acetylated tubulin (green) and gamma-tubulin in centrosomes (red) in maculae in *hdac1*$^{-/-}$ *hdac6*$^{-/-}$ *hdac10*$^{-/-}$ triple mutant. Scale bar - 10 µm.

Then, I investigated if hypoacetylation phenotype will affect ectopic cilia acetylation, which I have seen around maculae in *hdac1* mutants. For this reason, I generated triple mutants *hdac1*$^{-/-}$, *hdac6*$^{-/-}$ and *hdac10*$^{-/-}$ by outcrossing *hdac6*$^{-/-}$ and *hdac10*$^{-/-}$ homozygote mutant with *hdac1* heterozygote mutant. The offsprings were incrossed to identify fish carrying *hdac1*$^{-/-}$ mutation. Then remaining 75% was raised to adulthood and incrossed to identify triple mutants. Preliminary results from staining triple mutants for acetylated tubulin in cilia were intriguing as they suggest that removal of Hdac1

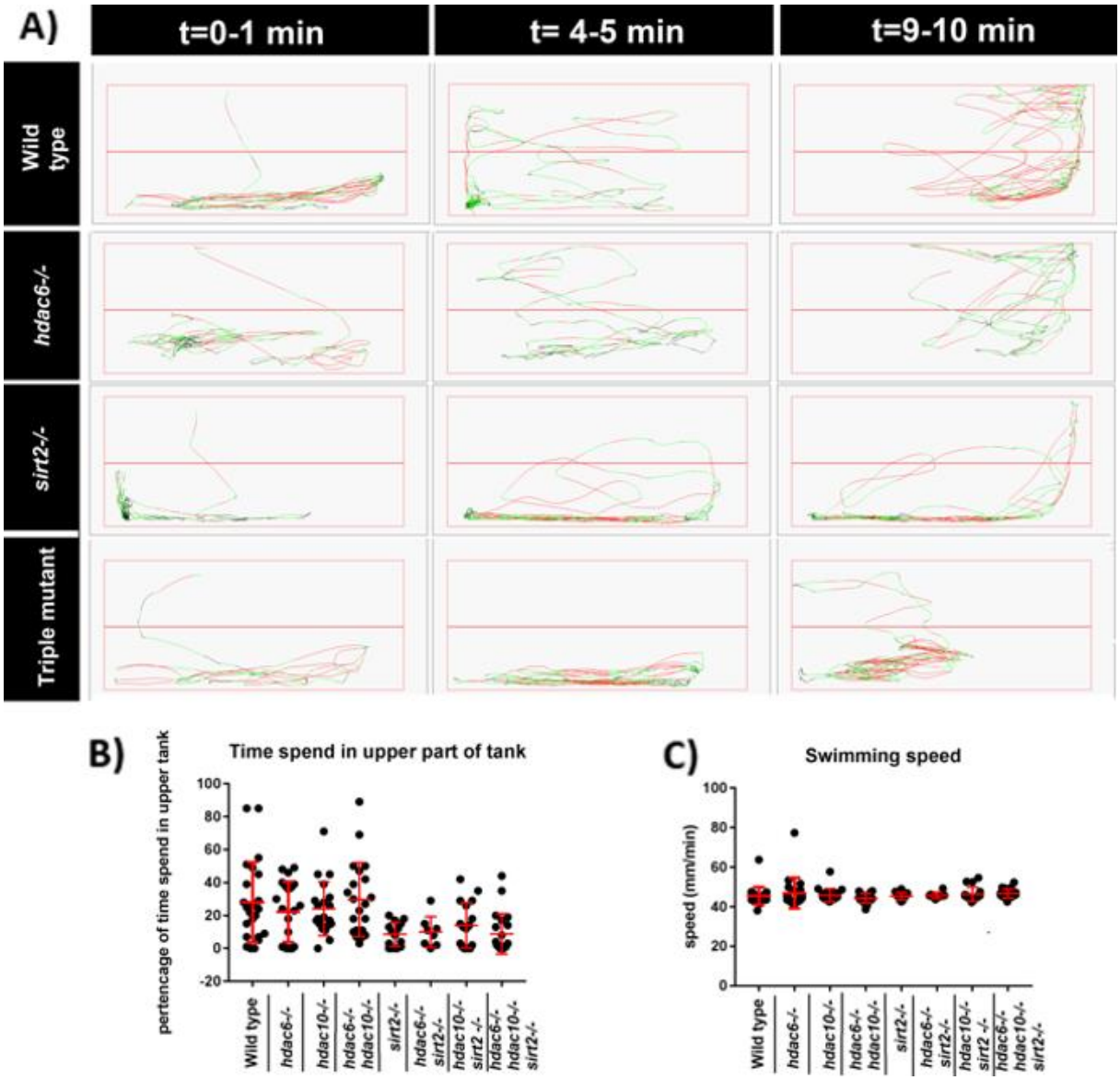

Fig. 47 Effect of Hdac6, Hdac10 and Sirt2 on an adult zebrafish behaviour and swimming pattern. Panel A) shows the swimming pattern of wild-type fish Ai) Shows *hdac6*$^{-/-}$ Aii) *sirt2*$^{-/-}$ and Aiii) Triple mutant of *hdac6*$^{-/-}$, *hdac10*$^{-/-}$ and *sirt2*$^{-/-}$. Panel B) shows the percentage of time spend in the upper part of the tank after the drop test. Panel C) shows the average speed with which fish were swimming during the experiments. P<0.05 (*) and P<0.01 (**) compared to wild-type student T.test mean with 95% CI.

7.3 Discussion

Studies have shown a significant role for histone deacetylases in development, physiology and diseases (Bitler et al., 2017; Dovey et al., 2010; Guo et al., 2007; Kaluza et al., 2011; Pang & Zhuang, 2010; Zuo et al., 2012). In this chapter, I describe the impact of mutations in HDAC IIb class proteins (Hdac6 and Hdac10), Hdac1, and Sirt2 on zebrafish. Previous studies conducted on mice showed no external phenotype in *Hdac6*, and *Sirt2* mutated animals (Bobrowska et al., 2012; Zhang et al., 2008). The reported observations included global hyperacetylation of cells and hyperactivity (Bobrowska et al., 2012; Fukada et al., 2012; Zhang et al., 2008). Zebrafish carrying these mutations do not display any apparent phenotypes, grow to adulthood and are fertile.

In comparison to mice, I did not see any hyperactivity as both mutated and wild-type fish swam at the same speed over 10 minute long experiments. Upon closer investigation, I discovered hypoacetylation of cilia in sensory tissues of the ear and eye. This phenotype is unusual as it would be expected to see somewhat over acetylation. No significant difference in strength of glutaminated tubulin signal assures that the observed difference is not due to increased glutamination. I would expect to see more acetylation in cilia as HDAC6 and Sirt2 are known to deacetylate lysine 40 of tubulin in microtubules (Kozikowski et al., 2008; Leroux, 2010; Miyake et al., 2016b; Rymut & Kelley, 2015). Despite the hypoacetylation, the morphology of cilia in observed structures seems unaffected. This is another surprising result as it was suggested that deacetylation of α-tubulin and cortactin was pointed at the key players in triggering ciliary disassembly (Pugacheva et al., 2007; Ran et al., 2015). The hypo acetylation phenotype of cilia, whatever seemingly weaker, was observed in single mutants of *hdac6*$^{-/-}$ as well. This led me to investigate if it is possible to reproduce the same phenotype with drug inhibition of Hdac6's catalytic activity in zebrafish embryos. Interestingly only embryos treated with 5uM CAY-10603 at day 0 for 3 days reproduced the phenotype, suggesting possible checkpoint in early development affecting homeostasis between acetylated and non-acetylated tubulin.

Furthermore of proper acetylation in cilia in *hdac1, hdac6* and *hdac10* mutants, as a mutation of *hdac1* results in the delay of the cell cycle and development retardation including ear (Dovey et al., 2010; Guo et al., 2007; He et al., 2016). Interestingly this phenomena seems to be limited to cilia in the ear, and the photoreceptors in the eye

as neither acetylation of the nasal pit or neuromast cilia seems to be affected. The result that I obtained from cryosections of retina showing possible changes in its morphology stays in contradiction with a study conducted on zebrafish which suggests that use of tubastatin A (HDAC6 inhibitor) rescued vision phenotype in zebrafish model with inherited blindness (Leyk et al., 2017). One possible explanation for this may be the lower amounts of enzymatic activity of acetyltransferases as a response to the abundance of acetylated proteins. However, this hypothesis has to be checked. These abnormalities in cilia acetylation seem to not have the visible effect on the livelihood of zebrafish. Behavioural tests did not show hyperactivity or balance problems as it was possible due to described acetylation role in the endurance of microtubules resulting in the possibility of cilia being easily damaged upon mechanical stress (Nicolson, 2017; Portran et al., 2017; Szyk et al., 2014). Neither of mutated fish displayed balance abnormality. However, mutants carrying the mutation for Sirt2 protein showed the different pattern of behaviours after being dropped to the tank. They did not explore the tank and remain in the lower area of it. This behaviour of zebrafish was associated with stress and anxiety and displayed by fish treated for example with stress hormone cortisol (Cachat et al., 2010; Egan et al., 2009). However, as the cilia hypoacetylation phenotype in cristae and maculae were displayed by fish as well, which have only *hdac6*$^{-/-}$ mutation in background and change in behaviour is only shown by fish with *sirt2*$^{-/-}$ mutation it is highly unlikely that this change is linked with cilia hypoacetylation but rather with the effect of Sirt2 on neuron development (Melchor & Strickland, 2006).

Chapter 8. Discussion

Overall, in this work, I established the basis for the usage of magnetic nanoparticles *in vitro* and zebrafish system and described the importance of Hdac1, Hdac6, Hdac10 and Sirt2 in zebrafish development. To my knowledge, it is the first time when both magnetosomes and ADEMTECH particles were used to change the direction of cell migration within zebrafish embryos. Furthermore, although previous work on HDAC6 and Sirt2 exists, we describe a novel phenotype of ciliary hypoacetylation in sensory cells of the ear and the eye in zebrafish mutants.

First, I described methods for both isolation and functionalisation of magnetosomes for injection purposes. This step was of crucial importance as studies have shown that uptake of magnetosomes and their internalisation within the cells strongly depend on magnetosomes aggregation (Alphandéry et al., 2012). These results are in agreement with the observation of the difference in dispersion of magnetosomes after injection into the 8 hours old zebrafish embryo. Magnetosomes without membranes created big clumps while magnetosomes with membranes dispersed within embryos cells. The difference depended on the presence or absence of magnetosomes' membranes. Subsequent steps involved establishment of working methods to visualise both magnetosomes and ADEMTECH particles. Using EZ-Link NHS-Biotin, streptavidin (native, labelled with AlexaFluor488 or Alexa Fluor 594) and biotinylated ATTO 594 die, I made nanoparticles easy to observe under the microscope both outside and within cells. Using anti-GFP antibodies, I managed to create magnetic nanoparticle complexes, recognising their target in solution and possibly *in vitro*. I was, however, unable to reproduce this in the zebrafish system. Low frequency of binding in MDCK cells with NPHP6 fused using GFP can be explained by the observation that the majority of magnetic particles are encapsulated in intercellular vesicles. This possibly prevented particles from reaching their target. Similar data on magnetic particles trapped within lysosomes were reported by other research groups.

Furthermore, results reported by other groups suggest that magnetic particles can be corroded by the strongly acidic environment within the lysosomes (Arbab et al., 2005; Byrne & Farrow, 2015; Moise et al., 2017; Wang et al., 2017). Entrapment of particles within lysosomes seems to be overcome by direct injection, instead of allowing magnetic particles to be absorbed by the cells in *in vitro* experiments (Chen et al., 2014; Etoc et al., 2013; Etoc et al., 2015). The inability of the functionalised magnetic

particles to bind their targets in zebrafish embryos may be explained in the same way as for observation *in vitro*, namely entrapment of particles within lysosomes. However, another possible explanation is the position of the protein fused to the GFP and its accessibility to antibodies. Centrin2 is found in centrioles which are surrounded by γ-tubulin and pericentrin, whereas NPHP6 with CEP290 are found in much easier accessible Y-links and necklace structures around the basal body of cilia (Dammermann et al., 2004; Prosser & Morrison, 2015; Reiter et al., 2012).

Furthermore, I tried to solve a well-known issue of magnetic particles becoming immobile within cells, even when the magnetic force is applied (Etoc et al., 2013; Master et al., 2015; Steketee et al., 2011). A possibility is that the membrane protein of magnetosomes, MamK that usually interacts with actin-like MamJ to arrange magnetosomes into chains could be interacting with the actin-related protein 2-B isoform X1 from *Danio rerio*. As MamK shares 42% similarities and 22% identities, it is likely to become immobilised within the actin cytoskeleton. However, testing this possibility did not reveal any direct interaction between actin and the magnetic particles used in neither pull down or fluorescently labelled actin experiments. On the other hand, *in vitro* experiments conducted on HeLa cells revealed an overlap of signals from phalloidin staining for actin and functionalised magnetosomes. Similar outcomes were reported in the literature and explained with the observation of actin filaments being connected to lysosomes, in which particles can be stored (Master et al., 2015).

Finally, experiments were conducted on migrating zebrafish embryo cells using magnetic particles demonstrating that despite the inability to pull magnetic particles toward the magnet, the force applied had to impact on the angle of migrating cells. Previously, similar results suggesting that cell migration can be altered with the usage of the magnetic nanoparticles, to my knowledge, were reported only in *in vitro* models (Kolosnjaj-Tabi et al., 2013; Shen et al., 2014). This shows that the usage of magnetic nanoparticles can provide a tool in research *in vivo* as well as *in vitro*. However, the mechanism underlying the change in angle of cell migration still has to be investigated. Literature data suggest a role of nanoparticles exerting the force on the microtubule cytoskeleton (Kolosnjaj-Tabi et al., 2013; Master et al., 2015; Shen et al., 2014). It is tempting to explain the overserved results with data obtained by Oster group and their model which demonstrates that just contractile force is enough to trigger gastrulation or neural tube formation in a simplified model (Weliky & Oster, 1990). To find mechanisms underlying the change in migration may be worth to screen affected cells

for changes in mRNA to discover possible candidate protein participating in cells responsible for mechanical cues.

Moreover, using literature data and Stokes law, I characterised the amount of force applied in my experiments as described previously (Fred Etoc et al., 2015). This enabled me to establish that force of ~4 pN was sufficient to induce a response in migrating cells. This force was created with a neodymium bar magnet, however moving the magnet in and out of the experimental setup, was affecting the imaging process by changing focus plane and introducing additional variability to the experiment, such as the change in position of magnetic field lines. For this reason, and to develop better control over the force applied, I designed and characterised electromagnetic tweezers. The electromagnetic tweezers were successfully implemented in research by several scientific groups, which proves that further development of the setup is imperative for gathering more data (Bryan, Dean, et al., 2010; Bryan, Smith, et al., 2010; Steketee et al., 2011).

Finally, in this work, I described the phenotype of the histone deacetylase 6 zebrafish mutants. HDAC6 and Sirtuin2 are proteins involved in a vast number of biological processes including cell migration, angiogenesis, metastasis and cell survival (Giblin et al., 2014; Kaluza et al., 2011; Pugacheva et al., 2007; Wang et al., 2014; Zhang et al., 2007). Most of the information about these proteins were obtained in *in vitro* work but data from experiments conducted *in vivo* did not show any significant changes in phenotype of mice lacking HDAC6 and Sirt2 protein except abundance of acetylated tubulin within the cells and hyperactivity (Bobrowska et al., 2012; Fukada et al., 2012; Zhang et al., 2008). In this work, I discovered and described the surprising phenotype of hypoacetylation of cilia in sensory cells of the ear and the retina. Acetylation of tubulin is portrayed as an important tubulin modification in cilia maintenance, and deacetylation of tubulin was suggested to be a triggering cilia disassembly (Pugacheva et al., 2007). My staining experiments have shown a significant drop in the acetylation of the tubulin in comparison to glutaminated tubulin in cilia of cristae and maculae hair cells without visibly affecting cilia morphology. It is possible that other tubulin modifications compensate for acetylation. It was reported that in Tetrahymena hyperglutamination could stabilise cilia (Wloga et al., 2010). Treatment of embryos at different stages of development with Hdac6 inhibitor CAY-10603 has shown that only treatment at 0 dpf causes hypoacetylation of cilia while treatment at 1 or 2 dpf did not affect. It would be of value to examine the level of TATs in zebrafish embryos treated

with CAY-10603 as it is possible that high level of acetylated tubulin may affect the expression of TAT as a control mechanism in tubulin turnover. Preventing structures developed in later stages of the cell differentiation from being acetylated. Moreover, published data about the connection of tubulin acetylation, microtubule endurance and possible changes in eye morphology makes it worth to observe these fish as they age, since they may display late onset problems with vision and hearing (Leyk et al., 2017). Finally, the mutation in the *sirt2* gene caused the change in adult zebrafish behaviour. Their swimming pattern resembled behaviour displayed by fish in distress (Egan et al., 2009). It is unlikely that this phenotype is connected with cilia deacetylation in sensory organs, as fish lacking HDAC6 showed cilia hypoacetylation phenotype but did not display changes in behaviour. Behavioural aberrations may occur as the result of changes in neurological development as Sirt2 is known to play an essential role in neuronal development (Melchor & Strickland, 2006).

The result showed in this work paved a path for future discoveries. The usage of nanoparticles already made its significant contribution in research regarding mechanosensation, treatment of tumours drug delivery and activation of pathways with usage of mechanical force (Alphandéry et al., 2017; Chen et al., 2014; Varchulova et al., 2017; Wang et al., 2017; Wheeler et al., 2016). Furthermore, it was reported that those magnetic particles could affect the cell migration pattern *in vitro* (Shen et al., 2014). In this work, I showed the relatively quick method of magnetic particle functionalization which allows for visualisation of both magnetosomes and ADEMTECH magnetic particles in cells both *in vitro* and *in vivo*. *In vitro* work showed that functionalized particles could attach to their target proteins within the cells. What more my experiments showed that even particles which are no able to bind their targets, with the magnetic force still could affect cells migration. These data, as well as further development of magnetic tweezers, may lead to the further improvement in the field such as the discovery of new protein candidates involved in mechanosensation or investigation of the role of organelles position in development, cellular differentiation and behaviour. One of the most interesting applications for magnetic nanoparticles in my opinion is possibility to temporal and special activation mechanosensing pathways at different stages of the embryo development or even stimulation of the reward system by mechanical activation of D1R+ neurons in mice (Desprat et al., 2008; Etoc et al., 2013; Wheeler et al., 2016). Further development of technics involving usage of magnetic particles may allow for investigation of the role of the particular proteins in

organelle orientation. In this work, I described *hdac1*$^{-/-}$, *hdac6*$^{-/-}$, *hdac10*$^{-/-}$ and *sirt2*$^{-/-}$ zebrafish mutants which can be used alongside with magnetic particles to determine the role of these proteins in centrosome behaviour. From the characterisation of these mutants, two surprising observations have arisen. First was hypoacetylation of cilia in sensory cells of the eye and ear. The second was the change of behaviour in *sirt2-/-* mutants. The hypoacetylation of cilia is particularly interesting as it was never reported before and may shed new light on this structure physiology. These observations may lead to deepening our understanding of the big group of various diseases called ciliopathies.

References

Agha, R., Ogawa, R., Pietramaggiori, G., & Orgill, D. P. (2011). A review of the role of mechanical forces in cutaneous wound healing. *Journal of Surgical Research*, *171*(2), 700–708. http://doi.org/10.1016/j.jss.2011.07.007

Albanese, A., Tang, P. S., & Chan, W. C. W. (2012). The Effect of Nanoparticle Size, Shape, and Surface Chemistry on Biological Systems. *Annual Review of Biomedical Engineering*, *14*, 1–16. http://doi.org/10.1146/annurev-bioeng-071811-150124

Alivisatos, A. P. (2008). Birth of a nanoscience building block. *ACS Nano*, *2*(8), 1514–1516. http://doi.org/10.1021/nn800485f

Alphandery, E. (2014). Applications of Magnetosomes Synthesized by Magnetotactic Bacteria in Medicine. *Frontiers in Bioengineering and Biotechnology*, *2*(March), 1–6. http://doi.org/10.3389/fbioe.2014.00005

Alphandéry, E., Guyot, F., & Chebbi, I. (2012). Preparation of chains of magnetosomes, isolated from *Magnetospirillum magneticum* strain AMB-1 magnetotactic bacteria, yielding efficient treatment of tumors using magnetic hyperthermia. *International Journal of Pharmaceutics*, *434*, 444–452. http://doi.org/10.1016/j.ijpharm.2012.06.015

Alphandéry, E., Idbaih, A., Adam, C., Delattre, J. Y., Schmitt, C., Guyot, F., & Chebbi, I. (2017). Chains of magnetosomes with controlled endotoxin release and partial tumor occupation induce full destruction of intracranial U87-Luc glioma in mice under the application of an alternating magnetic field. *Journal of Controlled Release*, *262*(July), 259–272. http://doi.org/10.1016/j.jconrel.2017.07.020

Aoyagi, S., & Archer, T. K. (2005). Modulating molecular chaperone Hsp90 functions through reversible acetylation. *Trends in Cell Biology*, *15*(11), 565–567. http://doi.org/10.1016/j.tcb.2005.09.003

Apopa, P. L., Qian, Y., Shao, R., Guo, N. L., Schwegler-Berry, D., Pacurari, M., … Flynn, D. C. (2009). Iron oxide nanoparticles induce human microvascular endothelial cell permeability through reactive oxygen species production and microtubule remodeling. *Particle and Fibre Toxicology*, *6*, 1. http://doi.org/10.1186/1743-8977-6-1

Arakaki, A., Nakazawa, H., Nemoto, M., Mori, T., & Matsunaga, T. (2008). Formation of magnetite by bacteria and its application. *Journal of The Royal Society*

Interface, *5*(26), 977–999. http://doi.org/10.1098/rsif.2008.0170

Arbab, A. S., Yocum, G. T., Rad, A. M., Khakoo, A. Y., Fellowes, V., Read, E. J., & Frank, J. A. (2005). Labeling of cells with ferumoxides-protamine sulfate complexes does not inhibit function or differentiation capacity of hematopoietic or mesenchymal stem cells. *NMR in Biomedicine*, *18*(8), 553–559. http://doi.org/10.1002/nbm.991

Asaoka, Y., Hata, S., Namae, M., Furutani-Seiki, M., & Nishina, H. (2014). The Hippo pathway controls a switch between retinal progenitor cell proliferation and photoreceptor cell differentiation in zebrafish. *PLoS ONE*, *9*(5). http://doi.org/10.1371/journal.pone.0097365

Asparuhova, M. B., Gelman, L., & Chiquet, M. (2009). Role of the actin cytoskeleton in tuning cellular responses to external mechanical stress. *Scandinavian Journal of Medicine and Science in Sports*, *19*(4), 490–499. http://doi.org/10.1111/j.1600-0838.2009.00928.x

Bance, B., Seetharaman, S., Etienne-manneville, S., Polarity, C., Unit, C., & Polarity, C. (2018). Microtubule acetylation but not detyrosination promotes focal adhesion dynamics and cell migration.

Bañobre-López, M., Teijeiro, A., & Rivas, J. (2013). Magnetic nanoparticle-based hyperthermia for cancer treatment. *Reports of Practical Oncology and Radiotherapy*, *18*(6), 397–400. http://doi.org/10.1016/j.rpor.2013.09.011

Behrouzkia, Z., Joveini, Z., Keshavarzi, B., Eyvazzadeh, N., & Aghdam, R. Z. (2016). Hyperthermia: How can it be used? *Oman Medical Journal*, *31*(2), 89–97. http://doi.org/10.5001/omj.2016.19

Betts, D. C., & Müller, R. (2014). Mechanical regulation of bone regeneration: Theories, models, and experiments. *Frontiers in Endocrinology*, *5*(DEC), 1–14. http://doi.org/10.3389/fendo.2014.00211

Bitler, B. G., Wu, S., Park, P. H., Hai, Y., Aird, K. M., Wang, Y., … Zhang, R. (2017). ARID1A-mutated ovarian cancers depend on HDAC6 activity. *Nature Cell Biology*, *19*(8). http://doi.org/10.1038/ncb3582

Blaser, H., Reichman-Fried, M., Castanon, I., Dumstrei, K., Marlow, F. L., Kawakami, K., … Raz, E. (2006). Migration of Zebrafish Primordial Germ Cells: A Role for Myosin Contraction and Cytoplasmic Flow. *Developmental Cell*, *11*, 613–627. http://doi.org/10.1016/j.devcel.2006.09.023

Bobinnec, Y., Khodjakov, A., Mir, L. M., Rieder, C. L., Eddé, B., & Bornens, M.

(1998). Centriole disassembly in vivo and its effect on centrosome structure and function in vertebrate cells. *Journal of Cell Biology*, *143*(6), 1575–1589. http://doi.org/10.1083/jcb.143.6.1575

Bobrowska, A., Donmez, G., Weiss, A., Guarente, L., & Bates, G. (2012). SIRT2 ablation has no effect on tubulin acetylation in brain, cholesterol biosynthesis or the progression of Huntington's disease phenotypes in vivo. *PloS One*, *7*(4), e34805. http://doi.org/10.1371/journal.pone.0034805

Boggs, A. E., Vitolo, M. I., Whipple, R. A., Charpentier, M. S., Goloubeva, O. G., Ioffe, O. B., … Martin, S. S. (2015). α-Tubulin acetylation elevated in metastatic and basal-like breast cancer cells promotes microtentacle formation, adhesion, and invasive migration. *Cancer Research*, *75*(1), 203–215. http://doi.org/10.1158/0008-5472.CAN-13-3563

Brehm, A., Miska, E. a, McCance, D. J., Reid, J. L., Bannister, A. J., & Kouzarides, T. (1998). Retinoblastoma protein recruits histone deacetylase to repress transcription. *Nature*, *391*(6667), 597–601. http://doi.org/10.1038/35404

Bryan, M. T., Dean, J., Schrefl, T., Thompson, F. E., Haycock, J., & Allwood, D. a. (2010). The effect of trapping superparamagnetic beads on domain wall motion. *Applied Physics Letters*, *96*, 3–6. http://doi.org/10.1063/1.3428775

Bryan, M. T., Smith, K. H., Real, M. E., Bashir, M. a., Fry, P. W., Fischer, P., … Haycock, J. W. (2010). Switchable cell trapping using superparamagnetic beads. *IEEE Magnetics Letters*, *1*. http://doi.org/10.1109/LMAG.2010.2046143

Burda, C., Chen, X., Narayanan, R., & El-Sayed, M. A. (2005). *Chemistry and properties of nanocrystals of different shapes*. *Chemical Reviews* (Vol. 105). http://doi.org/10.1021/cr030063a

Byrne, J. M., & Farrow, N. (2015). Nanoscale 2014- E Cespedes- Supporting, (August).

Cachat, J., Stewart, A., Grossman, L., Gaikwad, S., Kadri, F., Chung, K. M., … Kalueff, A. V. (2010). Measuring behavioral and endocrine responses to novelty stress in adult zebrafish. *Nature Protocols*, *5*(11), 1786–1799. http://doi.org/10.1038/nprot.2010.140

Campinho, P., Behrndt, M., Ranft, J., Risler, T., Minc, N., & Heisenberg, C.-P. (2013). Tension-oriented cell divisions limit anisotropic tissue tension in epithelial spreading during zebrafish epiboly. *Nature Cell Biology*, *15*(11), 1405–14.

http://doi.org/10.1038/ncb2869

Charras, G., & Paluch, E. (2008). Blebs lead the way: How to migrate without lamellipodia. *Nature Reviews Molecular Cell Biology*, *9*(9), 730–736. http://doi.org/10.1038/nrm2453

Chen, C. S., Mrksich, M., Huang, S., Whitesides, G. M., & Ingber, D. E. (1997). Geometric control of cell life and death. *Science (New York, N.Y.)*, *276*(May), 1425–1428. http://doi.org/10.1126/science.276.5317.1425

Chen, O., Riedemann, L., Etoc, F., Herrmann, H., Coppey, M., Barch, M., … Bawendi, M. G. (2014). ARTICLE Magneto-fluorescent core-shell supernanoparticles. *Nature Communications*, *5*, 1–8. http://doi.org/10.1038/ncomms6093

Cho, M. H., Lee, E. J., Son, M., Lee, J.-H., Yoo, D., Kim, J., … Cheon, J. (2012). A magnetic switch for the control of cell death signalling in in vitro and in vivo systems. *Nature Materials*, *11*(12), 1038–1043. http://doi.org/10.1038/nmat3430

Chowdhury, S. R., & Yanful, E. K. (2010). Arsenic and chromium removal by mixed magnetite-maghemite nanoparticles and the effect of phosphate on removal. *Journal of Environmental Management*, *91*(11), 2238–2247. http://doi.org/10.1016/j.jenvman.2010.06.003

Codelia, V., Sun, G., & Irvine, K. (2013). Regulation of YAP by Mechanical Strain through Jnk and Hippo Signaling. *Current Biology*, *24*(17), 2012–2017. http://doi.org/10.1016/j.cub.2014.07.034

Collinet, C., Rauzi, M., Lenne, P. F., & Lecuit, T. (2015). Local and tissue-scale forces drive oriented junction growth during tissue extension. *Nature Cell Biology*, *17*(10), 1247–1258. http://doi.org/10.1038/ncb3226

Dammermann, A., M??ller-Reichert, T., Pelletier, L., Habermann, B., Desai, A., & Oegema, K. (2004). Centriole assembly requires both centriolar and pericentriolar material proteins. *Developmental Cell*, *7*(6), 815–829. http://doi.org/10.1016/j.devcel.2004.10.015

Dang, I., Gorelik, R., Sousa-Blin, C., Derivery, E., Guérin, C., Linkner, J., … Gautreau, A. (2013). Inhibitory signalling to the Arp2/3 complex steers cell migration. *Nature*, *503*(7475), 281–284. http://doi.org/10.1038/nature12611

Dekens, M. P. S. (2003). The maternal-effect gene futile cycle is essential for pronuclear congression and mitotic spindle assembly in the zebrafish zygote. *Development*, *130*(17), 3907–3916. http://doi.org/10.1242/dev.00606

Delling, M., Indzhykulian, A. A., Liu, X., Li, Y., Xie, T., Corey, D. P., & Clapham, D. E. (2016). Primary cilia are not calcium-responsive mechanosensors. *Nature*, *531*(7596), 656–660. http://doi.org/10.1038/nature17426

Dennis, R. (n.d.). Mechanical Loading History Biology. *Bone*. http://doi.org/10.1016/0021-9290(87)90027-3

Desprat, N., Supatto, W., Pouille, P. A., Beaurepaire, E., & Farge, E. (2008). Tissue Deformation Modulates Twist Expression to Determine Anterior Midgut Differentiation in Drosophila Embryos. *Developmental Cell*, *15*, 470–477. http://doi.org/10.1016/j.devcel.2008.07.009

Dhanyamraju, P. K., Holz, P. S., Finkernagel, F., Fendrich, V., & Lauth, M. (2015). Histone deacetylase 6 represents a novel drug target in the oncogenic hedgehog signaling pathway. *Molecular Cancer Therapeutics*, *14*(3), 727–739. http://doi.org/10.1158/1535-7163.MCT-14-0481

Dovey, O. M., Foster, C. T., & Cowley, S. M. (2010). Histone deacetylase 1 (HDAC1), but not HDAC2, controls embryonic stem cell differentiation. *Proceedings of the National Academy of Sciences*, *107*(18), 8242–8247. http://doi.org/10.1073/pnas.1000478107

Dubey, J., Ratnakaran, N., & Koushika, S. P. (2015). Neurodegeneration and microtubule dynamics: death by a thousand cuts. *Frontiers in Cellular Neuroscience*, *9*(September), 1–15. http://doi.org/10.3389/fncel.2015.00343

Dupin, I., Camand, E., & Etienne-Manneville, S. (2009). Classical cadherins control nucleus and centrosome position and cell polarity. *Journal of Cell Biology*, *185*(5), 779–786. http://doi.org/10.1083/jcb.200812034

Dutcher, S. K. (2003). Elucidation of basal body and centriole functions in Chlamydomonas reinhardtii. *Traffic*, *4*(7), 443–451. http://doi.org/104 [pii] ET - 2003/06/11

Egan, R. J., Bergner, C. L., Hart, P. C., Cachat, J. M., Canavello, P. R., Elegante, M. F., … Kalueff, A. V. (2009). Understanding behavioral and physiological phenotypes of stress and anxiety in zebrafish. *Behavioural Brain Research*, *205*(1), 38–44. http://doi.org/10.1016/j.bbr.2009.06.022

El Yacoubi, S., Chopard, B., & Bandini, S. (n.d.). *LNCS 4173 - Cellular Automata*.

Elmore, S. (2007). Apoptosis: A Review of Programmed Cell Death. *Toxicologic Pathology*, *35*(4), 495–516. http://doi.org/10.1080/01926230701320337

Elric, J., & Etienne-Manneville, S. (2014). Centrosome positioning in polarized cells:

Common themes and variations. *Experimental Cell Research*, *328*(2), 240–248. http://doi.org/10.1016/j.yexcr.2014.09.004

Erck, C., Peris, L., Andrieux, A., Meissirel, C., Gruber, A. D., Vernet, M., … Wehland, J. (2005). A vital role of tubulin-tyrosine-ligase for neuronal organization. *Proceedings of the National Academy of Sciences*, *102*(22), 7853–7858. http://doi.org/10.1073/pnas.0409626102

Etienne-Manneville, S. (2014). Neighborly relations during collective migration. *Current Opinion in Cell Biology*, *30*(1), 51–59. http://doi.org/10.1016/j.ceb.2014.06.004

Etoc, F., Lisse, D., Bellaiche, Y., Piehler, J., Coppey, M., & Dahan, M. (2013). Subcellular control of Rac-GTPase signalling by magnetogenetic manipulation inside living cells. *Nature Nanotechnology*, *8*(3), 193–8. http://doi.org/10.1038/nnano.2013.23

Etoc, F., Vicario, C., Lisse, D., Siaugue, J.-M., Piehler, J., Coppey, M., & Dahan, M. (2015). Magnetogenetic Control of Protein Gradients Inside Living Cells with High Spatial and Temporal Resolution. *Nano Letters*, 150428133855000. http://doi.org/10.1021/acs.nanolett.5b00851

Farina, F., Gaillard, J., Guérin, C., Couté, Y., Sillibourne, J., Blanchoin, L., & Théry, M. (2016). The centrosome is an actin-organizing centre. *Nature Cell Biology*, *18*(1), 65–75. http://doi.org/10.1038/ncb3285

Finnin, M. S., Donigian, J. R., Cohen, a, Richon, V. M., Rifkind, R. a, Marks, P. a, … Pavletich, N. P. (1999). Structures of a histone deacetylase homologue bound to the TSA and SAHA inhibitors. *Nature*, *401*(6749), 188–193. http://doi.org/10.1038/43710

Forcioli-Conti, N., Est??ve, D., Bouloumi??, A., Dani, C., & Peraldi, P. (2016). The size of the primary cilium and acetylated tubulin are modulated during adipocyte differentiation: Analysis of HDAC6 functions in these processes. *Biochimie*, *124*, 112–123. http://doi.org/10.1016/j.biochi.2015.09.011

Freitag, S., Le Trong, I., Klumb, L., Stayton, P. S., & Stenkamp, R. E. (1997). Structural studies of the streptavidin binding loop. *Protein Science : A Publication of the Protein Society*, *6*(6), 1157–66. http://doi.org/10.1002/pro.5560060604

Fukada, M., Hanai, A., Nakayama, A., Suzuki, T., Miyata, N., Rodriguiz, R. M., … Kawaguchi, Y. (2012). Loss of deacetylation activity of Hdac6 affects emotional behavior in mice. *PLoS ONE*, *7*(2). http://doi.org/10.1371/journal.pone.0030924

Gardner, M. J., Putnam, S., Wong, A., Streubel, P. N., Kotiya, A., & Silva, M. J. (2013). variability : A mouse model, *16*(3), 298–303. http://doi.org/10.1007/s00776-011-0051-5.Differential

Giblin, W., Skinner, M. E., & Lombard, D. B. (2014). Sirtuins: Guardians of mammalian healthspan. *Trends in Genetics*, *30*(7), 271–286. http://doi.org/10.1016/j.tig.2014.04.007

Glickman, N. S., Kimmel, C. B., Jones, M. a, & Adams, R. J. (2003). Shaping the zebrafish notochord. *Development (Cambridge, England)*, *130*, 873–887. http://doi.org/10.1242/dev.00314

Gorby, Y. a., Beveridge, T. J., & Blakemore, R. P. (1988). Characterization of the bacterial magnetosome membrane. *Journal of Bacteriology*, *170*(2), 834–841.

Gramage, E., Li, J., & Hitchcock, P. (2014). The expression and function of midkine in the vertebrate retina. *British Journal of Pharmacology*, *171*(4), 913–923. http://doi.org/10.1111/bph.12495

Guo, C., Mi, J., Brautigan, D. L., & Larner, J. M. (2007). ATM regulates ionizing radiation-induced disruption of HDAC1:PP1:Rb complexes. *Cellular Signalling*, *19*(3), 504–510. http://doi.org/10.1016/j.cellsig.2006.08.001

Haberland, M., Montgomery, R. L., & Olson, E. N. (2009). The many roles of histone deacetylases in development and physiology: implications for disease and therapy. *Nature Reviews. Genetics*, *10*(1), 32–42. http://doi.org/10.1038/nrg2485

Hai, Y., Shinsky, S. A., Porter, N. J., & Christianson, D. W. (2017). Histone deacetylase 10 structure and molecular function as a polyamine deacetylase. *Nature Communications*, *8*(May), 1–9. http://doi.org/10.1038/ncomms15368

Harrison, M. R. M., Georgiou, A. S., Spaink, H. P., & Cunliffe, V. T. (2011). The epigenetic regulator Histone Deacetylase 1 promotes transcription of a core neurogenic programme in zebrafish embryos. *BMC Genomics*, *12*(1), 24. http://doi.org/10.1186/1471-2164-12-24

Harvey, K. F., & Hariharan, I. K. (2012). The Hippo pathway. *Cold Spring Harbor Perspectives in Biology*, *4*. http://doi.org/10.1101/cshperspect.a011288

Hassan, A. (2016). Single cell migration.

Hayashi, S., Mikami, T., Murai, Y., Takano, Y., & Imura, J. (2014). Alpha-tubulin nuclear overexpression is an indicator of poor prognosis in patients with non-Hodgkin's lymphoma. *International Journal of Molecular Medicine*, *34*(2), 483–490. http://doi.org/10.3892/ijmm.2014.1793

He, Y., Tang, D., Li, W., Chai, R., & Li, H. (2016). Histone deacetylase 1 is required for the development of the zebrafish inner ear. *Scientific Reports*, *6*, 16535. http://doi.org/10.1038/srep16535

Hedayatnasab, Z., Abnisa, F., & Daud, W. M. A. W. (2017). Review on magnetic nanoparticles for magnetic nanofluid hyperthermia application. *Materials and Design*, *123*, 174–196. http://doi.org/10.1016/j.matdes.2017.03.036

Heisenberg, C. P., Tada, M., Rauch, G. J., Saúde, L., Concha, M. L., Geisler, R., … Wilson, S. W. (2000). Silberblick/Wnt11 mediates convergent extension movements during zebrafish gastrulation. *Nature*, *405*(May), 76–81. http://doi.org/10.1038/35011068

Henstock, J. R., Rotherham, M., Rashidi, H., Shakesheff, K. M., & El Haj, A. J. (2014). Remotely Activated Mechanotransduction via Magnetic Nanoparticles Promotes Mineralization Synergistically With Bone Morphogenetic Protein 2: Applications for Injectable Cell Therapy. *Stem Cells Translational Medicine*, *3*(11), 1363–74. http://doi.org/10.5966/sctm.2014-0017

Hook, S. S., Orian, A., Cowley, S. M., & Eisenman, R. N. (2002). Histone deacetylase 6 binds polyubiquitin through its zinc finger (PAZ domain) and copurifies with deubiquitinating enzymes. *Proceedings of the National Academy of Sciences of the United States of America*, *99*(21), 13425–13430. http://doi.org/10.1073/pnas.172511699

Hu, J., Lo, I. M. C., & Chen, G. (2007). Performance and mechanism of chromate (VI) adsorption by δ-FeOOH-coated maghemite (γ-Fe2O3) nanoparticles. *Separation and Purification Technology*, *58*(1), 76–82. http://doi.org/10.1016/j.seppur.2007.07.023

Hubbert, C., Guardiola, A., Shao, R., Kawaguchi, Y., Ito, A., Nixon, A., … Yao, T.-P. (2002). HDAC6 is a microtubule-associated deacetylase. *Nature*, *417*(6887), 455–458. http://doi.org/10.1038/417455a

Huízar-Félix, A. M., Muñoz, D., Orue, I., Magén, C., Ibarra, A., Barandiarán, J. M., … Fdez-Gubieda, M. L. (2016). Assemblies of magnetite nanoparticles extracted from magnetotactic bacteria: A magnetic study. *Applied Physics Letters*, *108*(6). http://doi.org/10.1063/1.4941835

Jing, X., & Malicki, J. (2009). Zebrafish ale oko, an essential determinant of sensory neuron survival and the polarity of retinal radial glia, encodes the p50 subunit of dynactin. *Development (Cambridge, England)*, *136*, 2955–2964.

http://doi.org/10.1242/dev.037739

Kafer, J., Hayashi, T., Maree, A. F. M., Carthew, R. W., & Graner, F. (2007). Cell adhesion and cortex contractility determine cell patterning in the Drosophilaretina. *Proceedings of the National Academy of Sciences*, *104*(47), 18549–18554. http://doi.org/10.1073/pnas.0704235104

Kaluza, D., Kroll, J., Gesierich, S., Yao, T. P., Boon, R. A., Hergenreider, E., … Urbich, C. (2011). Class IIb HDAC6 regulates endothelial cell migration and angiogenesis by deacetylation of cortactin. *EMBO Journal*, *30*(20), 4142–4156. http://doi.org/10.1038/emboj.2011.298

Kaverina, I., & Straube, A. (2011). Regulation of cell migration by dynamic microtubules. *Seminars in Cell and Developmental Biology*, *22*(9), 968–974. http://doi.org/10.1016/j.semcdb.2011.09.017

Keller, R., Davidson, L. a., & Shook, D. R. (2003). How we are shaped: The biomechanics of gastrulation. *Differentiation*, *71*(3), 171–205. http://doi.org/10.1046/j.1432-0436.2003.710301.x

Kim, H. R., Richardson, J., van Eeden, F., & Ingham, P. W. (2010). Gli2a protein localization reveals a role for Iguana/DZIP1 in primary ciliogenesis and a dependence of Hedgehog signal transduction on primary cilia in the zebrafish. *BMC Biology*, *8*(1), 65. http://doi.org/10.1186/1741-7007-8-65

Kim, T. J., Joo, C., Seong, J., Vafabakhsh, R., Botvinick, E. L., Berns, M. W., … Wang, Y. (2015). Distinct mechanisms regulating mechanical force-induced Ca2+signals at the plasma membrane and the ER in human MSCs. *ELife*, *2015*(4), 1–14. http://doi.org/10.7554/eLife.04876

Kimmel, C. B., Ballard, W. W., Kimmel, S. R., Ullmann, B., & Schilling, T. F. (1995). Stages of embryonic development of the zebrafish. *Dev.Dynam.*, *203*, 253–310. http://doi.org/10.1002/aja.1002030302

Klein, E. a, Castagnino, P., Kothapalli, D., Yin, L., Byfield, F. J., Xu, T., … Assoian, R. K. (2010). NIH Public Access. *In Vivo*, *19*(18), 1511–1518. http://doi.org/10.1016/j.cub.2009.07.069.Cell

Kollman, J. M., Merdes, A., Mourey, L., & Agard, D. A. (2011). Microtubule nucleation by γ-tubulin complexes. *Nature Reviews Molecular Cell Biology*, *12*(11), 709–721. http://doi.org/10.1038/nrm3209

Kolosnjaj-Tabi, J., Wilhelm, C., Clément, O., & Gazeau, F. (2013). Cell labeling with magnetic nanoparticles: opportunity for magnetic cell imaging and cell

manipulation. *Journal of Nanobiotechnology*, *11 Suppl 1*(Suppl 1), S7. http://doi.org/10.1186/1477-3155-11-S1-S7

Komeili, A., Li, Z., Newman, D. K., & Jensen, G. J. (2006). Magnetosomes are cell membrane invaginations organized by the actin-like protein MamK. *Science (New York, N.Y.)*, *311*(2006), 242–245. http://doi.org/10.1126/science.1123231

Kozikowski, A. P., Tapadar, S., Luchini, D. N., Ki, H. K., & Billadeau, D. D. (2008). Use of the Nitrile Oxide Cycloaddition (NOC) reaction for molecular probe generation: A new class of enzyme selective histone deacetylase inhibitors (HDACIs) showing picomolar activity at HDAC6. *Journal of Medicinal Chemistry*, *51*(15), 4370–4373. http://doi.org/10.1021/jm8002894

Krause, M., & Gautreau, A. (2014). Steering cell migration: Lamellipodium dynamics and the regulation of directional persistence. *Nature Reviews Molecular Cell Biology*, *15*(9), 577–590. http://doi.org/10.1038/nrm3861

Krieg, M., Arboleda-Estudillo, Y., Puech, P. H., Käfer, J., Graner, F., Müller, D. J., & Heisenberg, C. P. (2008). Tensile forces govern germ-layer organization in zebrafish. *Nature Cell Biology*, *10*(4), 429–436. http://doi.org/10.1038/ncb1705

Kubo, T., Yanagisawa, H. -a., Liu, Z., Shibuya, R., Hirono, M., & Kamiya, R. (2014). A conserved flagella-associated protein in Chlamydomonas, FAP234, is essential for axonemal localization of tubulin polyglutamylase TTLL9. *Molecular Biology of the Cell*, *25*(1), 107–117. http://doi.org/10.1091/mbc.E13-07-0424

Kushner, E. J., Ferro, L. S., Liu, J., Durrant, J. R., Rogers, S. L., Dudley, A. C., & Bautch, V. L. (2014). Excess centrosomes disrupt endothelial cell migration via centrosome scattering, *206*(2), 257–272. http://doi.org/10.1083/jcb.201311013

Lecuit, T., & Lenne, P.-F. (2007). Cell surface mechanics and the control of cell shape, tissue patterns and morphogenesis. *Nature Reviews. Molecular Cell Biology*, *8*(August), 633–644. http://doi.org/10.1038/nrm2222

Lee, N., Kim, H., Choi, S. H., Park, M., Kim, D., Kim, H.-C., … Hyeon, T. (2011). Magnetosome-like ferrimagnetic iron oxide nanocubes for highly sensitive MRI of single cells and transplanted pancreatic islets. *Proceedings of the National Academy of Sciences of the United States of America*, *108*(7), 2662–2667. http://doi.org/10.1073/pnas.1016409108

Leroux, M. R. (2010). Tubulin acetyltransferase discovered: Ciliary role in the ancestral eukaryote expanded to neurons in metazoans. *Proceedings of the National Academy of Sciences*, *107*(50), 21238–21239.

http://doi.org/10.1073/pnas.1016396108

Lessey, E. C., Guilluy, C., & Burridge, K. (2012). From mechanical force to RhoA activation. *Biochemistry*, *51*(38), 7420–7432. http://doi.org/10.1021/bi300758e

Leyk, J., Daly, C., Janssen-Bienhold, U., Kennedy, B. N., & Richter-Landsberg, C. (2017). HDAC6 inhibition by tubastatin A is protective against oxidative stress in a photoreceptor cell line and restores visual function in a zebrafish model of inherited blindness. *Cell Death & Disease*, *8*(8), e3028. http://doi.org/10.1038/cddis.2017.415

Li, H., Li, Z., Liu, T., Xiao, X., Peng, Z., & Deng, L. (2008). A novel technology for biosorption and recovery hexavalent chromium in wastewater by bio-functional magnetic beads. *Bioresource Technology*, *99*(14), 6271–6279. http://doi.org/10.1016/j.biortech.2007.12.002

Lin, Y. T., Weng, C. H., & Chen, F. Y. (2008). Effective removal of AB24 dye by nano/micro-size zero-valent iron. *Separation and Purification Technology*, *64*(1), 26–30. http://doi.org/10.1016/j.seppur.2008.08.012

Ling, H., Peng, L., Seto, E., & Fukasawa, K. (2012). Suppression of centrosome duplication and amplifcation by deacetylases. *Cell Cycle*, *11*(20), 3779–3791. http://doi.org/10.4161/cc.21985

Magnaghi-Jaulin, L., Groisman, R., Naguibneva, I., Robin, P., Lorain, S., Le Villain, J. P., … Harel-Bellan, A. (1998). Retinoblastoma protein represses transcription by recruiting a histone deacetylase. *Nature*, *391*(6667), 601–605. http://doi.org/10.1038/35410

Malicki, J. (2000). Harnessing the power of forward genetics - Analysis of neuronal diversity and patterning in the zebrafish retina. *Trends in Neurosciences*, *23*, 531–541. http://doi.org/10.1016/S0166-2236(00)01655-6

Mammoto, A., Huang, S., Moore, K., Oh, P., & Ingber, D. E. (2004). Role of RhoA, mDia, and ROCK in cell shape-dependent control of the Skp2-p27kip-1 pathway and the G1/S transition. *Journal of Biological Chemistry*, *279*(25), 26323–26330. http://doi.org/10.1074/jbc.M402725200

Mammoto, T., & Ingber, D. E. (2010). Mechanical control of tissue and organ development. *Development (Cambridge, England)*, *137*, 1407–1420. http://doi.org/10.1242/dev.024166

Mao, H., Li, J., Dulińska-Molak, I., Kawazoe, N., Takeda, Y., Mamiya, H., & Chen, G. (2015). Cellular effects of magnetic nanoparticles explored by atomic force

microscopy. *Biomater. Sci.*, *3*(9), 1284–1290. http://doi.org/10.1039/C5BM00141B

Markides, H., Rotherham, M., & El Haj, a. J. (2012). Biocompatibility and toxicity of magnetic nanoparticles in regenerative medicine. *Journal of Nanomaterials*, *2012*, 13–15. http://doi.org/10.1155/2012/614094

Marlow, F., Zwartkruis, F., Malicki, J., Neuhauss, S. C., Abbas, L., Weaver, M., … Solnica-Krezel, L. (1998). Functional interactions of genes mediating convergent extension, knypek and trilobite, during the partitioning of the eye primordium in zebrafish. *Developmental Biology*, *203*, 382–399. http://doi.org/10.1006/dbio.1998.9032

Martin, A. C., Gelbart, M., Fernandez-Gonzalez, R., Kaschube, M., & Wieschaus, E. F. (2010). Integration of contractile forces during tissue invagination. *Journal of Cell Biology*, *188*(5), 735–749. http://doi.org/10.1083/jcb.200910099

Master, A. M., Williams, P. N., Pothayee, N., Zhang, R., Vishwasrao, H. M., Golovin, Y. I., … Kabanov, A. V. (2015). Remote Actuation of Magnetic Nanoparticles for Cancer Cell Selective Treatment Through Cytoskeletal Disruption. *Statewide Agricultural Land Use Baseline 2015*, *1*(919), 1–13. http://doi.org/10.1017/CBO9781107415324.004

Matsuyama, A., Shimazu, T., Sumida, Y., Saito, A., Yoshimatsu, Y., Seigneurin-Berny, D., … Yoshida, M. (2002). In vivo destabilization of dynamic microtubules by HDAC6-mediated deacetylation. *EMBO Journal*, *21*(24), 6820–6831. http://doi.org/10.1093/emboj/cdf682

Mayor, R., & Etienne-Manneville, S. (2016). The front and rear of collective cell migration. *Nature Reviews Molecular Cell Biology*, *17*(2), 97–109. http://doi.org/10.1038/nrm.2015.14

Melchor, J. P., & Strickland, S. (2006). Physiology and Pathology, *93*(4), 655–660.

Menegola, E., Di Renzo, F., Broccia, M. L., & Giavini, E. (2006). Inhibition of histone deacetylase as a new mechanism of teratogenesis. *Birth Defects Research Part C - Embryo Today: Reviews*, *78*(4), 345–353. http://doi.org/10.1002/bdrc.20082

Miesfeld, J. B., & Link, B. A. (2014). Establishment of transgenic lines to monitor and manipulate Yap/Taz-Tead activity in zebrafish reveals both evolutionarily conserved and divergent functions of the Hippo pathway. *Mechanisms of Development*, *133*(414), 177–188. http://doi.org/10.1016/j.mod.2014.02.003

Miyake, Y., Keusch, J. J., Wang, L., Saito, M., Hess, D., Wang, X., … Matthias, P.

(2016). Structural insights into HDAC6 tubulin deacetylation and its selective inhibition. *Nature Chemical Biology*, *12*(9), 748–54. http://doi.org/10.1038/nchembio.2140

Moise, S., Céspedes, E., Soukup, D., Byrne, J. M., El Haj, A. J., & Telling, N. D. (2017). The cellular magnetic response and biocompatibility of biogenic zinc- and cobalt-doped magnetite nanoparticles. *Scientific Reports*, *7*(November 2016), 1–11. http://doi.org/10.1038/srep39922

Mohammed, L., Gomaa, H. G., Ragab, D., & Zhu, J. (2017). Magnetic nanoparticles for environmental and biomedical applications: A review. *Particuology*, *30*, 1–14. http://doi.org/10.1016/j.partic.2016.06.001

Murat, D., Quinlan, A., Vali, H., & Komeili, A. (2010a). Comprehensive genetic dissection of the magnetosome gene island reveals the step-wise assembly of a prokaryotic organelle. *Proceedings of the National Academy of Sciences of the United States of America*, *107*, 5593–5598. http://doi.org/10.1073/pnas.0914439107

Murat, D., Quinlan, A., Vali, H., & Komeili, A. (2010b). Comprehensive genetic dissection of the magnetosome gene island reveals the step-wise assembly of a prokaryotic organelle. *Proceedings of the National Academy of Sciences of the United States of America*, *107*(6), 5593–5598. http://doi.org/10.1073/pnas.0914439107

Nicolson, T. (2005). The Genetics of Hearing and Balance in Zebrafish. *Annual Review of Genetics*, *39*(1), 9–22. http://doi.org/10.1146/annurev.genet.39.073003.105049

Nicolson, T. (2017). The genetics of hair-cell function in zebrafish. *Journal of Neurogenetics*, *31*(3), 102–112. http://doi.org/10.1080/01677063.2017.1342246

Nikonova, A. S., & Golemis, E. A. (2015). Control of ciliation in embryogenesis. *Nature Cell Biology*, *17*(2), 109–111. http://doi.org/10.1038/ncb3103

Nobes, C. D., & Hall, A. (1995). Rho, Rac, and Cdc42 GTPases regulate the assembly of multimolecular focal complexes associated with actin stress fibers, lamellipodia, and filopodia. *Cell*, *81*(1), 53–62. http://doi.org/10.1016/0092-8674(95)90370-4

Norden, C., Young, S., Link, B. a., & Harris, W. a. (2009). Actomyosin Is the Main Driver of Interkinetic Nuclear Migration in the Retina. *Cell*, *138*(6), 1195–1208. http://doi.org/10.1016/j.cell.2009.06.032

North, B. J., Marshall, B. L., Borra, M. T., Denu, J. M., Verdin, E., & Francisco, S. (2003). Is an NAD -Dependent Tubulin Deacetylase. *Molecular Cell*, *11*, 437–444. http://doi.org/10.1016/S1097-2765(03)00038-8

Novorol, C., Burkhardt, J., Wood, K. J., Iqbal, A., Roque, C., Coutts, N., … Harris, W. A. (2013). Microcephaly models in the developing zebrafish retinal neuroepithelium point to an underlying defect in metaphase progression. *Open Biology*, *3*(10), 130065. http://doi.org/10.1098/rsob.130065

Outeiro, T. F., Kontopoulos, E., Altmann, S. M., Kufareva, I., Strathearn, K. E., Amore, A. M., … Kazantsev, A. G. (2007). Models of Parkinson ' s Disease, *1968*(August 2006). http://doi.org/10.1159/000092318

Palomares, K. T. S., Gleason, R. E., Mason, Z. D., M, D., Einhorn, T. A., Gerstenfeld, L. C., & Morgan, E. F. (2009). NIH Public Access. *Control*, *27*(9), 1123–1132. http://doi.org/10.1002/jor.20863.Mechanical

Paluch, E. K., & Raz, E. (2013). The role and regulation of blebs in cell migration. *Current Opinion in Cell Biology*, *25*(5), 582–590. http://doi.org/10.1016/j.ceb.2013.05.005

Pang, M., & Zhuang, S. (2010). Histone Deacetylase: A Potential Therapeutic Target for Fibrotic Disorders. *Journal of Pharmacology and Experimental Therapeutics*, *335*(2), 266–272. http://doi.org/10.1124/jpet.110.168385

Park, J. S., Chu, J. S., Tsou, A. D., Diop, R., Wang, A., & Li, S. (2012). Seven year outcome-Chesterman, *32*(16), 3921–3930. http://doi.org/10.1016/j.biomaterials.2011.02.019.The

Parsons, J. T., Horwitz, A. R., & Schwartz, M. A. (2010). Cell adhesion: Integrating cytoskeletal dynamics and cellular tension. *Nature Reviews Molecular Cell Biology*, *11*(9), 633–643. http://doi.org/10.1038/nrm2957

Pathak, N., Austin-Tse, C. A., Liu, Y., Vasilyev, A., & Drummond, I. A. (2014). Cytoplasmic carboxypeptidase 5 regulates tubulin glutamylation and zebrafish cilia formation and function. *Molecular Biology of the Cell*, *25*(12), 1836–1844. http://doi.org/10.1091/mbc.E13-01-0033

Patwari, P., & Lee, R. T. (2008). Mechanical control of tissue morphogenesis. *Circulation Research*, *103*, 234–243. http://doi.org/10.1161/CIRCRESAHA.108.175331

Porazinski, S., Wang, H., Asaoka, Y., Behrndt, M., Miyamoto, T., Morita, H., … Furutani-Seiki, M. (2015). YAP is essential for tissue tension to ensure

vertebrate 3D body shape. *Nature*, 1–6. http://doi.org/10.1038/nature14215

Portran, D., Schaedel, L., Xu, Z., Théry, M., & Nachury, M. V. (2017). Tubulin acetylation protects long-lived microtubules against mechanical ageing. *Nature Cell Biology*, *19*(4), 391–398. http://doi.org/10.1038/ncb3481

Prosnitz, L. R., Maguire, P., Anderson, J. M., Scully, S. P., Harrelson, J. M., Jones, E. L., … Brizel, D. M. (1999). The treatment of high-grade soft tissue sarcomas with preoperative thermoradiotherapy. *International Journal of Radiation Oncology Biology Physics*, *45*(4), 941–949. http://doi.org/10.1016/S0360-3016(99)00272-2

Prosser, S. L., & Morrison, C. G. (2015). Centrin2 regulates CP110 removal in primary cilium formation. *Journal of Cell Biology*, *208*(6), 693–701. http://doi.org/10.1083/jcb.201411070

Pugacheva, E. N., Jablonski, S. A., Hartman, T. R., Henske, E. P., & Golemis, E. A. (2007). HEF1-Dependent Aurora A Activation Induces Disassembly of the Primary Cilium. *Cell*, *129*(7), 1351–1363. http://doi.org/10.1016/j.cell.2007.04.035

Quinones, G. B., Danowski, B. A., Devaraj, A., Singh, V., & Ligon, L. A. (2011). The posttranslational modification of tubulin undergoes a switch from detyrosination to acetylation as epithelial cells become polarized. *Molecular Biology of the Cell*, *22*(7), 1045–1057. http://doi.org/10.1091/mbc.E10-06-0519

Raimon Sunyer1, Vito Conte1, Jorge Escribano2, Alberto Elosegui-Artola1, Anna Labernadie1, Léo Valon1, Daniel Navajas1, 3, 4, José Manuel García-Aznar2, José J. Muñoz5, Pere Roca-Cusachs1, 3,*, Xavier Trepat1, 3, 6, 7,* Raimon Sunyer1, Vito Conte1, Jorge, 7. (2016). Re s ear ch | r e p o r t s. *Science*, *353*(6304), 1157–1161. http://doi.org/10.5061/dryad.r8h3n

Ran, J., Yang, Y., Li, D., Liu, M., & Zhou, J. (2015). Deacetylation of α-tubulin and cortactin is required for HDAC6 to trigger ciliary disassembly. *Scientific Reports*, *5*, 1–13. http://doi.org/10.1038/srep12917

Ranft, J., Basan, M., Elgeti, J., Joanny, J.-F., Prost, J., & Jülicher, F. (2010). Fluidization of tissues by cell division and apoptosis. *Proceedings of the National Academy of Sciences of the United States of America*, *107*(49), 20863–20868. http://doi.org/10.1073/pnas.1011086107

Reiter, J. F., Blacque, O. E., & Leroux, M. R. (2012). The base of the cilium: Roles for transition fibres and the transition zone in ciliary formation, maintenance and compartmentalization. *EMBO Reports*, *13*(7), 608–618.

http://doi.org/10.1038/embor.2012.73

Ridley, A. J., Paterson, H. F., Johnston, C. L., Diekmann, D., & Hall, A. (1992). The small GTP-binding protein rac regulates growth factor-induced membrane ruffling. *Cell*, *70*(3), 401–410. http://doi.org/10.1016/0092-8674(92)90164-8

Riolo, M. T., Cooper, Z. A., Holloway, M. P., Cheng, Y., Bianchi, C., Yakirevich, E., … Altura, R. A. (2012). Histone deacetylase 6 (HDAC6) deacetylates survivin for its nuclear export in breast cancer. *Journal of Biological Chemistry*, *287*(14), 10885–10893. http://doi.org/10.1074/jbc.M111.308791

Rioux, J. B., Philippe, N., Pereira, S., Pignol, D., Wu, L. F., & Ginet, N. (2010). A second actin-like mamk protein in *Magnetospirillum magneticum* AMB-1 encoded outside the genomic magnetosome island. *PLoS ONE*, *5*(2). http://doi.org/10.1371/journal.pone.0009151

Rogowski, K., Juge, F., van Dijk, J., Wloga, D., Strub, J. M., Levilliers, N., … Janke, C. (2009). Evolutionary Divergence of Enzymatic Mechanisms for Posttranslational Polyglycylation. *Cell*, *137*(6), 1076–1087. http://doi.org/10.1016/j.cell.2009.05.020

Rosińczuk, J., Taradaj, J., Dymarek, R., & Sopel, M. (2016). Mechanoregulation of wound healing and skin homeostasis. *BioMed Research International*, *2016*. http://doi.org/10.1155/2016/3943481

Rotherham, M., Henstock, J. R., Qutachi, O., & El Haj, A. J. (2017). Remote regulation of magnetic particle targeted Wnt signalling for bone tissue engineering. *Nanomedicine: Nanotechnology, Biology and Medicine*, 1–12. http://doi.org/10.1016/j.nano.2017.09.008

Ruhlen, R., & Marberry, K. (2014). The chondrocyte primary cilium. *Osteoarthritis and Cartilage*, *22*(8), 1071–1076. http://doi.org/10.1016/j.joca.2014.05.011

Ruprecht, V., Wieser, S., Callan-Jones, A., Smutny, M., Morita, H., Sako, K., … Heisenberg, C. P. (2015). Cortical contractility triggers a stochastic switch to fast amoeboid cell motility. *Cell*, *160*(4), 673–685. http://doi.org/10.1016/j.cell.2015.01.008

Rymut, S. M., & Kelley, T. J. (2015). Broader implications: Biological and clinical significance of microtubule acetylation. *Cell Health and Cytoskeleton*, *7*, 71–82. http://doi.org/10.2147/CHC.S77040

Rymut SM, Harker A, Corey DA, Burgess JD, Sun H, Clancy JP, & Kelley TJ. (2013). Reduced microtubule acetylation in cystic. *American Journal of Physiology -*

Lung Cellular & Molecular Physiology, *305*(6), L419–L431. http://doi.org/10.1152/ajplung.00411.2012

Sadoul, K., & Khochbin, S. (2016). The growing landscape of tubulin acetylation: lysine 40 and many more. *Biochemical Journal*, *473*(13), 1859–1868. http://doi.org/10.1042/BCJ20160172

Sathasivam, K., Woodman, B., Mahal, a, Bertaux, F., Wanker, E. E., Shima, D. T., & Bates, G. P. (2001). Centrosome disorganization in fibroblast cultures derived from R6/2 Huntington's disease (HD) transgenic mice and HD patients. *Human Molecular Genetics*, *10*(21), 2425–2435. http://doi.org/10.1093/hmg/10.21.2425

Satoh, A., Imai, S. I., & Guarente, L. (2017). The brain, sirtuins, and ageing. *Nature Reviews Neuroscience*, *18*(6), 362–374. http://doi.org/10.1038/nrn.2017.42

Shah, Y. Y., Maldonado-Camargo, L., Patel, N. S., Biedrzycki, A. H., Yarmola, E. G., Dobson, J., … Allen, K. D. (2017). Magnetic particle translation as a surrogate measure for synovial fluid mechanics. *Journal of Biomechanics*, *60*, 9–14. http://doi.org/10.1016/j.jbiomech.2017.05.015

Shen, H., Tong, S., Bao, G., & Wang, B. (2014). Structural responses of cells to intracellular magnetic force induced by superparamagnetic iron oxide nanoparticles. *Physical Chemistry Chemical Physics*, *16*, 1914–1920. http://doi.org/10.1039/C3CP51435H

Shen, Y. F., Tang, J., Nie, Z. H., Wang, Y. D., Ren, Y., & Zuo, L. (2009). Tailoring size and structural distortion of Fe3O4nanoparticles for the purification of contaminated water. *Bioresource Technology*, *100*(18), 4139–4146. http://doi.org/10.1016/j.biortech.2009.04.004

Skitzki, J. J., Repasky, E. A., & Evans, S. S. (2009). Hyperthermia as an immunotherapy strategy for cancer. *Current Opinion in Investigational Drugs (London, England : 2000)*, *10*(6), 550–8. http://doi.org/10.1016/j.pestbp.2011.02.012.Investigations

Smutny, M., Ákos, Z., Grigolon, S., Shamipour, S., Ruprecht, V., Čapek, D., … Heisenberg, C. P. (2017). Friction forces position the neural anlage. *Nature Cell Biology*, *19*(4), 306–317. http://doi.org/10.1038/ncb3492

Solnica-Krezel, L., & Sepich, D. S. (2012). Gastrulation: Making and Shaping Germ Layers. *Annual Review of Cell and Developmental Biology*, *28*, 687–717. http://doi.org/10.1146/annurev-cellbio-092910-154043

Song, Y., & Brady, S. T. (2015). Post-translational modifications of tubulin: Pathways

to functional diversity of microtubules. *Trends in Cell Biology*, *25*(3), 125–136. http://doi.org/10.1016/j.tcb.2014.10.004

Sosnovik, D. E., Nahrendorf, M., & Weissleder, R. (2008). Magnetic nanoparticles for MR imaging: Agents, techniques and cardiovascular applications. *Basic Research in Cardiology*, *103*(2), 122–130. http://doi.org/10.1007/s00395-008-0710-7

Staniland, S. S., Moisescu, C., & Benning, L. G. (2010). Cell division in magnetotactic bacteria splits magnetosome chain in half. *Journal of Basic Microbiology*, *50*, 392–396. http://doi.org/10.1002/jobm.200900408

Steketee, M. B., Moysidis, S. N., Jin, X.-L., Weinstein, J. E., Pita-Thomas, W., Raju, H. B., … Goldberg, J. L. (2011). Nanoparticle-mediated signaling endosome localization regulates growth cone motility and neurite growth. *Proceedings of the National Academy of Sciences*, *108*(47), 19042–19047. http://doi.org/10.1073/pnas.1019624108

Sun, J., Li, Y., Liang, X. J., & Wang, P. C. (2011). Bacterial magnetosome: A novel biogenetic magnetic targeted drug carrier with potential multifunctions. *Journal of Nanomaterials*, *2011*. http://doi.org/10.1155/2011/469031

Sütterlin, C., & Colanzi, A. (2010). The Golgi and the centrosome: Building a functional partnership. *Journal of Cell Biology*, *188*(5), 621–628. http://doi.org/10.1083/jcb.200910001

Szyk, A., Deaconescu, A. M., Spector, J., Goodman, B., Valenstein, M. L., Ziolkowska, N. E., … Roll-Mecak, A. (2014). Molecular basis for age-dependent microtubule acetylation by tubulin acetyltransferase. *Cell*, *157*(6), 1405–1415. http://doi.org/10.1016/j.cell.2014.03.061

Tam, P. P. L., & Behringer, R. R. (1997). Mouse gastrulation: The formation of a mammalian body plan. *Mechanisms of Development*, *68*(1–2), 3–25. http://doi.org/10.1016/S0925-4773(97)00123-8

Tanaka, T., Serneo, F. F., Higgins, C., Gambello, M. J., Wynshaw-Boris, A., & Gleeson, J. G. (2004). Lis1 and doublecortin function with dynein to mediate coupling of the nucleus to the centrosome in neuronal migration. *Journal of Cell Biology*, *165*(5), 709–721. http://doi.org/10.1083/jcb.200309025

Tang, N., & Marshall, W. F. (2012). Centrosome positioning in vertebrate development. http://doi.org/10.1242/jcs.038083

Tang, X., Gao, J. S., Guan, Y. jie, McLane, K. E., Yuan, Z. L., Ramratnam, B., &

Chin, Y. E. (2007). Acetylation-Dependent Signal Transduction for Type I Interferon Receptor. *Cell*, *131*(1), 93–105. http://doi.org/10.1016/j.cell.2007.07.034

Tay, C. Y., Cai, P., Setyawati, M. I., Fang, W., Tan, L. P., Hong, C. H. L., … Leong, D. T. (2014). Nanoparticles strengthen intracellular tension and retard cellular migration. *Nano Letters*, *14*, 83–88. http://doi.org/10.1021/nl4032549

Tay, C. Y., Fang, W., Setyawati, M. I., Chia, S. L., Tan, K. S., Hong, C. H. L., & Leong, D. T. (2014). Nano-hydroxyapatite and nano-titanium dioxide exhibit different subcellular distribution and apoptotic profile in human oral epithelium. *ACS Applied Materials and Interfaces*, *6*(9), 6248–6256. http://doi.org/10.1021/am501266a

Tay, C. Y., & Leong, D. T. (2014). Inorganic nanoparticles as tubulin binding agents for cancer therapy. *Nanomedicine*, *9*(14), 2075–2077. http://doi.org/10.2217/nnm.14.105

Thiam, H. R., Vargas, P., Carpi, N., Crespo, C. L., Raab, M., Terriac, E., … Piel, M. (2016). Perinuclear Arp2/3-driven actin polymerization enables nuclear deformation to facilitate cell migration through complex environments. *Nature Communications*, *7*, 1–14. http://doi.org/10.1038/ncomms10997

van den Tempel, N., Zelensky, A., Odijk, H., Laffeber, C., Schmidt, C., Brandsma, I., … Kanaar, R. (2019). On the Mechanism of Hyperthermia-Induced BRCA2 Protein Degradation. *Cancers*, *11*(1), 97. http://doi.org/10.3390/cancers11010097

Togenesis, T., Beckman, D. a, & Brent, R. L. (1984). Mechanisms of tera togenesis.

Tong, J. J., Liu, J., Bertos, N. R., & Yang, X.-J. (2002). Identification of HDAC10, a novel class II human histone deacetylase containing a leucine-rich domain. *Nucleic Acids Research*, *30*(5), 1114–1123. http://doi.org/10.1093/nar/30.5.1114

Topczewski, J., Sepich, D. S., Myers, D. C., Walker, C., Amores, A., Lele, Z., … Solnica-Krezel, L. (2001). The Zebrafish Glypican Knypek Controls Cell Polarity during Gastrulation Movements of Convergent Extension. *Developmental Cell*, *1*(2), 251–264. http://doi.org/10.1016/S1534-5807(01)00005-3

Udan, R. S., Kango-Singh, M., Nolo, R., Tao, C., & Halder, G. (2003). Hippo promotes proliferation arrest and apoptosis in the Salvador/Warts pathway. *Nature Cell Biology*, *5*(10), 914–920. http://doi.org/10.1038/ncb1050

Uebe, R., & Schüler, D. (2016). Magnetosome biogenesis in magnetotactic bacteria.

Nature Reviews Microbiology, *14*(10), 621–637. http://doi.org/10.1038/nrmicro.2016.99

Vagida, M. S., Arakelyan, A., Lebedeva, A. M., Grivel, J.-C., Shpektor, A. V, Yu Vasilieva, E., & Margolis, L. B. (2016). Analysis of Extracellular Vesicles Using Magnetic Nanoparticles in Blood of Patients with Acute Coronary Syndrome EXTRACELLULAR VESICLES IN ISCHEMIC HEART DISEASE. *Biochemistry (Moscow)*, *81*(4), 15–312. http://doi.org/10.1134/S0006297916040088

van Bergeijk, P., Hoogenraad, C. C., & Kapitein, L. C. (2015). Right Time, Right Place: Probing the Functions of Organelle Positioning. *Trends in Cell Biology*, *xx*, 1–14. http://doi.org/10.1016/j.tcb.2015.10.001

Varchulova Novakova, Z., Gasparova, I., Krajciova, L., Molcan, M., Varga, I., Timko, M., & Danisovic, L. (2017). Effect of magnetosomes on cell proliferation, apoptosis induction and expression of Bcl-2 in the human lung cancer cell line A549. *Biologia (Poland)*, *72*(5). http://doi.org/10.1515/biolog-2017-0059

Wang, G., Li, S., Gilbert, J., Gritton, H. J., Wang, Z., Li, Z., … Man, H. Y. (2017). Crucial Roles for SIRT2 and AMPA Receptor Acetylation in Synaptic Plasticity and Memory. *Cell Reports*, *20*(6), 1335–1347. http://doi.org/10.1016/j.celrep.2017.07.030

Wang, J., Chen, H., Seth, A., & McCulloch, C. A. (2003). Mechanical force regulation of myofibroblast differentiation in cardiac fibroblasts. *American Journal of Physiology - Heart and Circulatory Physiology*, *285*(5), H1871–H1881. http://doi.org/10.1152/ajpheart.00387.2003

Wang, P., Chen, C., Chen, C., Li, Y., Pan, W., & Song, T. (2017). The interaction of bacterial magnetosomes and human liver cancer cells in vitro. *Journal of Magnetism and Magnetic Materials*, *427*(June 2016), 105–110. http://doi.org/10.1016/j.jmmm.2016.10.106

Wang, Y., Zhou, L., Zhao, Y., Wang, S., Chen, L., Liu, L., … Ye, D. (2014). Regulation of G 6PD acetylation by SIRT2 and KAT9 modulates NADPH homeostasis and cell survival during oxidative stress #, (May), 1–17.

Wanna, Y., Chindaduang, A., Tumcharern, G., Phromyothin, D., Porntheerapat, S., Nukeaw, J., … Pratontep, S. (2016). Efficiency of SPIONs functionalized with polyethylene glycol bis(amine) for heavy metal removal. *Journal of Magnetism and Magnetic Materials*, *414*, 32–37. http://doi.org/10.1016/j.jmmm.2016.04.064

Weber, G. F., Bjerke, M. A., & DeSimone, D. W. (2012). A Mechanoresponsive

Cadherin-Keratin Complex Directs Polarized Protrusive Behavior and Collective Cell Migration. *Developmental Cell*, *22*(1), 104–115. http://doi.org/10.1016/j.devcel.2011.10.013

Wei, X., & Malicki, J. (2002). nagie oko, encoding a MAGUK-family protein, is essential for cellular patterning of the retina. *Nature Genetics*, *31*(june), 150–157. http://doi.org/10.1038/ng883

Weliky, M., & Oster, G. (1990). The mechanical basis of cell rearrangement. I. Epithelial morphogenesis during Fundulus epiboly. *Development (Cambridge, England)*, *109*(2), 373–386.

Westermann, S., & Weber, K. (2003). Post-translational modifications regulate microtubule function. *Nature Reviews Molecular Cell Biology*, *4*(12), 938–947. http://doi.org/10.1038/nrm1260

Wheeler, M. A., Smith, C. J., Ottolini, M., Barker, B. S., Purohit, A. M., Grippo, R. M., … Guler, A. D. (2016). Genetically targeted magnetic control of the nervous system. *Nat Neurosci*, *19*(5), 756–761. http://doi.org/10.1038/nn.4265

Wipff, P. J., Rifkin, D. B., Meister, J. J., & Hinz, B. (2007). Myofibroblast contraction activates latent TGF-β1 from the extracellular matrix. *Journal of Cell Biology*, *179*(6), 1311–1323. http://doi.org/10.1083/jcb.200704042

Wloga, D., Dave, D., Meagley, J., Rogowski, K., Jerka-Dziadosz, M., & Gaertig, J. (2010). Hyperglutamylation of tubulin can either stabilize or destabilize microtubules in the same cell. *Eukaryotic Cell*, *9*(1), 184–193. http://doi.org/10.1128/EC.00176-09

Wloga, D., Joachimiak, E., Louka, P., & Gaertig, J. (2017). Posttranslational modifications of Tubulin and cilia. *Cold Spring Harbor Perspectives in Biology*, *9*(6). http://doi.org/10.1101/cshperspect.a028159

Wong, I. Y., Javaid, S., Wong, E. A., Perk, S., Haber, D. A., Toner, M., & Irimia, D. (2014). Collective and individual migration following the epithelial-mesenchymal transition. *Nature Materials*, *13*(11), 1063–1071. http://doi.org/10.1038/nmat4062

Woodham, E. F., & Machesky, L. M. (2014). Polarised cell migration: Intrinsic and extrinsic drivers. *Current Opinion in Cell Biology*, *30*(1), 25–32. http://doi.org/10.1016/j.ceb.2014.05.006Yamaguchi, M. (2005). Histone deacetylase 1 regulates retinal neurogenesis in zebrafish by suppressing Wnt and Notch signaling pathways. *Development*, *132*(13), 3027–3043. http://doi.org/10.1242/dev.01881

Yoshino, T., Hirabe, H., Takahashi, M., Kuhara, M., Takeyama, H., & Matsunaga, T. (2008). Magnetic cell separation using nano-sized bacterial magnetic particles with reconstructed magnetosome membrane. *Biotechnology and Bioengineering*, *101*(3), 470–477. http://doi.org/10.1002/bit.21912

Yoshino, T., Kanetsuki, Y., & Matsunaga, T. (2005). The Potential of Genetically Engineered Magnetic Particles in Biomedical Applications.

Yoshino, T., & Matsunaga, T. (2006). Efficient and stable display of functional proteins on bacterial magnetic particles using Mms13 as a novel anchor molecule. *Applied and Environmental Microbiology*, *72*(1), 465–471. http://doi.org/10.1128/AEM.72.1.465-471.2006

Yu, F. X., & Guan, K. L. (2013). The Hippo pathway: Regulators and regulations. *Genes and Development*, *27*(2012), 355–371. http://doi.org/10.1101/gad.210773.112

Zhang, F., Su, B., Wang, C., Siedlak, S. L., Mondragon-Rodriguez, S., Lee, H. gon, … Zhu, X. (2015). Posttranslational modifications of α-tubulin in alzheimer disease. *Translational Neurodegeneration*, *4*(1), 1–9. http://doi.org/10.1186/s40035-015-0030-4

Zhang, X., Yuan, Z., Zhang, Y., Yong, S., Salas-Burgos, A., Koomen, J., … Seto, E. (2007). HDAC6 Modulates Cell Motility by Altering the Acetylation Level of Cortactin. *Molecular Cell*, *27*(2), 197–213. http://doi.org/10.1016/j.molcel.2007.05.033

Zhang, Y., Kwon, S., Yamaguchi, T., Cubizolles, F., Rousseaux, S., Kneissel, M., … Matthias, P. (2008). Mice Lacking Histone Deacetylase 6 Have Hyperacetylated Tubulin but Are Viable and Develop Normally. *Molecular and Cellular Biology*, *28*(5), 1688–1701. http://doi.org/10.1128/MCB.01154-06

Zhao, Y., Yang, J., Liao, W., Liu, X., Zhang, H., Wang, S., … Zhu, W.-G. (2010). Cytosolic FoxO1 is essential for the induction of autophagy and tumour suppressor activity. *Nature Cell Biology*, *12*(7), 665–675. http://doi.org/10.1038/ncb2069

Zhou, X., Fan, L. X., Li, K., Ramchandran, R., Calvet, J. P., & Li, X. (2014). SIRT2 regulates ciliogenesis and contributes to abnormal centrosome amplification caused by loss of polycystin-1. *Human Molecular Genetics*, *23*(6), 1644–1655. http://doi.org/10.1093/hmg/ddt556

Zuo, Q., Wu, W., Li, X., Zhao, L., & Chen, W. (2012). HDAC6 and SIRT2 promote

bladder cancer cell migration and invasion by targeting cortactin. *Oncology Reports*, *27*(3), 819–824. http://doi.org/10.3892/or.2011.1553